

University of Groningen

Prokaryotic respiration and production in the open ocean

Reinthal, Thomas

IMPORTANT NOTE: You are advised to consult the publisher's version (publisher's PDF) if you wish to cite from it. Please check the document version below.

Document Version

Publisher's PDF, also known as Version of record

Publication date:

2006

[Link to publication in University of Groningen/UMCG research database](#)

Citation for published version (APA):

Reinthal, T. (2006). Prokaryotic respiration and production in the open ocean. s.n.

Copyright

Other than for strictly personal use, it is not permitted to download or to forward/distribute the text or part of it without the consent of the author(s) and/or copyright holder(s), unless the work is under an open content license (like Creative Commons).

Take-down policy

If you believe that this document breaches copyright please contact us providing details, and we will remove access to the work immediately and investigate your claim.

Downloaded from the University of Groningen/UMCG research database (Pure): <http://www.rug.nl/research/portal>. For technical reasons the number of authors shown on this cover page is limited to 10 maximum.

Prokaryotic respiration and production in the open ocean

Cover illustration by T. Reinthaler

RIJKSUNIVERSITEIT GRONINGEN

Prokaryotic respiration and production in the open
ocean

Proefschrift

ter verkrijging van het doctoraat in de

Wiskunde en Natuurwetenschappen

aan de Rijksuniversiteit Groningen

op gezag van de

Rector Magnificus, dr. F. Zwarts,

in het openbaar te verdedigen op

vrijdag 3 februari 2006

om 14:45 uur

door

Thomas Reinthaler

geboren op 22 februari 1973

te Feldkirch (Oostenrijk)

Promotor: Prof. Dr. G. J. Herndl

Beoordelingscommissie: Prof. Dr. J. Arístegui
Prof. Dr. J. Middelburg
Prof. Dr. P. J. leB. Williams

Paranimfen: Corina P. D. Brussaard
Cornelia Maier

The work presented in this thesis was carried out at the Department of Biological Oceanography of the Royal Netherlands Institute for Sea Research (NIOZ). Financial support was provided by NWO-ALW and the European Commission 5th framework program.

To Barbara for her unconditional support.

Contents

Introduction	11
1 Automated spectrophotometric approach to determine oxygen concentrations in seawater via continuous-flow analysis	17
<i>Submitted to <i>Limnol. and Oceanogr.: Methods</i></i>	
2 Bacterial production and respiration in the sea-surface microlayer of the open Atlantic ocean	31
<i>Submitted to <i>Limnol. and Oceanogr.</i></i>	
3 Seasonal dynamics of bacterial growth efficiencies in relation to phytoplankton in the southern North Sea	53
<i>Published in <i>Aquat. Microbiol. Ecol.</i> (2005) 39:7-16</i>	
4 Prokaryotic respiration and production in the meso- and bathypelagic realm of the eastern and western North Atlantic basin	71
<i>Accepted at <i>Limnol. Oceanogr.</i></i>	
5 Relationship between bacterioplankton richness, respiration, and production in the southern North Sea	95
<i>Published in <i>Appl. Environ. Microbiol.</i> (2005) 71:2260-2266</i>	
Summary	113
Samenvatting	121
Acknowledgements	123
Curriculum Vitae	125

Introduction

The notion that heterotrophic bacteria are more abundant than any other functional group of organisms in the ocean emerged about two decades ago [19]. Heterotrophic bacteria are also ubiquitously present: from the boundary layer between the surface ocean and the atmosphere to the deepest trenches of the dark ocean and in the subsurface seafloor [16]. Heterotrophic bacteria fulfill two major functions in the oceanic carbon cycle. They utilize dissolved organic carbon (DOC) for biomass production [1, 8] but at the same time, convert a large part of this DOC into carbon dioxide [6]. Overall, more than 50% of the organic carbon synthesized by marine primary producers is channeled through bacterioplankton [9].

The ‘microbial loop’ and bacterial growth efficiency

In the ‘microbial loop’ hypothesis, as originally formulated, it has been suggested that bacteria efficiently convert DOC, not accessible to other heterotrophic organisms, into particulate organic carbon (POC) (i.e., bacterial biomass), which is grazed upon by eukaryotic microheterotrophs. Thus, DOC is made indirectly available via the ‘microbial loop’ to higher trophic levels. This conversion of DOC to POC by bacteria is only efficient from a food web point-of-view, if the bacterial growth efficiency is high [5]. The bacterial growth efficiency ($BGE = BP/BCD$) is the fraction of the bacterial carbon demand (BCD) used for bacterial production (BP). The BCD is the sum of BP and bacterial respiration (BR; $BCD = BP + BR$).

Earlier studies, using radiolabeled model compounds estimated BGEs ranging from 30 to 80% [11] which would render bacteria a significant source of POC. However, experiments with natural substrates revealed consistently lower BGE values [9]. This was the beginning of a debate on whether bacteria are more likely to act as a ‘link or sink’ of organic carbon for higher trophic levels [17]. An average BGE of ~20% has been calculated for various coastal and open ocean sites based on a compilation of recently published data [5]. It is generally assumed that the major source of DOC is phytoplankton primary production, thus autochthonously produced. Based on our current understanding of carbon transport mediated by mixing of water masses and to a much lower extent diffusion, low BGEs pose frequently the problem that the organic carbon demand of bacterioplankton often exceeds its supply. This, in turn, raises questions on the validity of our current understanding of oceanic mixing processes and the accuracy of the primary production and bacterial production measurements.

The revival of bacterioplankton respiration measurements

Although measurements on respiration in aquatic ecosystems date as far back as to the 1950s [15], we still know very little about respiration in the ocean. Until recently, the research focus in

unraveling the carbon cycle was on primary production rather than on heterotrophic processes [22]. This bias towards productivity measurements is probably due to the relatively simple and seemingly straightforward method to measure primary production using radiolabeled bicarbonate [18]. However, this method bears considerable, often overlooked problems and it is still unclear whether it is more a measure of gross or net production. Routinely, primary production is measured as particulate primary production only while dissolved production is usually not measured.

For a long time, the fate of organic carbon was thought to be almost exclusively determined by the grazing food chain, passing organic carbon on from lower to higher trophic levels with accompanied respiratory losses. Consequently, bacteria were not seen as a significant part of the biogeochemical carbon cycling. In the early 1970s, Williams [20] and Pomeroy [14] found that the major fraction of the respiratory activity of the water column is mediated by the fraction smaller than 3 μm . However, this conception was only inadequately taken into account by the ‘microbial loop hypothesis’ [2]. After the introduction of a sensitive technique to measure bacterial production using radiolabeled substrates [10, 12], respiration measurements have hardly been performed anymore. A revival of respiration measurements was caused by the notion that respiration tends to exceed phytoplankton net production in oligotrophic open ocean systems [6] rendering major parts of the ocean net heterotrophic. This was the basis for a series of new studies on the balance between production and respiration in the ocean [7, 21].

Respiration is the metabolic process of oxidizing reduced organic substrates to release energy. The energy is stored in ATP, which in turn drives the transport of substrate into the cell, excretion of metabolic end-products and cell maintenance mechanisms [4]. The term ‘respiration’ is used for a variety of different processes, but generally involves the transfer of protons and electrons from an internal donor to a receptor. In the case of heterotrophic bacteria, the donor is the organic matter taken up, while oxygen usually is the terminal electron acceptor and the oxidation process results in the formation of CO_2 .

The most widely used approach to measure BGE is the simultaneous measurements of bacterial production via the incorporation of radioactively labeled leucine [12] and respiration via oxygen consumption on samples incubated preferably over less than 24 h [3, 13]. While the measurements of bacterial production and respiration are principally straightforward from a technical point of view, it is difficult to estimate BGE accurately. To separate bacteria from the remaining plankton, usually filtration over 0.6 to 0.8 μm filters is applied which might lead to a severe underestimation of the total bacterial activity if an active bacterial community is attached to particles. Furthermore, the respiration rates might be close to the detection limit and conversion factors have to be used to convert the incorporated radioactive substrate into carbon units produced.

Thesis outline

The aim of this thesis was to advance our knowledge on the dynamics of bacterial production and bacterial respiration in the open ocean and linking microbial activity to the physico-chemical environment. Figure 1 shows the conducted cruises on which the presented results are based upon as presented in the following chapters.

Chapter 1—Although the currency in carbon cycling measurements is logically carbon, respiration in water is most often calculated from the decline in oxygen concentrations in enclosed samples over time. The method of choice is the Winkler titration technique [23]

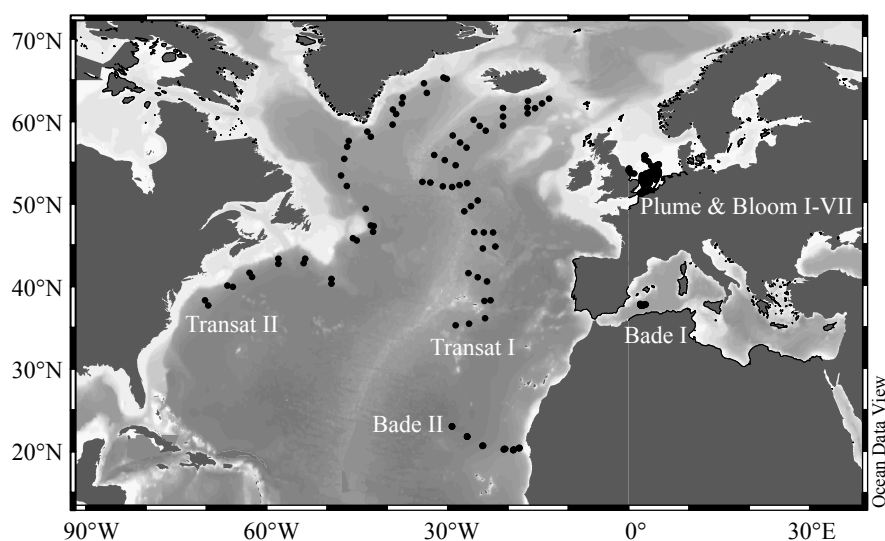


Figure 1: Map of the study sites. Plume and Bloom I-VII (Jun-Dec 2000 and May 2001) was a seasonal study investigating the nutrient flux in the southern North Sea; Transat I (Sept-Oct, 2002) and Transat II (May, 2003) focused on the prokaryotic activity in the North Atlantic Deep Water; Bade I (Sept-Oct, 2003) followed a stable eddy system in the Algerian Basin of the western Mediterranean Sea focusing on diel dynamics of prokaryotes and viruses; Bade II (Oct, 2004) followed a transect from the Mauritanian upwelling into the subtropical Atlantic gyre, focusing on prokaryotic dynamics along a trophic gradient. Black dots indicate the stations occupied; In total, 342 bacterial respiration and bacterial production measurements were performed; more information on the cruise programs can be found at www.nioz.nl.

because it provides sufficient precision to allow measurements in productive as well as in oligotrophic oceanic systems where respiration rates are usually extremely low. Thus far, the Winkler titration was a tedious task and time consuming. The use of a spectrophotometric determination of the concentration of total iodine and later refinements of the method made it possible to analyze samples more rapidly, however, for respiration measurements in oligotrophic regions this approach was found not to be sufficiently sensitive. In Chapter 1, we describe a method using the spectrophotometric Winkler approach in conjunction with an automated continuous-flow analyzing system. On board measurements along a gradient from high to low productivity proved, that the method allowed for precise and accurate measurements of oxygen concentrations even in oligotrophic environments.

Chapter 2—The sea-surface microlayer (SML) represents the boundary layer between the ocean and the atmosphere. It has been shown that dissolved organic matter in the SML is often enriched compared to the underlying water for reasons that are not entirely clear. Heterotrophic activity of the prokaryotic community in the SML could give important insight into exchange processes between the ocean and the atmosphere. In Chapter 2, we measured bacterial production and respiration and linked these parameters to patterns of potential substrate sources for bacteria.

Chapter 3—Seasonal studies in the open ocean are generally scarce because of constraints due to the weather conditions and availability of shiptime. In the southern North Sea, we conducted a seasonal survey studying the dynamics in bacterial respiration and production in relation to DOC and primary production. In total, we occupied 150 stations and compiled 102 BGE estimates.

Chapter 4—The dark ocean is one of the most under-sampled environments in our biosphere. Reported biological activity in the deep sea is low, however, until now methods were generally not sensitive enough to allow rate measurements at depths below 500 m. Model estimates on carbon fluxes suggest that respiration in the dark ocean represents up to half of the total respiration in the upper layers. However, even the highest current estimates on carbon input into the deep ocean do not match mineralization rates measured in the deep. In this chapter, bacterial production and respiration was measured in the meso- and bathypelagic of the North Atlantic supporting the current notion, that the carbon flux in the dark ocean mediated by the prokaryotic community might be either higher than previously assumed or that decompression of the prokaryotes leads to a stimulation of their activity.

Chapter 5—Currently, there is considerable scientific debate on the relation between diversity and ecosystem functioning. We investigated the relation between changes in the phylogenetic composition of the bacterioplankton community and the main function of bacteria in the carbon cycling, i.e., the remineralization of organic carbon, over seasonal cycles in the southern North Sea. The remineralization activity was found to be largely independent of the phylogenetic composition of the bacterioplankton community.

Bibliography

- [1] Azam F. 1998. Oceanography: Microbial control of oceanic carbon flux: The plot thickens. *Science* 280: 694-6
- [2] Azam F, Fenchel T, Field JG, Gray JS, Meyerreil LA, Thingstad F. 1983. The ecological role of water column microbes in the sea. *Marine Ecology-Progress Series* 10: 257-63
- [3] Biddanda B, Opsahl SB, R. 1994. Plankton respiration and carbon flux through bacterioplankton on the Louisiana shelf. *Limnology and Oceanography* 39: 1259-75
- [4] Del Giorgio PA, Cole JJ. 1998. Bacterial growth efficiency in natural aquatic systems. *Annual Review of Ecology and Systematics* 29: 503-41
- [5] Del Giorgio PA, Cole JJ. 2000. Bacterial energetics and growth efficiency. In *Microbial Ecology of the Oceans*, ed. DL Kirchman, pp. 289-325. New York: Wiley-Liss
- [6] Del Giorgio PA, Cole JJ, Cimperis A. 1997. Respiration rates of bacteria exceed phytoplankton in unproductive aquatic systems. *Nature* 385: 148-51
- [7] Duarte CM, Agusti S. 1998. The CO₂ balance of unproductive aquatic ecosystems. *Science* 281: 234-6
- [8] Ducklow HW. 2000. Bacterial production and biomass in the oceans. In *Microbial ecology of the oceans*, ed. DL Kirchman, pp. 85-120. New York: Wiley-Liss
- [9] Ducklow HW, Purdie DA, Williams PJJ, Davies JM. 1986. Bacterioplankton: a sink for carbon in a coastal marine plankton community. *Science* 232: 865-7
- [10] Fuhrman JA, Azam F. 1982. Thymidine incorporation as a measure of heterotrophic bacterioplankton production in marine surface waters: evaluation and field results. *Marine Biology* 66: 109-20

- [11] Jahnke RA, Craven DB. 1995. Quantifying the role of heterotrophic bacteria in the carbon cycle - a need for respiration rate measurements. *Limnology and Oceanography* 40: 436-41
- [12] Kirchman D, K'Ness E, Hodson RE. 1985. Leucine incorporation and its potential as a measure of protein synthesis by bacteria in natural aquatic systems. *Applied and Environmental Microbiology* 49: 599-607
- [13] Lemée R, Rochelle-Newall E, Van Wambeke F, Pizay M-D, Rinaldi P, Gattuso J-P. 2002. Seasonal variation of bacterial production, respiration and growth efficiency in the open NW Mediterranean Sea. *Aquatic Microbial Ecology* 29: 227-37
- [14] Pomeroy LR. 1974. The ocean's food web, a changing paradigm. *BioScience* 24: 499-504
- [15] Pomeroy LR, Johannes RE. 1966. Total plankton respiration. *Deep-Sea Research Part I* 13: 971-3
- [16] Schippers A, Neretin LN, Kallmeyer J, Ferdelman TG, Cragg BA, et al. 2005. Prokaryotic cells of the deep sub-seafloor biosphere identified as living bacteria. 433: 861-4
- [17] Sherr EB, Sherr BF, Albright LJ. 1987. Bacteria: link or sink? *Science* 235: 88-9
- [18] Steemann Nielsen E. 1952. The use of radio-active carbon (^{14}C) for measuring organic production in the sea. *Journal du Conseil permanent International pour l' Exploration de la Mer* 18: 117-40
- [19] Whitman WB, Coleman DC, Wiebe WJ. 1998. Prokaryotes: the unseen majority. *Proceedings of the National Academy of Sciences of the United States of America* 95: 6578-83
- [20] Williams PJL. 1970. Heterotrophic utilization of dissolved organic compounds in the sea. I. Size distribution of population and relationship between respiration and incorporation of growth substrates. *Journal of the Marine Biological Association of the United Kingdom* 50: 859-70
- [21] Williams PJIB. 1998. The balance of plankton respiration and photosynthesis in the open oceans. *Nature* 394: 55-7
- [22] Williams PJIB, Del Giorgio PA. 2005. Respiration in aquatic ecosystems: history and background. In *Respiration in aquatic ecosystems*, ed. PA Del Giorgio, PJIB Williams, pp. 1-17. New York: Oxford University Press
- [23] Winkler LW. 1888. Die Bestimmung des im Wasser gelösten Sauerstoffes. *Chemische Berichte* 27: 2843-55

Chapter 1

Automated spectrophotometric approach to determine oxygen concentrations in seawater via continuous-flow analysis¹

Thomas Reinthaler, Karel Bakker, Rinus Manuels, Jan van Ooijen and Gerhard J. Herndl

Oxygen consumption measurements are the most common approach to estimate remineralization of organic carbon to CO₂. A refined protocol of the spectrophotometric Winkler approach is presented, where a continuous-flow analyzer is coupled with a custom-made autosampler for 30 BOD bottles. The time required for analysis is 2 min per sample and the precision is 0.04% at ~200 mmol O₂ m⁻³. Thus, analysis speed and quality are significantly improved compared to the classical Winkler titration approach to determine O₂ concentrations. The accuracy of the method is 99.7 ± 0.2% as determined by measuring the oxygen concentrations of O₂-saturated seawater at 20°C. The measured absorption of the molecular iodine and the tri-iodide ion couple at 460 nm wavelength was linear up to an equivalent of 320 mmol O₂ m⁻³, which is within the range of open ocean oxygen concentrations. The instrument was tested on a cruise in the subtropical North Atlantic to determine community respiration (CR) and bacterial respiration (BR). Both CR and BR decreased by ~85% between the Mauritanian upwelling region and the oligotrophic gyre. Along this gradient, the contribution of BR to CR increased from 36 to 76%. The instrument proved highly suitable for work at sea and should allow more rapid and exact oxygen concentration measurements in the open ocean.

Introduction

Measurements of oxygen concentrations are used to characterize water masses in physical and chemical oceanography and to estimate the respiratory activity of single specimens or entire subsystems. The Winkler method [21] is considered the most accurate and cost-effective method to measure dissolved oxygen in water. The Winkler approach is also used to calibrate

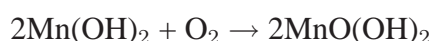
¹Submitted to *Limnol. and Oceanogr.: Methods*

the Clark-type oxygen sensors on conductivity-temperature-depth rosettes in sea-going research and limnology.

Recently, renewed interest on the respiratory activity of plankton emerged as it might be one of the missing key parameters in ocean carbon cycle models [8]. Because the remineralization of organic matter to CO₂ is of particular interest, the most direct way of measuring respiration is to follow the evolution of dissolved inorganic carbon (DIC) in bottle incubations. Similarly, differences in oxygen concentrations can be measured requiring, however, the use of a respiration quotient to convert oxygen consumption to CO₂ production. The small changes in concentration of either CO₂ or O₂ over time during these incubations, against a usually high background concentration, demand a high precision of the method.

Due to the high DIC background in seawater of ~2000 mmol DIC m⁻³ and the comparatively low resolution (~1 mmol DIC m⁻³) of the coulometric CO₂ analysis [11, 15], this approach is only feasible in oceanic systems with fairly high planktonic activity. The achievable resolution of the Winkler method of 0.06–0.2 mmol O₂ m⁻³ at an average oxygen concentration in seawater of 200 mmol O₂ m⁻³ is sufficient to detect the minute changes in these incubation experiments, even in oligotrophic systems. Dissolved gas analyzers potentially achieve a similar level of precision as sensitive Winkler approaches [12], however, these instruments are expensive and therefore not widely used. Thus, oxygen consumption measurements, following the Winkler approach, are still the most widely applied method to determine the metabolic activity of plankton communities.

The basis of the Winkler procedure is that the oxygen in a sea water sample is made to oxidize the iodide ion to iodine quantitatively and the amount of iodine generated is determined by measuring the absorption of the Tri-iodide colored solution in an oxygen bottle. Manganese chloride is added to a known amount of seawater, followed by the addition of an alkaline sodium hydroxide-potassium iodide solution. The resulting manganous hydroxide precipitate reacts with the dissolved oxygen in the water and forms a hydrated tetravalent oxide of manganese:



Upon acidification, the manganese hydroxides dissolve and the tetravalent manganese acts as an oxidizing agent and liberates free iodine from the iodide ions:



in which I₃⁻ is the complex being formed according to the equation 3I₂ → 2I₃⁻, because there is an excess of I⁻.

The precision and the time needed for titration in the classical Winkler method have been improved by the automation of the end-point detection [3, 9, 20], however, commonly it still takes ~4 to 6 min to titrate a sample. The faster spectrophotometric approach to determine O₂ was introduced by Broenkow and Cline [2] and is based on measuring the absorbance of the I₂/I₃⁻ couple. After several improvements on analysis speed and standardization [14, 17] and the choice of wavelength [13], this technique might have the potential to replace the Winkler titration for most applications in biological oceanography and aquatic ecology, particularly if the particle load of the water is low such as in open ocean systems.

To further improve the spectrophotometric approach for measuring oxygen concentrations, we developed a fully automated analysis system using a custom-made autosampler in

conjunction with a continuous-flow analyzer. With this system, the time required to perform high quality oxygen concentration measurements is significantly reduced and ultimately, the analysis is coupled to an analytical control commonly not possible in conventional Winkler titration.

Materials and procedures

Glass bottles—Oxygen bottles made from borosilicate glass with a nominal volume in the range of 116–122 cm³ were calibrated to the mm³ level, according to the recommendations of the World Ocean Circulation Experiment (WOCE) [6]. For identification of bottles and the corresponding volume, the borosilicate glass bottles were engraved with a unique number. A set of these bottles was assigned for the calibration of the flow-through analyzer. In respiration experiments many bottles (up to 400 in our case) are incubated at the same time and the numbering system usually employed is tedious and frequently leads to confusion. With a more simple system of few numbers and color coded oxygen bottles it is easier to keep track of the samples. A difference in volume of $\leq \pm 0.5$ cm³ between bottles, analyzed in a single run on the flow-through analyzer, results in an uncertainty $\leq 0.02\%$ (for the calculation of the bottle volume correction factor see equation 2) and the resulting variations in measured oxygen concentrations in the bottles are below the detection limit of the Winkler method. Therefore, we sorted and color-coded the oxygen bottles according to their volume in classes of $\leq \pm 0.5$ cm³. We usually perform oxygen concentration measurements in triplicates. For simple identification of the respiration experiments consisting of t_0 and t_1 incubations, batches of 6 oxygen bottles were labeled with one unique number. Furthermore, all the t_0 bottles were labeled with a unique colored adhesive tape around the bottle neck.

Chemicals—We used the common Winkler reagents to determine oxygen concentrations at the following concentrations: A) manganese chloride (MnCl₂·4H₂O; 600 g dm⁻³; 3 mol L⁻¹), B) alkaline iodide reagent (NaOH; 250 g dm⁻³; 6 mol L⁻¹ + KI; 350 g dm⁻³; 2 mol L⁻¹), and C) sulfuric acid (H₂SO₄; 10 mol L⁻¹). After preparation, the reagent grade chemicals were filtered through Whatman GF/F filters and subsequently stored in dark glass bottles at ~20°C. The standard stock solution was prepared with potassium iodate (KIO₃; Malinckrodt Baker; primary standard). KIO₃ was dried at 180°C for 6 h, and 2.5 g of KIO₃ dissolved in 250 cm³ ultrapure Milli-Q water. Thus, 1 cm³ of stock solution of KIO₃ is equivalent to 70.1 mmol O₂ m⁻³. The prepared stock solution was aliquoted into small polycarbonate bottles and stored in a chamber with 100% humidity to prevent evaporation of water and therefore concentration of the stock solution.

Spectrophotometer—A Technicon TRAACS 800 continuous-flow analyzing system (Bran + Luebbe, Germany) was used equipped with a standard tungsten filament lamp and a fixed filter for 460 ± 10 nm wavelength (Fig. 1.1). The flow cell had a volume of 7.85 mm³ and the flow rate was set to ~ 1 cm³ min⁻¹. To further stabilize the signal, a heat exchange element was installed in front of the cuvette. The continuous-flow analyzer was controlled via the standard TRAACS analysis software (AACE version 5.40).

Autosampler—The principal components of the custom-made autosampler are an electronic board controlling an electric motor and the pneumatic sampling arm driven by compressed air at ~ 4 bar (Fig. 1.1). The motor and the sampling arm can be programmed via an RS232 connection by a computer with a simple DOS program. Programmable parameters include sampling time, flushing time with wash solution and the number of picks for both the sample and the wash

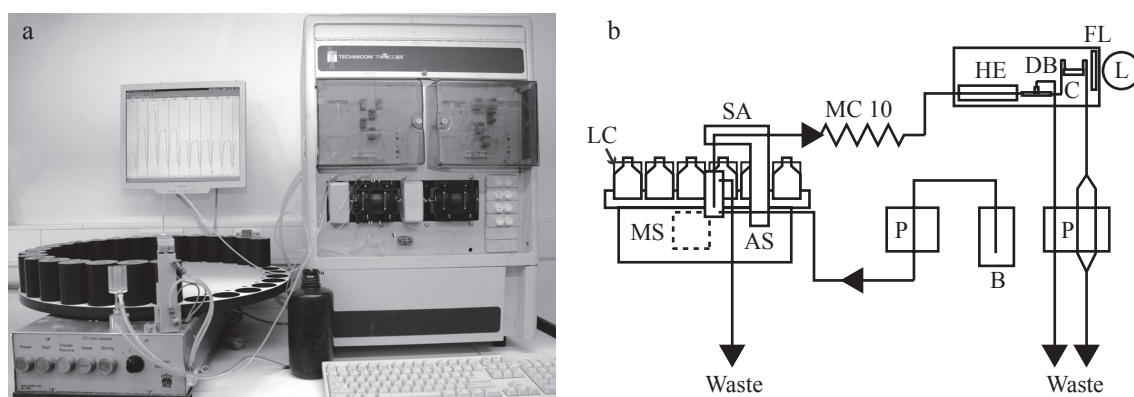


Figure 1.1: Setup of the autosampler and the continuous-flow analyzer in the temperature controlled container (a) and schematic diagram of the sample flow path through the analysis system (b). Autosampler (AS), sampling arm (SA), light cover for the bottles (LC), magnetic stirrer (MS), mixing coil (MC; 10 turns), heat exchange element (HE), de-bubbler (DB), flow-through cuvette (C), filter (FL; cutoff at 460 nm), light source (L), peristaltic pump (P), wash solution container (B). Arrows indicate the flow of sample, wash and waste water through the system.

solution. A built-in magnetic stirrer agitates the sample just before it is turned into the sampling position. The platform holds up to 30 bottles and a pneumatic pin fixes the platform firmly in place when the sample is in picking position. A sensor at the sampling arm automatically stops the autosampler at empty tray positions.

Sampling procedure and handling—The general sampling procedure and handling of samples followed the recommendations of Carritt and Carpenter [4]. For respiration measurements, seawater samples were transferred into a batch 6 oxygen bottles (from one volume class) via Tygon tubing, overflowing each bottle by at least three volumes. For community respiration measurements the seawater was tapped directly from the CTD, for bacterial respiration the seawater was first filtered over 0.8- μm polycarbonate filters and then siphoned into oxygen bottles. Triplicate samples were taken for t_0 and t_1 measurements. To fix the oxygen content in a bottle, 1 cm³ of reagent A followed by 2 cm³ of reagent B was added with high precision dispensers (Fortuna Optifix basic; precision $\pm 0.1\%$) near the bottom. The precise addition of chemical A and B is important because it dilutes the sample, therefore a dummy sample was spiked with the reagents prior to the actual samples which reassures air-free and smoothly working dispensers. Subsequently the bottles were stoppered and shaken vigorously to mix the chemicals. For incubation and storage, the bottles were immersed in waterbaths (kept at in situ temperature) to avoid drying of the bottle neck and losing the stopper seal. After ~ 20 min the fixed bottles were shaken again to assure complete reaction of the chemicals. Shortly before the measurements on the TRAACS system, 1 cm³ of reagent C was added to the fixed samples. After adding reagent C, a magnetic stirring bar was carefully introduced and the bottles were immediately covered with Parafilm to avoid losses of volatile compounds. The bottles were covered with a dark plastic cylinder shielding off light to prevent photooxidation of the I₂/I₃ mixture and stirred until the precipitate in the bottles was completely dissolved. Finally the samples were placed on the autosampler.

Calibration procedure—For the preparation of the wash solution, drift standards and instrument calibration standards, particle poor seawater from below the euphotic zone was

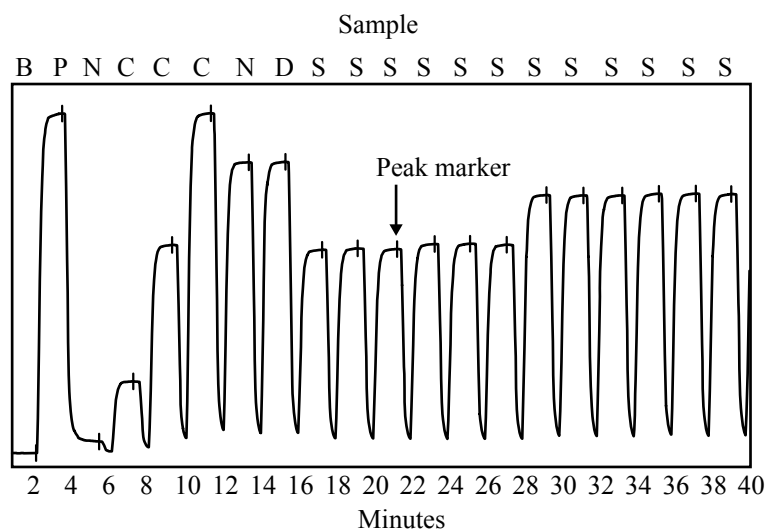


Figure 1.2: Example of a peak chart from respiration measurements on the continuous-flow analysis system conducted during the BADE-2 cruise. Baseline readings of the wash solution (B), primer as indicator of maximum peak height (P), calibration standards (C), sensitivity drift standards (D) and samples (S) are shown. The peak marker is set in a pre-defined peak window (for explanation see Text). Minutes indicate the analysis time.

collected into an 80-L polycarbonate carboy and acclimatized at 20°C. For occasional checks of instrument performance between different runs, reference samples were prepared. For the reference samples, the seawater was bubbled with air at 20°C for 24 h to reach saturation concentrations of oxygen. Subsequently, oxygen bottles were filled and fixed according to the procedure described above. A 3–4 point calibration line was constructed as follows: Seawater was filled into oxygen bottles with known volume; subsequently the reagents A, B and C were added in reverse order. After each addition the bottles were stoppered and shaken. Finally, the KIO_3 standard solution was added with adjustable volume electronic pipettes of 100, 250 and 1000 mm^3 (precision <0.05% and <0.15%; Biohit) and a magnetic stirrer was inserted into the bottle to homogenize the solution. The calibration line was usually constructed in the range for previously found oxygen concentrations of surface samples of ~ 150 to $300 \text{ mmol O}_2 \text{ m}^{-3}$. With flow-through systems it is necessary to provide a low-concentration marker or baseline to separate consecutive peaks. Thus, after each sample, the system was flushed with washing fluid. To minimize potential carry-over of the absorption signal from the washing fluid to the following sample, the wash solution was adjusted to an oxygen concentration slightly lower than the expected lowest value in the samples. Calibrating the instrument in a narrow range also increases the sensitivity of the photomultiplier to small changes in absorbance. To correct for changes in the sensitivity of the photomultiplier during a run, 2 drift standards with known concentration were placed after the calibration standards. Drift standards were set at around the medium expected concentration in the sample batch. The same pair of drift standards was also placed after 30 samples as well as at the end of each run. Both, wash solution and drift standards were prepared similar to the calibration standards. Because the calibration- and sensitivity standards are prepared with seawater and include all the chemicals used for normal samples a conventional blank used in titration is not necessary. All preparations and measurements were done in a temperature-controlled container set at 20°C.

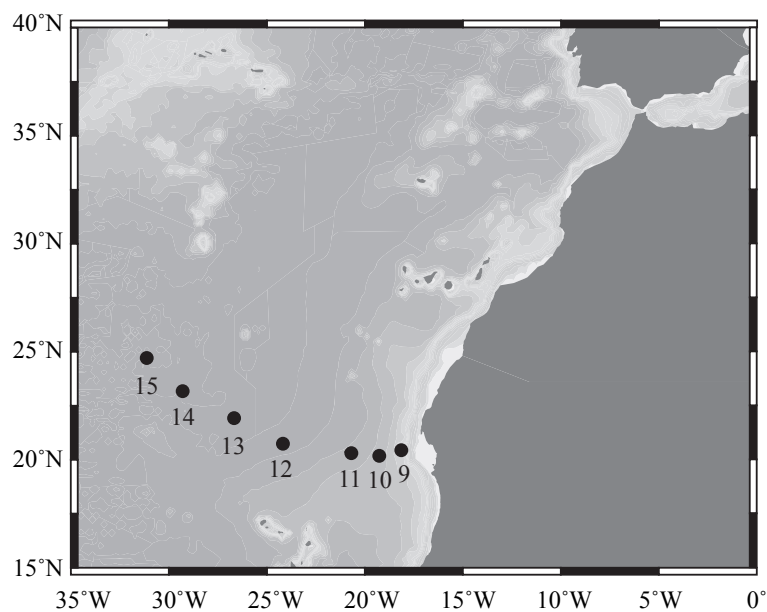


Figure 1.3: Map of the cruise track during BADE-2 from the Mauritanian upwelling (Station 9) into the subtropical North Atlantic gyre (Station 13 to 15).

Software and calculation—The software automatically detects a peak as the highest reading within an expected peak window and an adjustable smoothing parameter averages successive data points for improved peak identification (Fig. 1.2). The system measures relative absorbance on the scale of the calibration line and the oxygen concentrations are calculated internally from the calibration line via the TRAACS analysis software with the following formula:

$$\text{O}_2 \text{ (mmol O}_2 \text{ m}^{-3}\text{)} = [(\text{Abs}_{\text{corr}}/\text{slope}) \times \text{Bot}_f] - \text{O}_{2r}$$

Where Abs_{corr} is the absorbance at 460 nm corrected for sensitivity drift of the instrument; O_{2r} is the amount of dissolved O_2 in the reagents which will co-precipitate in the $\text{MnO}(\text{OH})_2$ precipitate. Bot_f is the volume correction factor for bottles in a range of $\leq \pm 0.5 \text{ cm}^3$ and was calculated by:

$$\text{Bot}_f = [\text{Bot}_V + R_C] / [\text{Bot}_V - (R_A + R_B)]$$

Where Bot_V is the average bottle volume of the batch in cm^3 ; $R_{A,B,C}$ is the volume of the respective added reagents. The intercept and slope of the calibration line are calculated by a linear regression model. The final export file contains corrected concentrations, as well as the raw analog data for manual calculation.

ASSESSMENT

Sample collection and analysis—Initial tests of the method were performed in the laboratory. The performance of the setup at sea was tested during the BADE-2 cruise (September to October 2004), where we followed the dynamics of microbial respiration and prokaryotic production from the coastal upwelling into the subtropical North Atlantic gyre at $\sim 20^\circ\text{N}$ (Fig. 1.3).

Choice of wavelength—Because one of the most important aspects in oxygen determinations is the total iodine, Labasque et al. [13] suggested to measure the absorbance

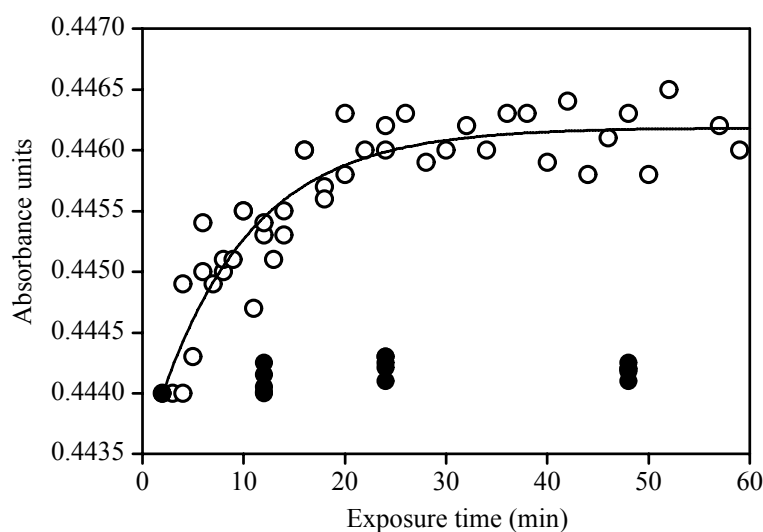


Figure 1.4: Photochemical effect of ambient light on absorbance over time (open circles; 3 experiments). The model is for illustration purposes and recalculated to oxygen concentrations it indicates an increase of $\sim 0.9 \text{ mmol O}_2 \text{ m}^{-3}$ within 30 min. Full circles indicate measurements in bottles covered with black plastic cylinders; 6 samples were measured at 0, 12, 24 and 48 min.

at the intersection point of absorbance of the I_2/I_3 couple at 466 nm. Due to limitations in the availability of fixed wavelength filters for the TRAACS system, we measure at $460 \pm 10 \text{ nm}$. While at 466 nm, oxygen concentrations of up to $900 \text{ mmol O}_2 \text{ m}^{-3}$ can be measured [13], the limit of linearity of the calibration at 460 nm is probably lower. However, most open ocean profiles show oxygen concentrations $< 320 \text{ mmol O}_2 \text{ m}^{-3}$ (eWOCCE Data5). Up to $320 \text{ mmol O}_2 \text{ m}^{-3}$, our calibration lines measured at 460 nm were always linear (data not shown). Additionally, on a moving ship the absorbance reading is more stable when a fixed wavelength filter is used rather than a movable mirror as in many general purpose spectrophotometers.

Volatilization of iodine—Volatilization of iodine is recognized as a potential problem in the Winkler method, especially when exposing the sample to air [4]. In closed systems and with the sampling probe inserted near the bottom of the bottle, vaporization of iodine is not detectable over short time periods [14]. However, the samples spend up to 60 min on the autosampler, therefore the bottles were covered immediately with Parafilm after sulfuric acid addition. While Parafilm itself is not completely gas tight, we found no systematic decrease in absorbance over a period of 60 min.

Photochemistry in fixed samples—After acidification with the sulfuric acid, the color of the samples darkens considerably due to ambient laboratory light. The influence of light on the analysis had not been emphasized before. In experiments ($n = 3$), the influence of light exposure of samples on the absorbance was measured at 2 min intervals for 60 min (Fig. 1.4). The maximum increase in absorbance over this 60 min period corresponded to an average increase of $\sim 0.9 \text{ mmol O}_2 \text{ m}^{-3}$ which would add a significant and variable error to the analysis. No increase in absorbance was detected in bottles held in the dark (Fig. 1.4). Although the reasons for this photochemical effect are not clear, traces of copper in the $\text{MnCl}_2 \cdot 4\text{H}_2\text{O}$ solution could be responsible for oxidation processes during light exposure (Van Bennekom unpublished). To prevent a light-induced increase in absorbance, we immediately covered the bottles with black

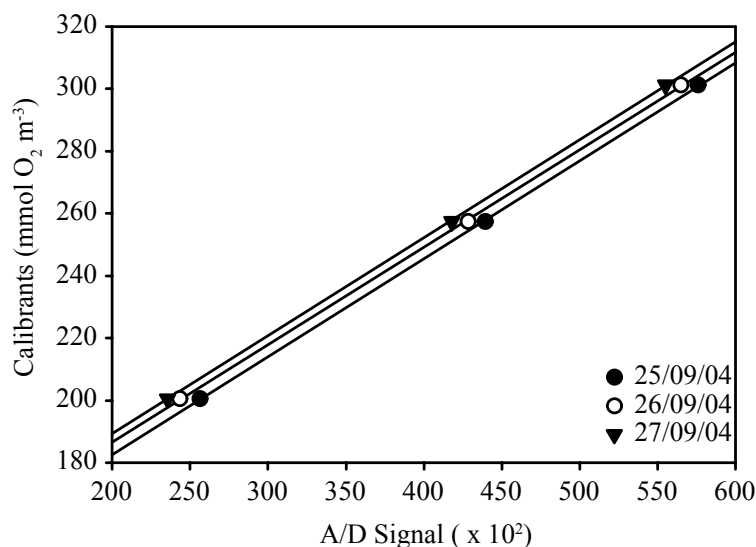


Figure 1.5: Example of measurements of calibration lines on 3 consecutive days using stored calibrants. The slopes of the 3 calibration lines are not significantly different. The calculations to test for differences among the slopes were done according to Zar [22]. X-axis shows the raw analog to digital output of the spectrophotometer (values $\times 10^2$).

plastic cylinders after acidification (see Fig. 1.1b).

Calibration—The continuous-flow system has to be calibrated with known concentrations of oxygen for each run. The preparation of calibrants requires particular care and is time consuming. If the calibration of oxygen sensors is the ultimate goal, a new set of calibration standards should be used for each run because the intercept slightly changes between runs, probably due to aging of the feed tubing. If differences in oxygen concentrations between samples are the main purpose of the measurement such as for the determination of respiration rates, the slope of the calibration line is important. We tested whether the standards of a calibration line can be stored and used for several days. The slopes of the calibration lines determined with standards stored for up to 3 d were not significantly different from each other ($F_{3,4} p = 0.757$; Fig. 1.5).

Accuracy and Precision—Certified reference material for oxygen measurements is not available, which would be important to intercalibrate the various oxygen methods applied in the different laboratories. Thus, we aimed at testing the accuracy of our method on O_2 -saturated samples in the laboratory. Seawater (20 L) was irradiated with UVB to inhibit biological oxygen production or consumption. Subsequently the seawater was kept in the dark at 20°C and saturated with oxygen via an aerator and stirring for 2 d. The aerator was turned off 1 h prior to sampling to prevent over-saturation of the water. Finally, 8 BOD bottles with known volume were filled according to the recommendations and measured according to the procedure described above. The theoretical oxygen concentration in saturated seawater was calculated taking the water temperature, salinity and air pressure into account [19]. The accuracy of our measurements was $99.7 \pm 0.2\%$ ($n = 40$; 4 experiments).

The precision of our method and the instrument was tested at sea, which is the main application site of our system. For calibrating oxygen sensors, WOCE demanded a precision of the Winkler method of $<0.2\%$ [6]. However, for respiration measurements the precision

Table 1.1: Precision of triplicate measurements during a cruise in the subtropical Atlantic over a range of oxygen concentrations. Average oxygen concentrations measured (O_2); range in oxygen concentrations from which relative standard deviations were calculated (O_2 range); average standard deviation of triplicate measurements (ASD); relative standard deviation ($RSD = SD/mean \times 100$); confidence interval (CI). Saturated samples (SAT) and samples directly tapped from the CTD.

	O_2	O_2 range	ASD	CI		RSD	CI	
	(mmol m^{-3})	(mmol m^{-3})	(mmol m^{-3})	-95%	+95%	%	-95%	+95%
SAT	213.62	186.55-232.93	0.08	0.06	0.09	0.04	0.03	0.06
($n = 78$)	(8.21)		(0.06)			(0.03)		
CTD	200.13	120.23-229.79	0.10	0.08	0.12	0.05	0.04	0.06
($n = 66$)	(24.44)		(0.08)			(0.04)		

*top numbers are averages of the water masses; number in parenthesis are standard deviations of the mean.

should be better. The precision of triplicate seawater samples used as t_0 for bacterial respiration measurements was on average 0.04% ($n = 78$; Table 1.1) including errors due to preparation and handling of the samples. The precision of triplicate samples tapped directly from the CTD was slightly lower and 0.05% ($n = 66$; Table 1.1).

Field study of microbial production and respiration—We measured community respiration (CR) in unfiltered seawater and bacterial respiration (BR) in 0.8- μm filtered seawater (assuming that respiration in the 0.8- μm filtered fraction is dominated by bacteria) collected in the euphotic layer along a transect from the Mauritanian upwelling into the subtropical North Atlantic gyre. Samples for nutrients, DOC, primary and bacterial production were taken as well but will be presented elsewhere. For the respiration measurements, we incubated triplicate BOD bottles in a water bath in the dark at in situ temperature ($\pm 1^\circ\text{C}$). T_0 bottles were fixed immediately with the Winkler reagents and t_1 bottles were fixed after an incubation time of 12 to 24 h depending on the expected microbial activity. CR and BR decreased significantly with depth down to ~120 m ($r^2 = 0.72$, $p < 0.0001$, $n = 61$ for CR and $r^2 = 0.52$, $p < 0.0001$, $n = 62$ for BR; Fig. 1.6). Both, CR and BR were in the range of reported respiration rates for upwelling and oligotrophic systems [7, 10, 16].

Most of the variability in respiration between the upwelling stations and the oligotrophic gyre waters were found in the top 40 m. Thus, for the illustration of the method only the near surface layer was analyzed to assess lateral trends. Both CR and BR significantly decreased by $\sim 86 \pm 56\%$ ($3.26\text{--}0.46 \text{ mmol } O_2 \text{ m}^{-3} \text{ d}^{-1}$) and $\sim 84 \pm 41\%$ ($1.22 \text{ to } 0.20 \text{ mmol } O_2 \text{ m}^{-3} \text{ d}^{-1}$) respectively, from the upwelling area to the oligotrophic gyre (Fig. 1.7). BR explained ~61% of the variability in CR (Fig. 1.8). This suggests that BR comprises a major fraction of CR over a broad trophic spectrum. The contribution of BR to CR increases from the upwelling region towards the gyre with lowest values in the upwelling area ($36 \pm 12\%$) and the highest contribution in the oligotrophic gyre reaching $76 \pm 24\%$ (Fig. 1.9). Average BR as percentage of CR over the full transect was $\sim 55 \pm 19\%$ which is in general agreement with the few studies available for open ocean systems [16]. However, as indicated by our data, bacterial respiration might not always be the dominant fraction of oceanic community respiration.

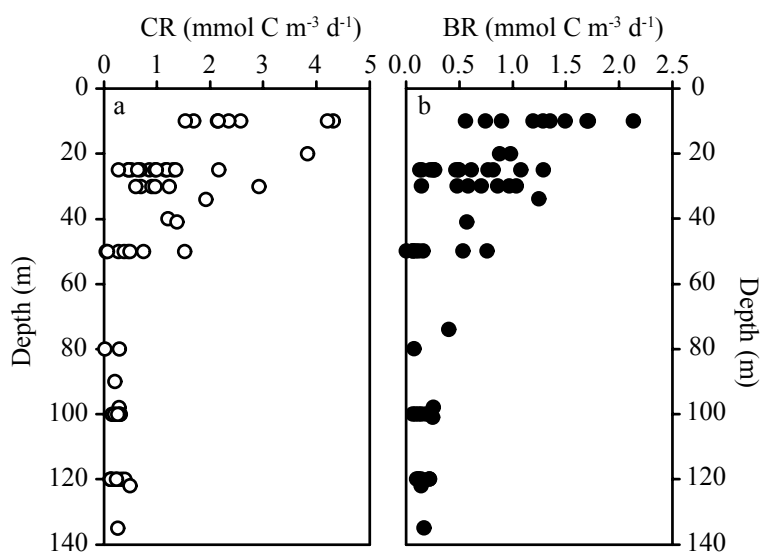


Figure 1.6: Depth profiles of (a) total community respiration (CR; mmol O₂ m⁻³ d⁻¹) measured on unfiltered and (b) bacterial respiration (BR; mmol O₂ m⁻³ d⁻¹) measured on 0.8- μ m filtered seawater.

DISCUSSION

Recently, respiration was proposed to be a better estimator for system productivity than primary production [8]. Thus, mapping of respiration in open oceans is similarly important as primary production measurements. For large parts of the ocean, data on respiration do not exist and the lack of spatial resolution makes it impossible to draw firm conclusions on systems' remineralization rates on a global scale. One reason why there are orders of magnitude more estimates on organic matter production (i.e., primary production) than on remineralization is probably that the Winkler titration to measure oxygen consumption is considered tedious and labor intensive. Our main motivation was therefore, to develop a continuous-flow analysis setup to increase the number of oxygen determinations at high precision.

An alternative method allowing high precision oxygen determinations is membrane inlet mass spectrometry (MIMS). With the transportable MIMS, it is possible to measure a variety of oceanic trace gases with high sample throughput [12, 18]. As the determination of oxygen with MIMS is flow-rate dependent, the ratio between oxygen and argon is used. Consequently, measurements of absolute oxygen concentrations are as of yet difficult to measure with high precision.

Recently, a method for measuring respiration with oxygen microprobes was presented [1]. The method apparently performs quite well in the laboratory, however, the frailty and sensitivity of the probes against movement precludes their use on ships. Uncertainty in the linearity of oxygen consumption over time represents a potential problem in endpoint measurements and can be detected in the continuous recording of the oxygen concentration with microprobes [1]. However, with a precision of 0.5%, the oxygen microprobes are not sufficiently sensitive to measure microbial respiration in open ocean systems.

The spectrophotometric oxygen analysis is straightforward and the rugged instrumentation is easy to repair on board. Depending on the spectrophotometer, a reading is recorded when the absorbance is stable as judged by the analyst, or alternatively, at a preset time point the

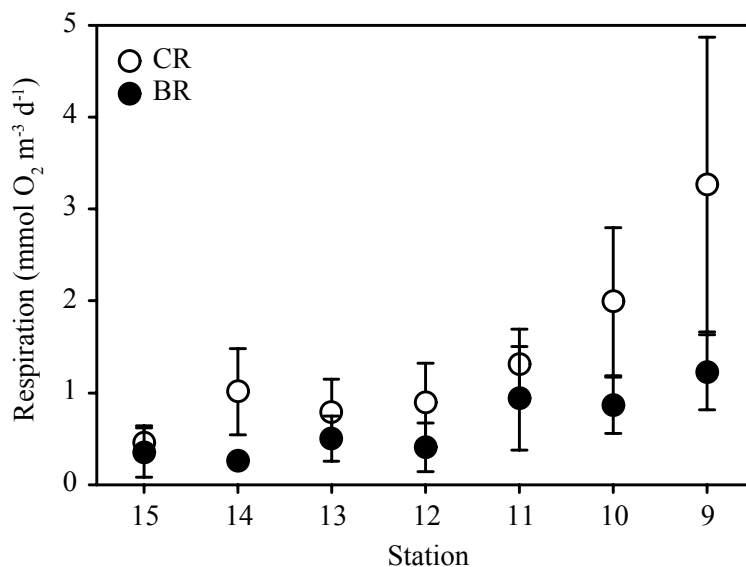


Figure 1.7: Lateral trend in total community respiration (CR; $\text{mmol O}_2 \text{ m}^{-3} \text{ d}^{-1}$) and bacterial respiration (BR; $\text{mmol O}_2 \text{ m}^{-3} \text{ d}^{-1}$) from the Mauritanian upwelling (Station 9) towards the subtropical North Atlantic gyre (Station 13 to 15; see Fig. 1.3). Data points are averages of the respiration measurements over a depth range of 10–40 m ($n = 5$ per station); error bars show standard deviations.

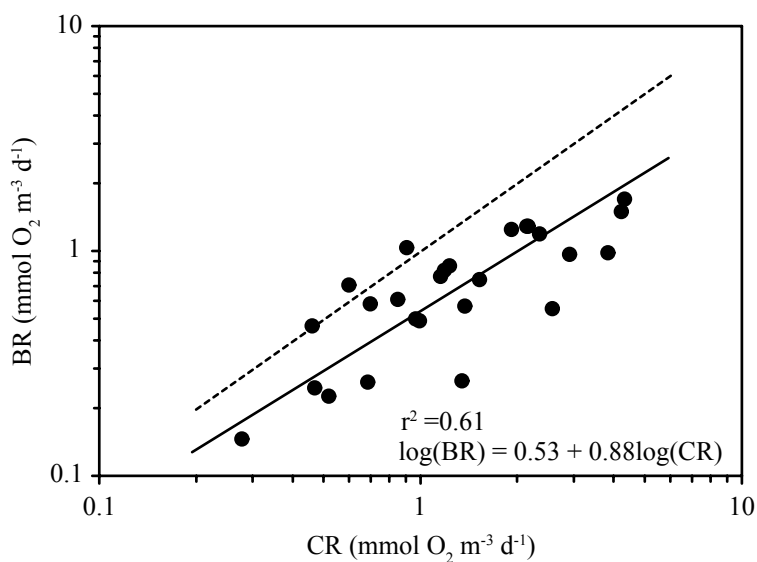


Figure 1.8: Relationship between total community respiration (CR; $\text{mmol O}_2 \text{ m}^{-3} \text{ d}^{-1}$) and bacterial respiration (BR; $\text{mmol O}_2 \text{ m}^{-3} \text{ d}^{-1}$). The full line represents a reduced major axis (RMA) regression; dotted line indicates 1:1 relation.

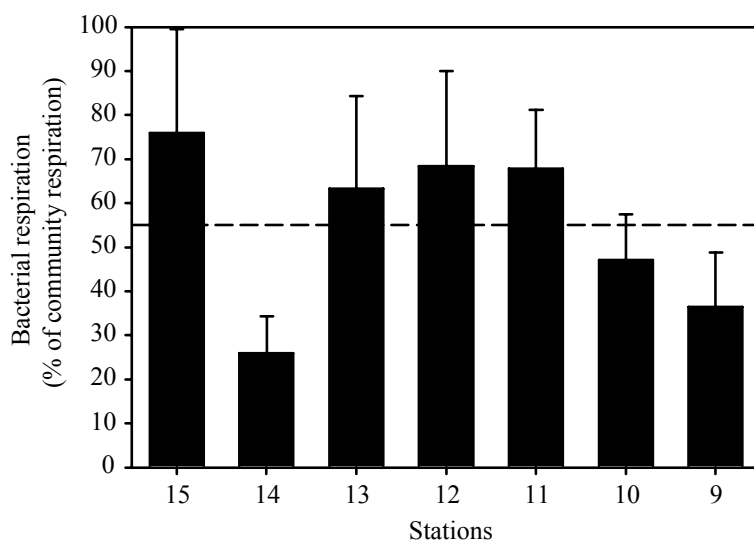


Figure 1.9: Bacterial respiration (BR) expressed as percentage of total community respiration (CR) at the different stations from the Mauritanian upwelling to the subtropical North Atlantic gyre. Error bars show standard errors ($n = 5$); the dotted line indicates the grand average over all the stations.

instrument averages over a certain time. Nevertheless, several readings per sample should be taken. The continuous flow analysis allows for more control on the actually recorded concentration. The data are saved automatically and can be exported in various ways, either as raw data for manual calculations or as drift and baseline corrected concentrations calculated from the calibration line in either ASCII or Excel format. Furthermore, optical control of the peak chart helps to quickly identify outliers. The measurement is fast (~ 2 min per sample) and only a minimum of supervision is necessary.

So far, the precision may have distracted scientists from using the spectrophotometric approach. Labasque et al. [13] and Pai et al. [14] report a shipboard precision of $\sim 0.12\%$ while the overall precision of the data reported here is 0.04% . We suggest that this improved precision is a result of the automation of the measurement and the correction possibilities for the gain and baseline drift of the instrument.

COMMENTS AND RECOMMENDATIONS

During experiments in the subtropical Atlantic, we experienced only moderate sea state. A problem with spectrophotometers on board ships is the instable filament in the tungsten lamp. When measuring during rough sea state, the readings can be considerably biased. To avoid this problem, installation of a light emitting diode eliminates this source of erroneous measurements. The tubing and the cuvette diameter are small and potentially can get clogged by particles in the sample. Therefore, it is necessary to flush the system with a cleaning solution (2% Hellmanex, Hellma Germany) and Milli-Q water after each run. The manganese hydroxide which forms on the dispenser tip of the bottle containing the NaOH/KI reagent contaminates the blanks. For cleaning, we recommend using a dilute solution of sulfuric acid with a few mL of NaOH/KI.

Although we used a TRAACS system, in principle any spectrophotometer with appropriate software for peak detection can be used. Oxygen measurements as proposed here with a

continuous-flow analyzing system in conjunction with an autosampler should be a useful tool for open ocean expeditions where high sample throughput and high quality data are essential.

Acknowledgments

The Dept. Marine Technology (MT) of the NIOZ and particularly Herman Boekel is gratefully acknowledged for constructing the autosampler. Thanks to the technicians of the electronics group of MT for designing the electronic configuration and Dirk J. Buijsman for software programming of the autosampler. Financial support was provided by NIOZ-MRF and the Dutch Science Foundation (NWO-ALW), project 811.33.004 to G.J.H.

Bibliography

- [1] Briand E, Pringault O, Jacquet S, Torreton J-P. 2004. The use of oxygen microprobes to measure bacterial respiration for determining bacterioplankton growth efficiency. *Limnology and Oceanography: Methods* 2: 406-16
- [2] Broenkow WW, Cline JD. 1969. Colorimetric determinations of dissolved oxygen at low concentrations. *Limnology and Oceanography* 14: 450-4
- [3] Bryan JR, Riley JP, Williams PJIB. 1976. A Winkler procedure for making precise measurements of oxygen concentration for productivity and related studies. *Journal of Experimental Marine Biology and Ecology* 21: 191-7
- [4] Carritt DE, Carpenter JH. 1966. Comparison and evaluation of currently employed modifications of Winkler method for determining dissolved oxygen in seawater - a NASCO Report. *Journal of Marine Research* 24: 287-318
- [5] Committee Wdp. 2002. *WOCE global data*, WOCE international project office, Southampton UK
- [6] Culberson CH. 1991. *Dissolved oxygen. Rep. WHP 91-1*, Woods Hole, Massachusetts, USA
- [7] Del Giorgio PA, Cole JJ. 2000. Bacterial energetics and growth efficiency. In *Microbial Ecology of the Oceans*, ed. DL Kirchman, pp. 289-325. New York: Wiley-Liss
- [8] Del Giorgio PA, Williams PJIB. 2005. The global significance of respiration in aquatic ecosystems: from single cells to the biosphere. In *Respiration in aquatic ecosystems*, ed. PA Del Giorgio, PJIB Williams, pp. 267-303. New York: Oxford University Press
- [9] Furuya K, Harada K. 1995. An automated precise Winkler titration for determining dissolved oxygen on board ship. *Journal of Oceanography* 51: 375-83
- [10] Gonzalez N, Anadon R, Viesca L. 2003. Carbon flux through the microbial community in a temperate sea during summer: role of bacterial metabolism. *Aquatic Microbial Ecology* 33: 117-26

- [11] Johnson KM, Wills KD, Butler DB, Johnson WK, Wong CS. 1993. Coulometric total carbon dioxide analysis for marine studies: maximizing the performance of an automated gas extraction system and coulometric detector. *Marine Chemistry* 44: 167-87
- [12] Kana TM, Darkangelo C, Hunt MD, Oldham JB, Bennett GE, Cornwell JC. 1994. Membrane inlet mass spectrometer for rapid high precision determination of N₂, O₂, and Ar in environmental water samples. *Analytical Chemistry* 66: 4166-70
- [13] Labasque T, Chaumery C, Aminot A, Kergoat G. 2004. Spectrophotometric Winkler determination of dissolved oxygen: re-examination of critical factors and reliability. *Marine Chemistry* 88: 53-60
- [14] Pai S-C, Gong G-C, Liu K-K. 1993. Determination of dissolved oxygen in seawater by direct spectrophotometry of total Iodine. *Marine Chemistry* 41: 343-51
- [15] Robinson C, Williams PJIB. 1999. Plankton net community production and dark respiration in the Arabian Sea during September 1994. *Deep-Sea Research Part II* 46: 745-65
- [16] Robinson C, Williams PJIB. 2005. Respiration and its measurement in surface marine waters. In *Respiration in aquatic ecosystems*, ed. PA Del Giorgio, PJIB Williams, pp. 147-80. New York: Oxford University Press
- [17] Roland F, Caraco NF, Cole JJ, Del Giorgio PA. 1999. Rapid and precise determination of dissolved oxygen by spectrophotometry: evaluation of interference from color and turbidity. *Limnology and Oceanography* 44: 1148-54
- [18] Tortell PD. 2005. Dissolved gas measurements in oceanic waters made by membrane inlet mass spectrometry. *Limnology and Oceanography: Methods* 3: 24-37
- [19] UNESCO. 1973. International oceanographic tables. pp. 195. Paris: NIO-UNESCO
- [20] Williams PJIB, Jenkinson NW. 1982. A transportable microprocessor-controlled precise Winkler titration suitable for field and shipboard use. *Limnology and Oceanography* 27: 576-84
- [21] Winkler LW. 1888. Die Bestimmung des im Wasser gelösten Sauerstoffes. *Chemische Berichte* 27: 2843-55
- [22] Zar JH. 1999. *Biostatistical analysis*. Upper Saddle River, NJ: Prentice-Hall. 931 pp.

Chapter 2

Bacterial production and respiration in the sea-surface microlayer of the open Atlantic ocean¹

Thomas Reinthaler and Gerhard J. Herndl

Bacterial production and bacterial respiration was measured along with DOC, inorganic nutrients and dissolved amino acids in the sea-surface microlayer (SML) and the underlying water (ULW) of the subtropical Atlantic gyre (SATL) and the and western Mediterranean Sea (WMED). DON, DOP and amino acids were significantly enriched in the SML as compared to the ULW, however, bacterial production was consistently low ranging from 0.001–0.05 $\mu\text{mol C L}^{-1} \text{d}^{-1}$ in the SATL and $\sim 0.07 \pm 0.07 \mu\text{mol C L}^{-1} \text{d}^{-1}$ in the WMED. In contrast, bacterial respiration was high, with rates between 3.6 and 9.5 $\mu\text{mol O}_2 \text{ L}^{-1} \text{d}^{-1}$ in both study areas, resulting in extremely low bacterial growth efficiencies (BGEs) of 0.2–1.7% in the SML. In the ULW, bacterial production and respiration were in the range typical for surface waters at both open ocean sites, however, BGE was highly variable ($13.8 \pm 14.6\%$ in the SATL and $8.6 \pm 10.1\%$ in the WMED). The low bacterial production and the low BGE coincided with high contributions of dissolved free amino acids (DFAA) to the total amino acid pool in the SML indicating accumulation of DFAA due to retarded DFAA availability or bacterial uptake.

Introduction

The sea-surface microlayer (SML) is the boundary layer between the atmosphere and the oceans, covering $\sim 70\%$ of the earth's surface. Although the average thickness of the SML is only about 10–250 μm [11], this interface is important in mediating the exchange of gases and organic and inorganic matter between the atmosphere and the bulk surface waters [30].

It is well-established that the SML is a unique environment with considerable variability in both its chemical and biological characteristics compared to those of the underlying waters

¹Submitted to *Limnol. and Oceanogr.*

(ULW). Dissolved compounds such as nutrients, dissolved organic carbon (DOC) and amino acids are often enriched in the SML, especially in the visible slicks of near-shore environments [41]. The enrichment of these compounds in the SML has been attributed to surface active matter collected by rising gas bubbles in the upper water column [21] or by Longmuir circulations in the open ocean [17]. With increasing distance from the coast, atmospheric deposition of matter might become increasingly important for the development of a SML [42].

Despite the long-lasting interest in the physico-chemical properties of the SML, studies on microbial metabolism in the SML are still scarce. For microbes, the SML might be a stressful environment. The SML receives intense solar irradiation, especially in the low wavelength range of UVB (300-320 nm) which is detrimental to DNA containing organisms [35]. Nevertheless, distinct neustonic communities and higher activity of the neuston than in the plankton community below the SML have been reported for coastal systems [1, 8, 13]. The main function of heterotrophic bacteria in all aquatic environments is the production of biomass and the remineralization of DOC to CO₂ [10]. The bacterial growth efficiency (BGE) relates biomass production to the bacterial uptake of DOC. Thus, the BGE serves as an indicator whether bacteria are more acting as a 'link' or 'sink' for DOC. Enhanced respiration rates in the SML for a variety of environments have been measured, albeit indirectly, with either radiolabeled organic model compounds or via electron transport system estimates [31, 38].

The only study directly measuring oxygen consumption of the total microbial community in the SML at a coastal site also found high rates of carbon remineralization [33]. However, measurements on respiration rates of open ocean SML prokaryotic communities are not available, although the global extension of the SML likely makes it an important site of CO₂ production in direct exchange with the atmosphere. In a gradient from high productive to low productive North Atlantic waters, a strongly negative relationship between planktonic net community production and CO₂ fluxes in the top 2 cm layer has been found recently, thus suggesting an important biological component controlling the exchange of CO₂ across the air-sea interface [7]. In this study, we aimed at determining the variability of the SML and selected biological and chemical parameters along trophic gradients and elucidating the dynamics in these parameters in the open ocean SML. The ultimate goal was to test the hypothesis that the bacterial SML community and its activity is largely independent from the bacterial activity in the adjacent ULW and largely governed by the prevailing atmospheric conditions such as solar radiation and wind stress. To address this hypothesis, we measured at two open ocean sites, bacterial production and respiration together with an extensive set of physico-chemical parameters. We studied a gradient from a highly productive system to an oligotrophic environment, following a transect from the Mauritanian upwelling into the subtropical North Atlantic gyre. The other sampling site was located in the Algerian basin of the western Mediterranean Sea, where we followed the biological dynamics in a stable eddy system. We found that potentially labile substrates for bacterial growth such as amino acids were accumulating in the SML, while bacterial production was low. In contrast to bacterial production, bacterial respiration was significantly enhanced compared to the underlying bulk water resulting in consistently low BGE in the SML.

Methods

Study sites and sampling—Samples of the surface microlayer (SML) and the underlying water (ULW) were collected at two open ocean sites. In the eastern subtropical North Atlantic

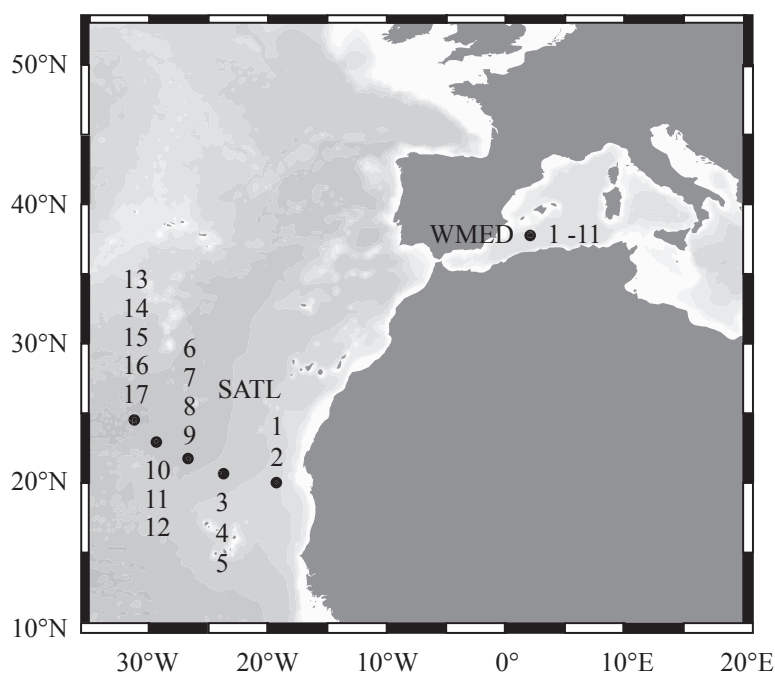


Figure 2.1: Map of the study area in the subtropical Atlantic (SATL) and in the western Mediterranean Sea (WMED). In the SATL, a transect from the highly productive Mauritanian upwelling area into the oligotrophic gyre was followed. In the WMED, a stable eddy system was sampled over a two weeks period. Dots and numbers indicate the individual stations occupied.

(SATL), we followed a transect from the productive Mauritanian upwelling region ($20^{\circ}25'N$, $18^{\circ}10'W$) into the oligotrophic gyre ($24^{\circ}39'N$, $31^{\circ}10'W$; Fig. 2.1) during Sep–Oct 04. In the Algerian basin of the western Mediterranean Sea (WMED), we followed a stable eddy system (at $37^{\circ}50'N$ and $2^{\circ}05'E$) for a period of three weeks in Sep–Oct 03 (Fig. 2.1). To track the anticyclonic eddy, a drifting buoy was deployed near the center of the eddy and sampling took place within 500 m of the buoy. The positions of the individual sampling stations and the time of sampling are given in Table 2.1.

Samples of the SML and the ULW (~ 30 cm depth) were taken from a drifting inflatable boat upwind the mother ship. If the weather permitted, sampling was conducted in the morning, at noon and in the late afternoon. SML samples were taken with a glass plate sampler. The dimension of the glass plate was $500 \times 250 \times 4$ mm. The glass plate was introduced vertically into the water and gently withdrawn [18]. To remove excess water, the plate was allowed to drain for a few seconds before the plate was inserted into a slot with a teflon wiper on each side. The wiper blades scrapped off the SML and the sample was collected in a 1.5 L glass bottle. Per dip, 5–10 mL of SML was collected. Thus, the thickness of the collected SML was between 40–80 μm (volume of the sample/area of the sampler). This estimated SML thickness is in the range of reported values for glass plate samplers [18].

The ULW was sampled with a glass bottle filled at 30 cm depth. All the glassware including the glass plate and teflon wipers were kept in an acid bath (0.1 N HCl) until sampling. All the sampling gear was vigorously rinsed with sampling water prior to sampling. With two glass plate samplers used concurrently ~ 3 L of SML were sampled within 1.5 h. Back on board of the ship, the sample was split for the different parameters and either preserved for later analyses

Table 2.1: Overview on the sampling positions, dates and time of visited stations (STN) in the subtropical Atlantic (SATL) and the western Mediterranean (WMED).

STN	SATL				WMED			
	Date	Time (Local)	Lat (°N)	Lon (°E)	Date	Time (Local)	Lat (°N)	Lon (°E)
1	09/25/04	07:45	20.03	-19.27	09/29/03	10:00	37.74	2.02
2	09/25/04	13:15	20.03	-19.27	09/29/03	15:00	37.76	2.02
3	09/29/04	08:30	20.69	-24.06	09/29/03	19:00	37.76	2.01
4	09/29/04	13:15	20.69	-24.06	09/30/03	10:00	37.77	1.98
5	09/29/04	17:00	20.69	-24.06	09/30/03	16:00	37.80	1.97
6	10/02/04	13:15	21.77	-26.71	09/30/03	20:00	37.81	1.95
7	10/02/04	17:00	21.77	-26.71	10/04/03	10:00	37.87	2.15
8	10/03/04	08:00	21.76	-26.64	10/04/03	15:30	37.87	2.15
9	10/03/04	13:15	21.71	-26.65	10/05/03	10:30	37.78	2.20
10	10/05/04	08:00	23.00	-29.39	10/05/03	15:30	37.75	2.20
11	10/05/04	13:15	22.97	-29.43	10/05/03	19:00	37.72	2.18
12	10/05/04	17:00	22.99	-29.44				
13	10/07/04	07:45	24.60	-31.24				
14	10/07/04	13:15	24.58	-31.24				
15	10/07/04	17:00	24.57	-31.23				
16	10/08/04	07:45	24.49	-31.25				
17	10/08/04	10:30	24.47	-31.26				

or analyzed immediately as described below.

Dissolved organic carbon (DOC)— Samples for DOC were filtered through rinsed 0.2- μm polycarbonate filters and sealed in pre-combusted (450°C for 4 h) glass ampoules after adding 50 μL of 40 % phosphoric acid. Subsequently, the samples were stored frozen at -20°C . DOC concentrations were determined back in the lab by the high temperature combustion method using a Shimadzu TOC-5000 analyzer [5]. Standards were prepared with potassium hydrogen phthalate (Nacalai Tesque, Inc. Kyoto, Japan). Ultrapure Milli-Q blanks were run before and after the sample analyses. The Milli-Q blank was on average $16.3 \pm 6.8 \mu\text{mol C L}^{-1}$. Per sample, the mean concentration of triplicate injections was calculated. The average analytical precision of the instrument was $< 3\%$.

Dissolved organic nitrogen (DON) and dissolved organic phosphorus (DOP)—Total dissolved nitrogen (TDN) and total dissolved phosphorus (TDP) were analyzed with a TRAACS 800 continuous-flow analysis system following the persulfate oxidation method [39]. DON concentrations were calculated by subtracting the sum of the inorganic nitrogen species from TDN concentrations. Similarly, DOP concentrations were calculated by subtracting PO_4^{3-} from TDP. The recovery of DON and DOP was estimated by measuring a mixture of 10 different organic compounds containing known concentrations of N and P. To increase the recovery of DOP, samples were kept under pressure at 110°C for 90 min instead of 45 min. The recovery efficiency for these model compounds was 97% for both DON and DOP.

Inorganic nutrients—The methods for nutrient measurements principally followed JGOFS recommendations (JGOFS protocols 1994). The concentrations of dissolved inorganic nutrients (NH_4^+ , NO_3^- , NO_2^- , PO_4^{3-}) were determined immediately after collecting the samples and gentle filtration through 0.2- μm filters (Acrodisc, Gelman Science) with a TRAACS

autoanalyzer system. NH_4^+ was detected with the indo-phenolblue method (pH 10.5) at 630 nm [20]. NO_2^- was detected after diazotation with sulfanilamide and *N*-(1-naphtyl)-ethylene diammonium-dichloride as the reddish-purple dye complex at 540 nm. NO_3^- was reduced in a copper cadmium coil to nitrite (with imidazole as a buffer) and then measured as nitrite. Inorganic PO_4^{3-} was determined via the molybdenum blue complex at 880 nm.

Amino acid analysis—Up to 20 mL of sample was filtered through pre-rinsed 0.2- μm polycarbonate filters (Millipore GTTP, 25 mm). Subsequently, 8 mL of the filtrate was transferred into a combusted glass ampoule, sealed and stored at -20°C until analyses. The filtration unit and filters were rinsed with 20 mL of 0.1N HCl and Milli-Q water prior to filtration. Concentrations of total dissolved hydrolyzable amino acids (THAA) and dissolved free amino acids (DFAA) were measured by high-performance liquid chromatography, separating fluorescent *o*-phthaldialdehyde (OPA) derivatives [29]. For chiral separation *n*-isobutryl-L-cysteine (IBLC) was used as thiol group [12]. Analyses were performed on a temperature controlled Dionex HPLC system, equipped with a guard column (Security Guard, Phenomenex) and a following stationary phase column (Syngeri 4 μ MAX-RP 80A, Phenomenex). Amino acids were separated with a gradient of sodium acetate (25 mmol L^{-1} , pH 6.0; Solvent A) and methanol (Lichrosolv, Merck, HPLC grade, Solvent B), starting with 96% A to 40% A at 75 min, then 0% A at 80 min until 90 min. At 95 min the system was returned to 96% A and equilibrated for 5 min. Fluorescence was quantified at 330 nm excitation and 445 nm emission wavelength with a RF-2000 fluorescence detector.

For sample hydrolysis, 500 μL of 12 mol L^{-1} HCl was added to 500 μL of sample in a 2 mL glass vial. Then, 10 μL of ascorbic acid (0.1 mmol L^{-1} final concentration) was added and the mixture was flushed for 10 min with nitrogen, sealed and heated to 110°C for 20 h. Subsequently, the samples were dried under nitrogen gas (grade 5) and 500 μL borate buffer (0.5 mol L^{-1} , pH 10.4) was added to the resulting pellet. The sample was sonicated until the pellet was in a fine suspension and after centrifugation for 1 min at 4000 g, 250 μL of the supernatant were transferred to a glass insert.

The OPA/IBLC reagent was prepared by dissolving 20 mg of OPA and 48 mg of IBLC in 1.25 mL methanol and 8.75 mL borate buffer (1 mol L^{-1} ; pH 10.4). Aliquots of the reagent were stored at -20°C in amber glass vials until use. Derivatization took place in the autosampler of the HPLC system, where 30 μL of the OPA/IBLC reagent were added to 100 μL of sample and mixed automatically. Finally, 100 μL of sample was injected into the HPLC system and measured as described above. Dissolved combined amino acids (DCAA) were calculated as the difference between THAA and DFAA. Depending on the method used, a variable fraction of amino acids might isomerize during acid hydrolysis, thus resulting in quantification errors of L- and D-enantiomers. However, the liquid-phase hydrolysis we employed did not result in significant racemization of free amino acids as revealed by previous tests and shown also elsewhere [24].

Bacterial abundance—One mL samples of unfiltered and 0.8- μm filtered seawater were fixed with paraformaldehyde (1% final conc.) for 10 min. Subsequently, the samples were stained with SYTO Green (Molecular Probes; 5 $\mu\text{mol L}^{-1}$ final conc.) at room temperature in the dark for 10 min. Analyses were done on a FACSCalibur flow cytometer (BD Biosciences). Counts were performed with the argon laser at 488 nm set at an energy output of 15 mW. Prokaryotic cells were enumerated according to their right-angle light scatter and green fluorescence measured at 530 nm. To calibrate the system, a known concentration of beads was counted with the flow cytometer and cross-checked with epifluorescence microscopy.

Bacterial production—Bacterial production in unfiltered and 0.8- μm filtered seawater was measured by [^3H]-leucine incorporation (specific activity: 157 Ci mmol^{-1} for the WMED and 160 Ci mmol^{-1} for the SATL; final concentration 10 nmol L^{-1}). Usually, a 1:1 mixture of hot to cold leucine was added. Two 5 mL samples and 1 blank were incubated in the dark. The blank was fixed immediately with concentrated 0.2- μm filtered formaldehyde (4% final conc., v/v) 10 min prior to adding the tracer. After incubating the samples and the blank at in situ temperature for 0.5–1.5 h, depending on the expected activity, the samples were fixed with formaldehyde (4% final conc.), filtered onto 0.2- μm polycarbonate filters (Millipore GTTP; 25 mm diameter) supported by a Millipore HAWP cellulose nitrate filter and rinsed twice with 10 mL ice-cold 5% trichloroacetic acid (Sigma Chemicals) for 5 min. Tests showed that polycarbonate filters were superior over the commonly used cellulose nitrate and cellulose acetate filters as polycarbonate filters adsorb significantly less leucine resulting in lower blanks and less variability among replicate samples. The polycarbonate filters were placed in scintillation vials and stored at -20°C in the dark until the radioactivity of the filters was determined in the lab. One mL of ethylacetate was added and after 10 min, 8 mL of scintillation cocktail (Insta-Gel Plus, Canberra Packard). The radioactivity incorporated into cells was counted in a liquid scintillation counter (LKB Wallac, Model 1212). Leucine incorporated into bacterial biomass was converted to carbon production using the theoretical conversion factor of 1.5 kg C mol^{-1} Leu assuming no isotope dilution [25].

Bacterial respiration—The 0.8- μm filtrate was collected in a glass flask and subsequently transferred to calibrated borosilicate glass BOD-bottles with a nominal volume of 120 cm^{-3} using silicon tubing fixed to the spigot of the glass flask. For the determination of the initial O_2 concentration (t_0), samples were fixed immediately with Winkler reagents and incubated together with the live samples in water baths in the dark at in situ temperature ($\pm 1^\circ\text{C}$) for 12 to 24 h when the incubations were terminated (t_1). Whenever possible, quadruplicate bottles were used for the determination of the initial and final O_2 concentration. All the glassware was washed with 10% HCl and thoroughly rinsed with Milli-Q water prior to use. Oxygen concentrations of the t_0 and t_1 bottles were measured spectrophotometrically in a single run following the standard protocol for the determination of oxygen by Winkler titration [9]. Measurements were done in a temperature-controlled laboratory container (set at 20°C) on a Technicon TRAACS 800 continuous-flow analysis system, connected to a custom-made autosampler as described in Reinthaler et al. [36]. The amount of total iodine was determined at a wavelength of 460 nm. The spectrophotometer was calibrated using standard additions of potassium iodate (J.T. Baker ACS grade KIO_3) to BOD bottles filled with seawater and adding Winkler chemicals in reverse order. The coefficient of variation between triplicate samples was on average 0.04% at 214 $\mu\text{mol O}_2 \text{ L}^{-1}$. The final oxygen consumption rates were converted to carbon units using a respiratory quotient of 1.

Calculations and statistics—The enrichment factor was calculated by dividing concentrations or rates determined for the SML by those for the ULW ($\text{EF} = \text{SML}/\text{ULW}$). Statistical analysis was done with the software package STATISTICA from Statsoft.

Results

Physical properties—Along the transect in the subtropical Atlantic (SATL), salinity increased towards the oligotrophic gyre from 36.1 to 37.7 (Fig. 2.2a) and the surface water temperature increased from 25.8–27.3 $^\circ\text{C}$ (Fig. 2.2b). The wind speed measured around sampling time was

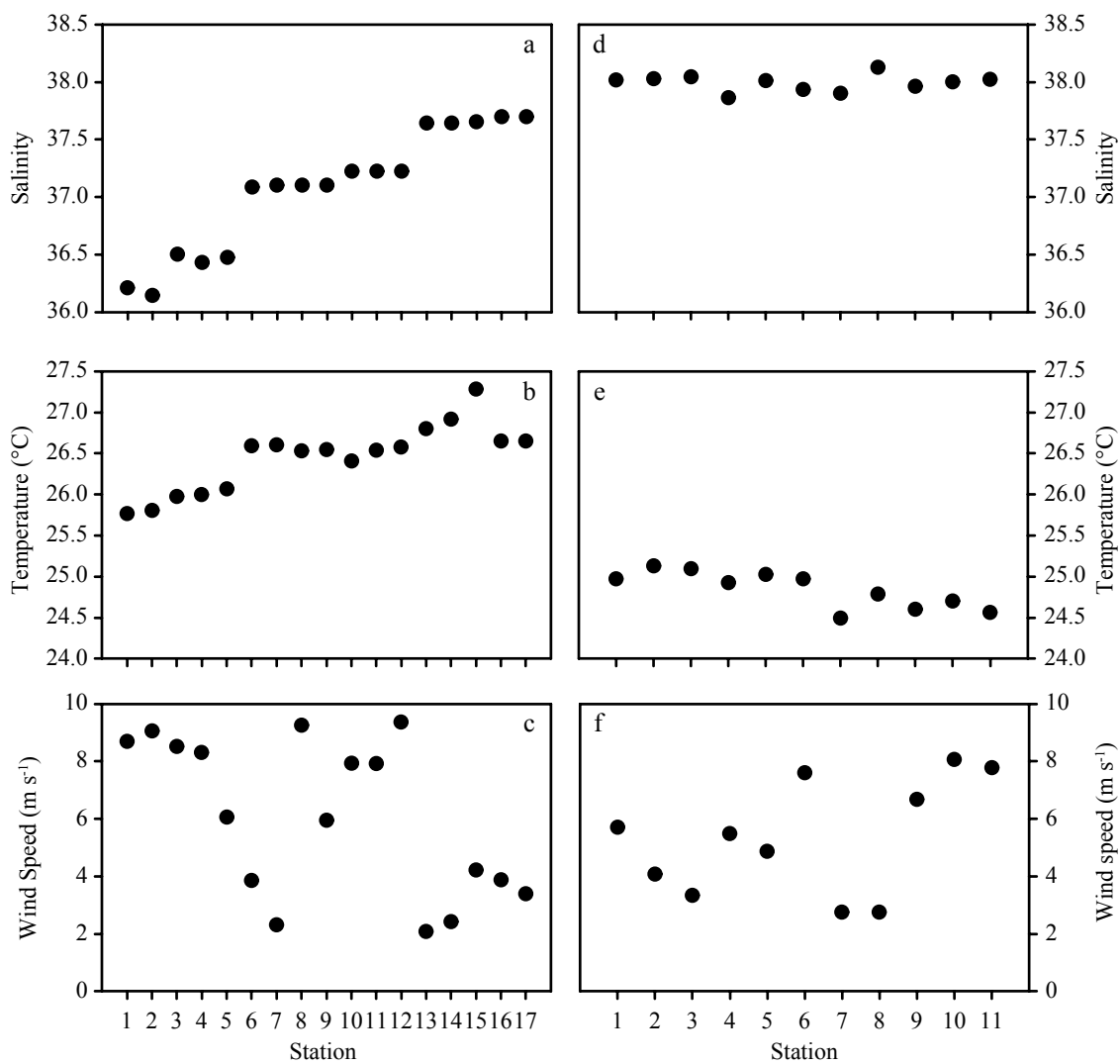


Figure 2.2: Salinity, temperature ($^{\circ}\text{C}$) and wind speed (m s^{-1}) at the different stations in the subtropical Atlantic (a-c) and the western Mediterranean (d-f).

variable ranging from 2–9 m s⁻¹ (Fig. 2.2c). In the western Mediterranean Sea (WMED), salinity was uniform with 38.0 ± 0.1 (Fig. 2.2d) and the surface temperature was rather constant averaging $24.8 \pm 0.3^\circ\text{C}$ (Fig. 2.2e). Wind speed during sampling in the WMED varied between 3–8 m s⁻¹ (Fig. 2.2f).

DOC, DON, DOP and inorganic nutrient concentrations—The concentrations of DOC, DON and DOP and inorganic nutrients are summarized in Table 2.2. Highest DOC concentrations were measured in the SML of the subtropical Atlantic shelf region, gradually decreasing along the transect from 439.2 to $\sim 110 \mu\text{mol C L}^{-1}$ in the oligotrophic gyre. DOC concentrations in the underlying water (ULW) of the SATL were persistently lower compared to the SML (by $\sim 30\%$) and decreased from 344.7 to $\sim 85 \mu\text{mol C L}^{-1}$. DOC concentrations in the SML were positively related to the DOC concentrations in the ULW ($r^2 = 0.87$; $p < 0.0001$). In the eddy system of the WMED, DOC concentrations in the SML were about twice as high as in the ULW averaging $143.1 \pm 25.3 \mu\text{mol C L}^{-1}$ in the SML and $78.0 \pm 10.8 \mu\text{mol C L}^{-1}$ in the ULW (Table 2.2). Thus, at both study sites, the SML was significantly enriched in DOC as compared to the ULW with enrichment factors ranging from 1.1–2.4 (Wilcoxon matched pairs test; $p = 0.005$, $n = 17$ and $p = 0.005$, $n = 10$ for the SATL and the WMED, respectively; Table 2.3).

DON concentrations in the SML of the SATL were on average more than three times higher than in the ULW (range: 7.9–37.4 $\mu\text{mol L}^{-1}$; Table 2.2). In the WMED, mean DON concentrations of the SML and ULW were similar to those obtained for the SATL (Table 2.2). Due to the higher enrichment in DON as compared to DOC in the SML at both sites (Table 2.3), DOC:DON ratios for the SML (9.9 ± 7.5 for SATL, 8.1 ± 2.4 for WMED) were substantially lower than for the ULW (Table 2.4). In contrast to DOC, no relationship was found between DON concentrations in the SML and the ULW at both study sites ($r^2 = 0.02$, $p = 0.6$ and $r^2 = 0.004$, $p = 0.8$ for the SATL and the WMED, respectively). Only for the SATL, DOP concentrations are available. DOP concentrations decreased from the upwelling region towards the oligotrophic gyre from 0.34 to 0.17 $\mu\text{mol L}^{-1}$ in the SML and from 0.26 to 0.12 $\mu\text{mol L}^{-1}$ in the ULW (Table 2.2). Thus, DOP was barely enriched in the SML as compared to the ULW in contrast to DOC and particularly to DON (Table 2.3). As for DOC, a positive relationship was found between DOP concentrations in the SML and the ULW ($r^2 = 0.74$; $p < 0.0001$). The mean DOC:DOP ratio was similar in the SML and ULW, however, DON:DOP ratios were on average 78.3 ± 33.0 in the SML and thus, significantly higher than the average DON:DOP ratio in the ULW (average: 28.9 ± 5.9 ; Mann-Whitney U test; $p < 0.0001$), reflecting the enrichment in DON of the SML (Table 2.2, 2.4).

At both study sites, inorganic nutrient concentrations were typically low in the ULW reflecting open oceanic surface water conditions (Table 2.2). In the SML of the WMED, mean ammonium and nitrate concentrations were about one order of magnitude higher than in the ULW (Table 2.2). In the SML of the SATL, only the mean ammonium concentration was an order of magnitude higher than in the ULW, the nitrate concentration was only about twice as high in the SML than in the ULW (Table 2.2, 2.3). Phosphate in the SML of the SATL and WMED was enriched by a factor of 2 and 3, respectively (Table 2.3). Dissolved inorganic nitrogen concentrations showed no relationship between the SML and the ULW in the SATL and the WMED ($r^2 = 0.09$, $p = 0.2$ and $r^2 = 0.09$, $p = 0.8$, respectively). In the SATL, however, phosphate concentrations were positively correlated between the SML and ULW ($r^2 = 0.91$; $p < 0.0001$). In contrast to the SATL, no such relationship was found for the WMED ($r^2 = 0.01$, $p = 0.7$). Dissolved inorganic nitrogen to phosphorus (DIN:DIP) ratios in the ULW were close to

Table 2.2: Concentrations of DOC, DON, DOP and inorganic nutrients ($\mu\text{mol L}^{-1}$) as well as the DIN:DIP measured at the different stations (STN) in the surface microlayer (SML) and the underlying water (ULW) of the SATL and the WMED.

STN	DOC		DON		DOP		NH ₄		NO ₃		NO ₂		PO ₄		DIN:DIP	
	SML	ULW	SML	ULW	SML	ULW	SML	ULW	SML	ULW	SML	ULW	SML	ULW	SML	ULW
SATL																
1	439.2	344.7	11.8	6.0	0.34	0.26	2.050	0.155	0.190	0.050	0.036	0.022	0.152	0.108	15.0	2.1
2	370.5	208.5	37.4	6.2	0.33	0.31	3.733	0.136	0.440	0.000	0.044	0.010	0.212	0.102	19.9	1.4
3	186.3	158.1	19.7	6.5	0.28	0.25	0.917	0.175	0.200	0.050	0.017	0.011	0.182	0.157	6.2	1.5
4	207.6	88.7	30.0	6.4	0.28	0.23	3.272	0.233	0.120	0.040	0.026	0.012	0.437	0.192	7.8	1.5
5	142.8	88.8	12.8	5.7	0.23	0.23	1.050	0.155	0.090	0.020	0.014	0.011	0.166	0.148	7.0	1.3
6	110.0	81.4	13.3	5.5	0.23	0.23	1.876	0.185	0.034	0.028	0.017	0.012	0.044	0.043	43.8	5.2
7	121.1	86.8	14.6	5.8	0.27	0.19	2.055	0.289	0.024	0.035	0.018	0.013	0.044	0.028	47.7	12.0
8	121.1	81.9	14.9	5.3	0.24	0.20	0.694	0.188	0.078	0.070	0.017	0.019	0.038	0.018	20.8	15.4
9	102.0	82.2	12.8	5.6	0.24	0.21	0.802	0.194	0.039	0.020	0.015	0.013	0.036	0.022	23.8	10.3
10	98.3	79.2	13.5	5.0	0.23	0.18	0.143	0.573	0.029	0.205	0.013	0.012	0.011	0.031	16.8	25.5
11	116.2	87.8	13.5	5.6	0.22	0.21	1.452	0.265	0.046	0.047	0.018	0.013	0.036	0.025	42.1	13.0
12	174.4	82.2	21.6	4.9	0.22	0.17	2.196	0.193	0.049	0.004	0.015	0.012	0.036	0.021	62.8	10.0
13	110.6	82.1	11.6	6.3	0.20	0.14	1.076	0.242	0.020	0.043	0.010	0.009	0.025	0.008	44.2	36.8
14	97.7	80.8	24.0	5.0	0.21	0.15	4.047	0.201	0.103	0.008	0.011	0.009	0.052	0.009	80.0	24.2
15	95.6	83.3	24.2	4.6	0.22	0.15	1.515	0.175	0.042	0.004	0.009	0.010	0.043	0.008	36.4	23.6
16	115.8	85.5	7.9	4.5	0.14	0.13	0.542	0.275	0.027	0.220	0.007	0.009	0.022	0.012	26.2	42.0
17	131.4	87.9	27.0	4.7	0.17	0.12	2.482	0.175	0.016	0.019	0.010	0.006	0.02	0.007	125.4	28.6
Average	161.2	111.2	18.3	5.5	0.24	0.20	1.76	0.22	0.09	0.05	0.02	0.01	0.09	0.06	36.8	15.0
SD	98.0	69.2	7.9	0.7	0.05	0.05	1.13	0.10	0.11	0.06	0.01	0.00	0.11	0.06	30.6	13.0
WMED																
1	152.4	82.1	19.6	7.1	-	-	4.097	0.510	0.526	0.060	0.025	0.009	0.029	0.018	160.3	32.2
2	138.4	69.7	17.1	3.5	-	-	3.806	0.133	0.711	0.002	0.032	0.012	0.034	0.014	133.8	10.5
3	124.6	82.4	17.4	4.5	-	-	2.674	0.220	0.368	0.036	0.013	0.005	0.019	0.012	160.8	21.8
4	150.2	73.3	18.8	3.7	-	-	2.969	0.141	0.371	0.032	0.020	0.004	0.042	0.010	80.0	17.7
5	129.5	75.6	17.5	6.0	-	-	1.750	0.371	0.520	0.003	0.022	0.006	0.044	0.021	52.1	18.1
6	118.7	73.6	16.6	3.9	-	-	1.278	0.134	0.387	0.010	0.022	0.008	0.024	0.011	70.3	13.8
7	157.4	105.5	11.0	5.1	-	-	1.046	0.250	0.362	0.107	0.040	0.014	0.035	0.019	41.4	19.5
8	-	-	18.5	5.6	-	-	1.331	0.181	0.280	0.026	0.024	0.007	0.051	0.015	32.1	14.3
9	103.0	67.0	11.1	4.3	-	-	1.402	0.161	0.214	0.003	0.024	0.006	0.033	0.017	49.7	10.0
10	170.0	74.0	27.2	4.4	-	-	2.798	0.125	0.289	0.003	0.025	0.010	0.075	0.011	41.5	12.5
11	187.0	77.0	31.5	4.2	-	-	2.136	0.139	0.261	0.001	0.019	0.008	0.071	0.012	34.0	12.3
Average	143.1	78.0	18.7	4.8	-	-	2.30	0.22	0.39	0.03	0.02	0.01	0.04	0.01	77.8	16.6
SD	25.3	10.8	6.0	1.1	-	-	1.05	0.12	0.14	0.03	0.01	0.00	0.02	0.00	50.0	6.4

‘-’, not measured

Table 2.3: Summary of enrichment factors (EF = SML/ULW) for selected chemical and biological parameters at the different stations (STN) in the subtropical Atlantic (SATL) and the western Mediterranean Sea (WMED).

STN	DOC	DON	DOP	NH ₄	NO ₃	NO ₂	PO ₄	DTAA	DFAA	DCAABA	BA	BP	BR
SATL													
1	1.3	2.0	1.3	13.2	3.8	1.6	1.4	5.1	17.8	3.8	1.1	0.04	8.3
2	1.8	6.0	1.1	27.4	–	4.4	2.1	43.3	229.4	26.1	1.4	0.03	66.8
3	1.2	3.0	1.1	5.2	4.0	1.5	1.2	18.1	157.9	5.4	0.7	0.04	29.7
4	2.3	4.7	1.2	14.0	3.0	2.2	2.3	15.9	34.9	10.5	0.9	0.03	1.9
5	1.6	2.2	1.0	6.8	4.5	1.3	1.1	6.9	29.6	4.7	0.8	0.11	9.1
6	1.4	2.4	1.0	10.1	1.2	1.4	1.0	9.6	22.6	6.7	1.0	0.04	22.7
7	1.4	2.5	1.4	7.1	0.7	1.4	1.6	7.9	36.7	5.2	1.5	0.07	4.9
8	1.5	2.8	1.2	3.7	1.1	0.9	2.1	10.9	58.6	5.8	0.9	0.16	6.4
9	1.2	2.3	1.1	4.1	2.0	1.2	1.6	6.6	15.1	4.6	0.7	0.03	16.7
10	1.2	2.7	1.3	0.2	0.1	1.1	0.4	5.5	32.0	3.4	1.1	0.04	36.6
11	1.3	2.4	1.0	5.5	1.0	1.4	1.4	9.0	25.4	5.5	0.9	0.13	18.7
12	2.1	4.4	1.3	11.4	12.3	1.3	1.7	28.1	206.4	12.6	1.0	0.07	12.9
13	1.3	1.8	1.4	4.4	0.5	1.1	3.1	7.6	62.7	3.8	1.0	0.23	5.8
14	1.2	4.8	1.4	20.1	12.9	1.2	5.8	3.3	7.6	2.6	1.1	0.26	3.4
15	1.1	5.3	1.4	8.7	10.5	0.9	5.4	2.7	16.4	1.7	1.2	0.59	5.9
16	1.4	1.8	1.1	2.0	0.1	0.8	1.8	7.0	33.3	3.7	–	0.24	8.0
17	1.5	5.7	1.4	14.2	0.8	1.7	2.9	7.5	21.8	4.4	–	0.10	1.6
Average	1.5	3.3	1.2	9.3	3.7	1.5	2.2	11.5	59.3	6.5	1.0	0.13	15.3
SD	0.3	1.4	0.2	7.0	4.3	0.8	1.4	10.3	68.8	5.7	0.2	0.14	16.6
WMED													
1	1.9	2.8	–	8.0	8.8	2.8	1.6	5.5	6.2	4.0	1.2	0.54	1.0
2	2.0	4.9	–	28.6	355.5	2.7	2.4	10.4	25.8	5.5	1.1	0.26	3.1
3	1.5	3.9	–	12.2	10.2	2.6	1.6	8.6	10.1	7.7	1.0	0.33	1.0
4	2.0	5.1	–	21.1	11.6	5.0	4.2	18.9	–	5.8	1.1	0.56	2.3
5	1.7	2.9	–	4.7	173.3	3.7	2.1	11.9	26.1	8.1	1.2	0.15	16.3
6	1.6	4.2	–	9.5	38.7	2.8	2.2	7.1	14.0	2.7	1.0	0.25	1.4
7	1.5	2.1	–	4.2	3.4	2.9	1.8	–	–	–	1.1	2.93	1.1
8	–	3.3	–	7.4	10.8	3.4	3.4	–	–	–	1.2	0.15	1.5
9	1.5	2.6	–	8.7	71.3	4.0	1.9	–	–	–	1.1	1.32	0.3
10	2.3	6.1	–	22.4	96.3	2.5	6.8	–	–	–	1.2	0.87	139.5
11	2.4	7.5	–	15.4	261.0	2.4	5.9	–	–	–	1.1	0.50	0.4
Average	1.8	4.1	–	12.9	94.6	3.1	3.1	10.4	16.5	5.6	1.1	0.72	15.3
SD	0.3	1.6	–	8.0	119.3	0.8	1.8	4.8	9.1	2.1	0.1	0.81	41.5

‘–’ not measured

Table 2.4: DOC:DON, DOC:DOP, DON:DOP ratios calculated for the different stations (STN) in the surface microlayer (SML) and the underlying water (ULW) of the SATL. DOC:DON ratios of the WMED are also shown.

STN	DOC:DON		DOC:DOP		DON:DOP		DOC:DON	
	SML	ULW	SML	ULW	SML	ULW	SML	ULW
	SATL						WMED	
1	37.1	57.2	1275.8	1330.6	34.3	23.3	7.8	11.6
2	9.9	33.4	1116.6	674.2	112.6	20.2	8.1	19.9
3	9.4	24.5	672.7	621.9	71.2	25.4	7.1	18.3
4	6.9	13.9	731.9	386.7	105.8	27.9	8.0	19.8
5	11.1	15.5	625.7	381.8	56.1	24.7	7.4	12.7
6	8.3	14.7	482.4	350.4	58.4	23.8	7.2	18.8
7	8.3	15.0	450.7	449.9	54.4	29.9	14.3	20.6
8	8.1	15.3	502.9	403.7	61.8	26.4	0.0	0.0
9	8.0	14.6	432.2	386.5	54.1	26.5	9.3	15.8
10	7.3	15.9	432.5	450.3	59.3	28.3	6.3	16.7
11	8.6	15.7	530.7	412.3	61.8	26.2	5.9	18.3
12	8.1	16.8	784.4	485.2	97.2	28.8	–	–
13	9.5	13.1	554.8	566.6	58.3	43.4	–	–
14	4.1	16.2	473.7	535.9	116.4	33.1	–	–
15	4.0	18.2	437.2	549.0	110.5	30.2	–	–
16	14.6	19.2	840.9	654.0	57.6	34.1	–	–
17	4.9	18.5	786.9	739.9	161.5	39.9	–	–
Average	9.9	19.9	654.8	551.7	78.3	28.9	8.1	17.2
SD	7.5	10.8	246.7	232.3	33.0	5.9	2.4	3.1

‘–’ not measured

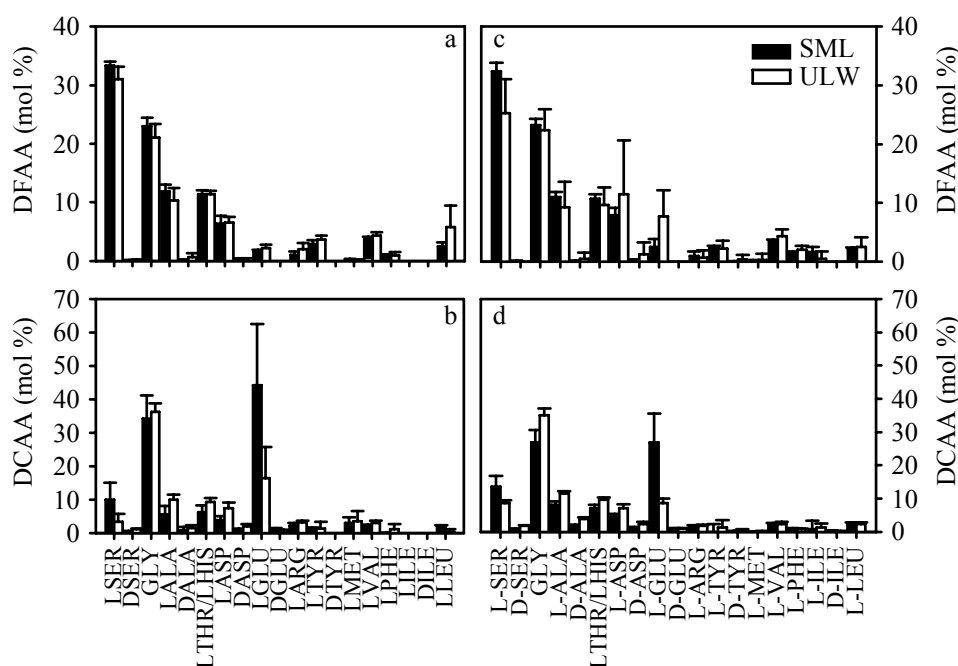


Figure 2.3: Average mole percentages of the L- and D-amino acids in the SML and ULW of the subtropical Atlantic (a-b) and the western Mediterranean (c-d). Error bars denote standard deviations.

Redfield (~ 16) while in the SML, mean DIN:DIP was 36.8 ± 30.6 and 77.8 ± 50.0 in the SATL and WMED, respectively (Table 2.2).

Patterns in total dissolved hydrolysable amino acids (THAA), dissolved free amino acids (DFAA), and dissolved combined amino acids (DCAA)—In the SATL, the concentrations of THAA in the SML ranged from 1.1 – $25.8 \mu\text{mol L}^{-1}$ and in the ULW from 0.3 – $0.6 \mu\text{mol L}^{-1}$, with no clear pattern along the transect (Table 2.5). In the SML, the contribution of DFAA to the THAA pool was remarkably high, averaging $47 \pm 10\%$ and was significantly lower in ULW with $12 \pm 5\%$ (Mann-Whitney U test; $p < 0.0001$; $n = 17$; Table 2.5). In the SML of the WMED, THAA concentrations varied within a narrow range from 2.8 – $5.3 \mu\text{mol L}^{-1}$. THAA concentrations in the ULW were similar to those obtained in the SATL and ranged between 0.3 – $1.0 \mu\text{mol L}^{-1}$ (Table 2.5). In the SML of the WMED, the contribution of DFAA to the THAA was even higher than in the SATL averaging $61 \pm 14\%$ (Table 2.5). Remarkably, in the ULW of the WMED, the DFAA contribution to the THAA pool was three times higher than in the SATL (Table 2.5).

Composition of the dissolved THAA pool—Generally, the composition of DFAA pool in the SML was similar to that of the ULW with L-serine, L-glycine, L-alanine, L-threonine/histidine and L-aspartic acid contributing $85.5 \pm 2.5\%$ and $78.5 \pm 8.2\%$ to the DFAA pool in the SML and ULW, respectively (Fig. 2.3a, c). The mol-percent distribution in the DCAA pool was significantly different (Analysis of variance; $p < 0.05$) from that of the DFAA pool with L-glycine and L-glutamic acid contributing 62.5 ± 12.0 and $48.1 \pm 6.5\%$ to the DCAA in the SML and ULW, respectively (Fig. 2.3b, d). L-glutamic acid was found to contribute about 3 times more to the DCAA pool in the SML than in the ULW. Thus, the composition of the DCAA pool in the SML did not resemble its composition in the ULW as closely as the DFAA pool. No relationship of individual amino acid mol-percentages or pooled dissolved amino acid

Table 2.5: Concentrations of dissolved total hydrolysable amino acids (THAA; $\mu\text{mol L}^{-1}$), dissolved free amino acids (DFAA; $\mu\text{mol L}^{-1}$), dissolved combined amino acids (DCAA; $\mu\text{mol L}^{-1}$) and the percentage of DFAA of THAA measured at the different stations (STN) in the subtropical Atlantic (SATL) and the western Mediterranean Sea (WMED).

STN	THAA ($\mu\text{mol L}^{-1}$)		DFAA ($\mu\text{mol L}^{-1}$)		DCAA ($\mu\text{mol L}^{-1}$)		DFAA/THAA (%)	
	SML	ULW	SML	ULW	SML	ULW	SML	ULW
SATL								
1	2.70	0.53	0.87	0.05	1.83	0.48	32	9
2	25.82	0.60	11.58	0.05	14.25	0.55	45	8
3	8.14	0.45	5.90	0.04	2.23	0.41	73	8
4	9.02	0.57	4.37	0.13	4.65	0.44	48	22
5	3.29	0.48	1.27	0.04	2.02	0.43	39	9
6	3.97	0.42	1.68	0.07	2.29	0.34	42	18
7	3.17	0.40	1.27	0.03	1.9	0.37	40	9
8	5.01	0.46	2.59	0.04	2.41	0.42	52	10
9	3.39	0.51	1.48	0.1	1.91	0.42	44	19
10	2.11	0.38	0.88	0.03	1.23	0.36	42	7
11	4.55	0.51	2.27	0.09	2.29	0.42	50	18
12	10.86	0.39	6.38	0.03	4.47	0.36	59	8
13	2.58	0.34	1.36	0.02	1.23	0.32	53	6
14	1.36	0.41	0.43	0.06	0.93	0.35	31	14
15	1.14	0.42	0.46	0.03	0.68	0.39	40	7
16	2.72	0.39	1.43	0.04	1.30	0.35	52	11
17	2.87	0.38	1.47	0.07	1.40	0.32	51	18
Average	5.45	0.45	2.69	0.05	2.77	0.39	47	12
SD	5.91	0.07	2.89	0.03	3.15	0.06	10	5
WMED								
1	5.26	0.96	3.76	0.60	1.55	0.39	71	63
2	3.37	0.32	1.89	0.07	1.51	0.27	56	23
3	4.80	0.56	2.11	0.21	2.72	0.35	44	37
4	4.92	0.26	3.42	–	1.52	0.26	70	–
5	5.08	0.43	2.38	0.09	2.71	0.33	47	21
6	2.82	0.40	2.19	0.16	0.64	0.24	78	39
Average	4.37	0.49	2.63	0.23	1.78	0.31	61	37
SD	1.02	0.25	0.77	0.22	0.80	0.06	14	17

‘–’ not measured

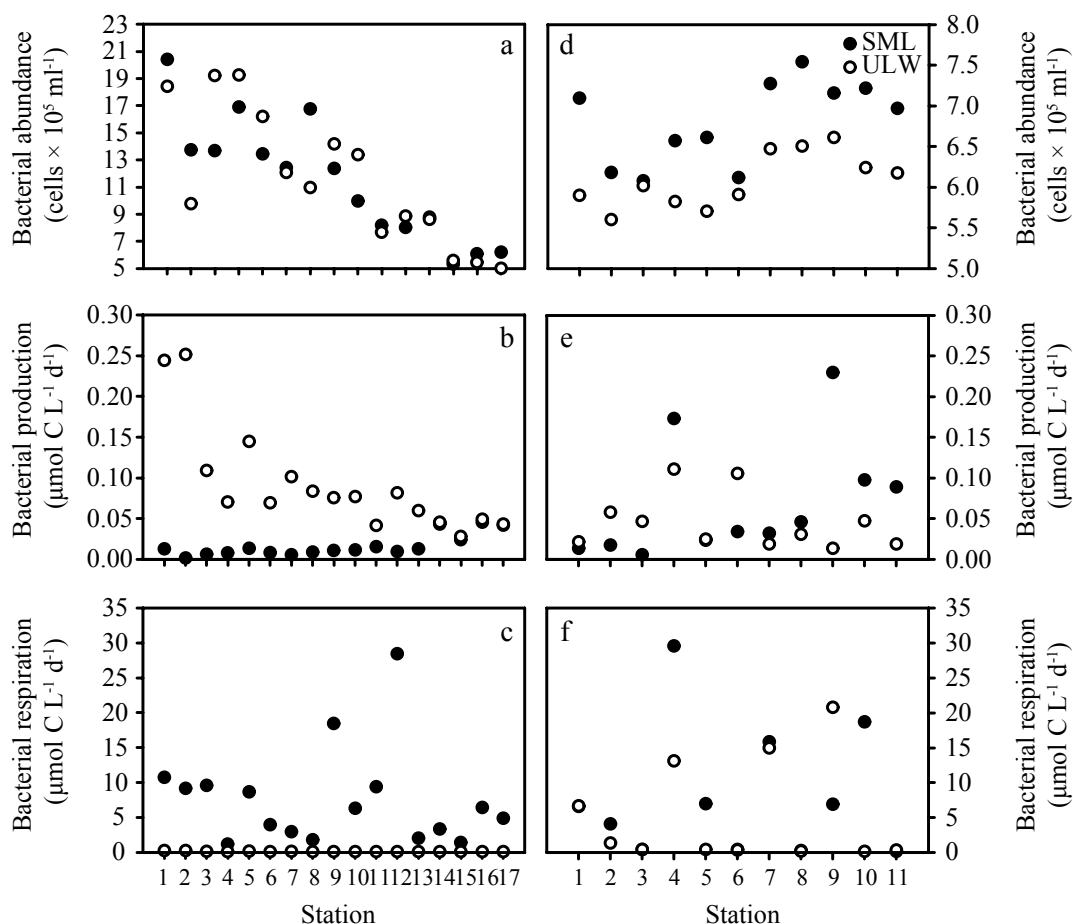


Figure 2.4: Bacterial abundance (cells × 10⁵ mL⁻¹), production and respiration measured in the surface microlayer (SML) and the underlying water (ULW) at the different stations in the subtropical Atlantic (a, c, e) and the western Mediterranean eddy (b, d, f).

concentrations was found between the SML and ULW. D-enantiomeric forms of the individual amino acids generally contributed < 3% to the THAA pool.

Mean concentrations of individual DFAAs in the SML ranged from 16 nmol L⁻¹ up to 876 nmol L⁻¹ (Data not shown). The DFAA concentrations in the ULW were generally significantly lower than in the SML ranging from ~1 to 14 nmol L⁻¹ (Analysis of variance; $p < 0.05$). DFAA concentrations of individual amino acids in the SML and ULW of the SATL were not significantly different from concentrations measured in the WMED (Analysis of variance; $p < 0.05$). The mean DCAA concentrations at both study sites ranged from ~2–789 nmol L⁻¹ in the SML and from ~3–138 nmol L⁻¹ in the ULW, however, similar to DFAA, concentrations in the ULW were significantly lower than in the SML (Analysis of variance; $p < 0.05$).

Bacterial abundance— In the SATL, bacterial abundance in the SML and the ULW decreased by a factor of 4 from the upwelling region to the subtropical Atlantic gyre (Fig. 2.4a) with no apparent enrichment in the SML (Wilcoxon matched pairs test; $p = 0.9$, $n = 15$; Table 2.3). Bacterial abundance in the SML was positively related to that in the ULW ($r^2 = 0.67$; $p < 0.001$).

Bacterial abundance in the WMED did not exhibit a specific trend over time (Fig. 2.4b).

Mean bacterial abundance was $6.8 \pm 0.5 \times 10^8$ cells L^{-1} in the SML and in the ULW $6.1 \pm 0.3 \times 10^8$ cells L^{-1} . Bacterial abundance in the SML of the WMED was enriched by a factor of 1.1 ± 0.1 (Wilcoxon matched pairs test; $p = 0.003$, $n = 11$; Table 2.3). As for SATL, in the WMED, bacterial abundance between SML and ULW was positively related ($r^2 = 0.56$; $p < 0.01$).

Bacterial production—In the SATL, bacterial production in the SML was generally low ranging from 0.001–0.014 $\mu\text{mol C L}^{-1} \text{d}^{-1}$ (Fig. 2.4c). In the ULW, bacterial production declined from the highly productive upwelling region to the gyre from 0.204 $\mu\text{mol C L}^{-1} \text{d}^{-1}$ to ~ 0.021 $\mu\text{mol C L}^{-1} \text{d}^{-1}$ (Fig. 2.4c). Thus, in the upwelling region, bacterial production in the SML was about one order of magnitude lower than in the ULW (Table 2.3). In the gyre, however, bacterial production was similar in the SML and the ULW (Table 2.3). In the WMED, bacterial production in the SML was not significantly different from that in the ULW (Wilcoxon matched pairs test; $p = 0.04$, $n = 11$; Fig. 2.4d). Enrichment factors for bacterial production in the SML of the WMED ranged from 0.1–16.8 and were therefore highly variable (Table 2.3). Bacterial production in the SML and ULW was not related with each other ($r^2 = 0.04$; $p = 0.4$ and $r^2 = 0.11$; $p = 0.3$ for SATL and WMED, respectively).

Bacterial respiration — In the SML of the SATL, bacterial respiration was high in the upwelling region (9.5 ± 0.9 $\mu\text{mol O}_2 \text{L}^{-1} \text{d}^{-1}$) and decreasing towards the oligotrophic gyre ($\sim 3.6 \pm 2.0$ $\mu\text{mol O}_2 \text{L}^{-1} \text{d}^{-1}$; Fig. 2.4e). In contrast, bacterial respiration in the ULW was consistently low along the transect (0.8 ± 0.8 $\mu\text{mol O}_2 \text{L}^{-1} \text{d}^{-1}$). Thus, contrary to bacterial production, bacterial respiration was significantly higher in the SML than in the ULW (Wilcoxon matched pairs test; $p = 0.0003$, $n = 17$) over the entire transect with enrichment factors ranging from 1.6–66. Generally, lower enrichment factors were found in the oligotrophic gyre region than in the upwelling region (Table 2.3). In the WMED, bacterial respiration exhibited high variability between the different stations. On average, bacterial respiration in the SML and ULW was similar although considerable differences in the respiration rates between SML and ULW were detected at individual stations (Fig. 2.4f). Comparing the average bacterial respiration between the two study sites for the SML and ULW separately, no significant difference was found (Student's *t*-test; $p = 0.2$ and $p = 0.1$ for the SML and ULW, respectively). As for bacterial production, bacterial respiration of the SML and ULW was not related at both sites ($r^2 = 0.45$; $p = 0.07$ and $r^2 = 0.23$; $p = 0.13$ for SATL and WMED, respectively).

Discussion

Problems and assumptions in methodology—It is well documented that different methods to sample the SML vary in their collection efficiency for different biological and chemical components. Most commonly, a metal screen sampler is used [15] which allows for relatively fast sampling of up to 100 mL per dip. However, it was found that the resulting SML sample is diluted with ULW [19]. The glass plate sampler [18] is the better choice for studies of dissolved hydrophobic matter, such as amino acids and nutrients [32] and probably also for bacteria [1, 37].

A potential problem for rate measurements in the SML is the alteration of the originally high-surface low-volume habitat and its confinement in flasks required to perform these rate measurements, as the interactions of the SML with the ULW and the atmosphere are disrupted. In this study, incubations were kept as short as possible (~ 0.5 h for bacterial production and ~ 14 h for respiration measurements in the SML), yet property changes in specific physical and chemical parameters could potentially lead to over- or underestimations of the actual rates.

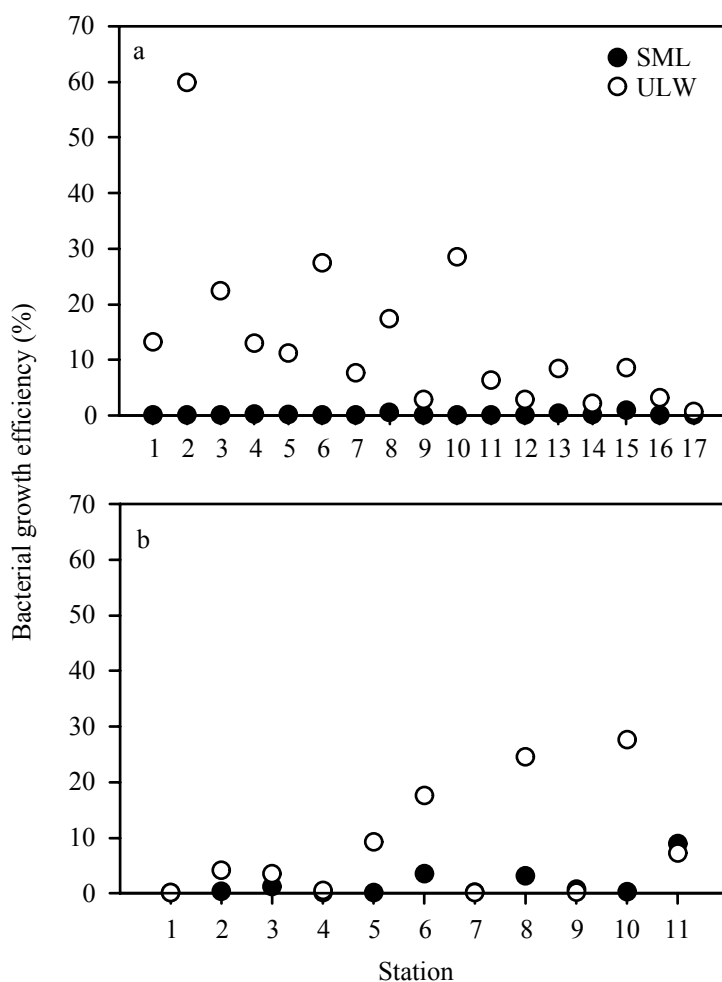


Figure 2.5: Bacterial growth efficiency (%) in the surface microlayer (SML) and the underlying water (ULW) at the stations along the transect in the subtropical Atlantic (a) and at the stations sampled in the western Mediterranean eddy (b).

Bacterial growth efficiencies (BGEs)—Generally, BGEs in aquatic systems vary over a large range from <1 to >60% [10]. At the SATL study site, mean BGE ($BGE = BP / (BP + BR)$) was $0.2 \pm 0.2\%$ in the SML and $13.8 \pm 14.6\%$ in the ULW with higher BGEs in the upwelling region than in the oligotrophic gyre (Fig. 2.5a). In the WMED, BGE was on average $1.7 \pm 2.7\%$ in the SML and $8.6 \pm 10.1\%$ in the ULW (Fig. 2.5b). As indicated by the high standard deviation as compared to the mean, there was considerable spatial (in the SATL) and temporal (in the WMED eddy) variability in the BGE particularly in the ULW.

To calculate BGE, it is necessary to filter the seawater to exclude the autotrophic plankton. Fractionating the community, however, might alter the bacterial activity during the incubations. The limitation in sample volume prevented experiments testing the linearity of oxygen consumption in the bottles. In the SATL, however, we also measured total community respiration of unfiltered seawater samples. Bacterial and total community respiration were highly related ($r^2 = 0.84$, $p < 0.0001$, $n = 17$ and $r^2 = 0.59$, $p < 0.01$, $n = 15$ in the SML and the ULW respectively; data not shown) and bacterial respiration was on average $58.4 \pm 22.1\%$ of the total respiration. Thus, we assume that our respiration measurements were not

altered dramatically due to the fractionation of the total community.

Bacterial production was extremely low in the SML (Fig. 2.4c, d). Bacterial production measured in unfiltered and 0.8- μm filtered seawater was highly correlated in both the SML and the ULW (Spearman rank correlation; $r = 0.95$, $p < 0.01$), however, bacterial production in the 0.8- μm filtered seawater was frequently $\sim 30\%$ lower compared to that in unfiltered seawater.

The only other reported BGE values for SML bacteria range from 18–83% at the French Mediterranean coast [33]. The values were calculated using the average of the bacterial production measured at time zero and after 24 h. Following this approach for some of our samples from the SATL, we arrive at a BGE of $30.4 \pm 15.8\%$ for the SML ($n = 12$) and $40.1 \pm 23.3\%$ for the ULW ($n = 10$). However, the relationship between bacterial production measured in unfiltered and 0.8- μm filtered seawater was weak after 12–18 h. Respiration measurements integrate over longer time scales (~ 12 – 24 h) than bacterial production measurements (~ 1 h), and it has been shown repeatedly that despite increased growth in incubations, oxygen consumption is linear [6]. Thus, there is no *a priori* reason to assume that averaging bacterial production over the incubation period is the better strategy to obtain accurate BGE estimates.

For the WMED, bacterial production was measured only at initial time points. However, for a few samples we followed the growth of bacterial cells over the duration of the incubations to calculate bacterial production from the increase in cell abundance. Applying a mean carbon content of $15 \text{ fg C cell}^{-1}$, we calculated a BGE of $36.8 \pm 42.4\%$ and $57.5 \pm 36.8\%$ for the SML and ULW, respectively. Mean BGEs calculated with this alternative method seem high, compared to the main body of BGE for the surface open ocean ranging from ~ 15 – 20% [10] and would indicate that available substrate is efficiently utilized. The high contribution of DFAA to the THAA pool we obtained in this study support the notion of low BGEs in the SML [27].

Accumulation of dissolved organic material— Mechanisms of dissolved organic matter (DOM) accumulation are complex. The SML is exposed to direct UV irradiation, which renders initially labile organic matter more refractory and vice versa [34]. Nevertheless, it has been shown recently on several bacterial strains from the SML and ULW of a coastal site that bacterioneuston are not fundamentally different in their response to UV stress from strains isolated from deeper water layers [2]. For efficient DOM assimilation by bacteria, the elemental composition of DOM should match the C:N:P ratio of the bacteria of about 50:10:1 [16]. Higher C:N ratios of DOM were shown to lead to decreasing growth efficiencies [16, 27]. Under these conditions, bacteria must process relatively more carbon to cover the nitrogen demand for biosynthesis. The DOM in the ULW was depleted in DON (C:N = 18.2 ± 9.3 ; average of SATL and WMED), while the DOM of the SML was nitrogen rich (C:N = 8.9 ± 6.2 ; average of SATL and WMED) as compared to DOC:DON ratios ranging between 8 and 16 in surface waters of the North Atlantic and the N-W Mediterranean Sea [3, 23] (Table 2.4). No relationship between C:N ratios and BGE, however, was found in the present study. DOC:DOP ratios in the SML and ULW of the SATL tended to be in the upper range of ratios reported for surface North Atlantic waters, whereas DON:DOP ratios were either lower in the ULW or much higher in the SML than reported for the surface ocean [3, 40]. We found an inverse relationship between bacterial production and DOP ($r^2 = 0.51$; $p = 0.001$), however, no relationship was found for bacterial production with DOC ($r^2 = 0.10$, $p = 0.2$). This is counterintuitive as one would expect higher bacterial production in the upwelling area with high DOP and DON concentrations and potentially fresh DOM released by phytoplankton. DFAA usually covers a considerable fraction of the bacterial nitrogen demand [26]. In the SML, DFAA were considerably enriched as compared to the concentrations in the ULW also measured elsewhere [28] (Table 2.5). DFAA

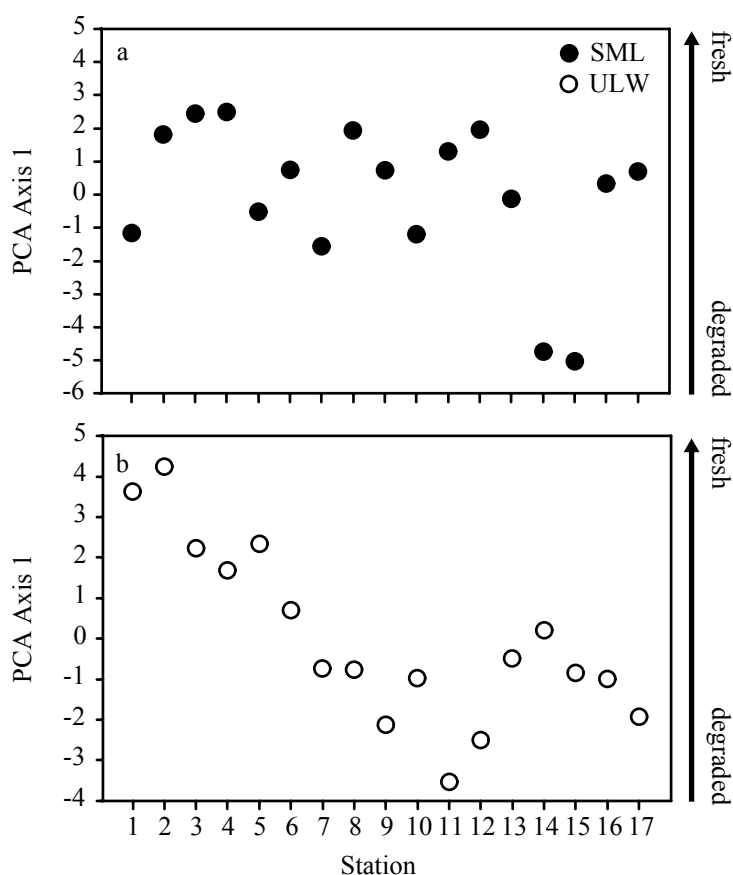


Figure 2.6: Degradation of the amino acid pool in the surface microlayer (SML) (a) and the underlying water (ULW) (b) of the subtropical Atlantic. The degradation index (PCA axis 1) is based on a principal component analysis of the mole percentages of the individual amino acids in the dissolved total dissolved amino acid pool (THAA). High scores indicate more freshly produced amino acids, while low scores are an indication of a relatively degraded amino acid pool.

was on average 47–61% of THAA in the SML (Table 2.5), however, the percentage of the DFAA pool was significantly lower in the ULW (~12–37%). The enrichment of DFAA in the SML suggests that bacteria in the SML are apparently inhibited in their uptake of DFAA which might also explain the low BGE (Fig. 2.5).

Changes in the amino acid composition have been suggested as indicator of organic matter diagenesis [4]. To characterize the changes in the amino acid pool along the transect in the SATL, a principal component analysis (PCA) was used based on a matrix of mole percentages of the different amino acids in the SML and ULW (Fig. 2.6). The site scores along axis 1 are interpreted as relative degradation state of the THAA pool, with more negative site scores representing more decomposed material and more positive scores indicating more freshly produced DOM. Using this approach, we found a rather variable pattern in the SML of the SATL, reflecting the complex production and degradation of amino acids in the SML (Fig. 2.6a). In the ULW, however, the DOM pool became more refractory and degraded from the upwelling area towards the oligotrophic gyre (Fig. 2.6b). Further evidence for increasing degradation of the amino acid pool towards the oligotrophic gyre comes from the increase in the D/L ratio of alanine and aspartic acid (Fig. 2.7). The D-isomers of alanine, aspartic acid, serine and glutamic

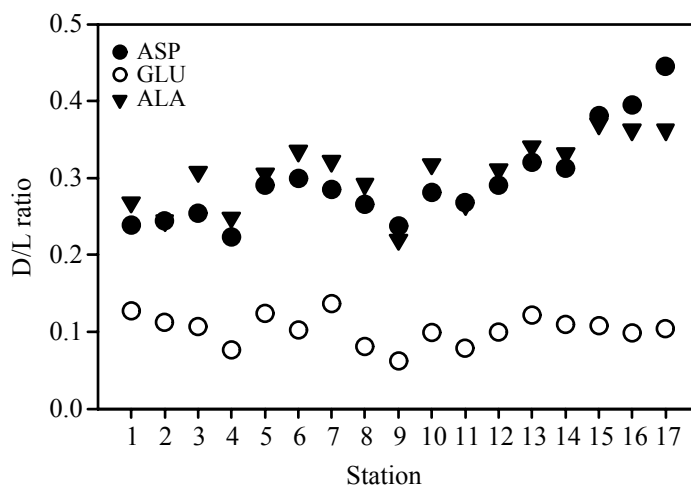


Figure 2.7: D/L amino acid ratios for aspartic acid (ASP), glutamic acid (GLU) and alanine (ALA) in the ULW of the subtropical Atlantic.

acid are mainly derived from the bacterial cell wall [22]. Thus, the gradually increasing D/L ratio of aspartic acid and alanine in the ULW suggests preferential utilization of L-amino acids (Fig. 2.7). While the pattern in D/L ratios showed no clear trend in the SML (data not shown), the decreasing BGE in the ULW of the SATL was linked to the diagenesis of the amino acid pool.

In addition to the relationship between wind speed and DOC and DOP in the SML ($r^2 = 0.27$; $p < 0.05$ and $r^2 = 0.37$; $p < 0.05$ for DOC and DOP, respectively), the significant correlation between the SML and the ULW might indicate an exchange of DOC and DOP between both water layers. Inorganic nitrogen, DON and amino acids were highly enriched in the SML and the variability of nitrogen in the SML is independent of that in the ULW.

We found, that the SML in the open ocean is a highly variable environment with generally low bacterial biomass production and high respiration. Bacterial production was not related to bacterial respiration and bacterial growth efficiency was mainly determined by respiration. It has been suggested, that the limitation in the supply of growth substrate in oligotrophic systems might lead to a high degree of uncoupling between production and respiration [10]. Despite the significant enrichments in dissolved organic matter in the SML, where concentrations of e.g. dissolved organic nutrients and amino acids were generally higher than commonly reported for oligotrophic systems, the low bacterial production in combination with high bacterial respiration suggests that the DOM pool of the SML pool, and particularly the amino acid pool is not readily available for the bacteria.

Acknowledgements

We thank the captain and crew of the RV *Pelagia* for their support at sea. Special thanks go to Karel Bakker, Santiago Gonzales and Arjan Smith for help with the DON and DOP, DOC and amino acid analysis, respectively. Eva Sintes performed the flow cytometry analyses of the bacterial community. The BADE cruises were supported by the Dutch Science Foundation (NWO-ALW), project 812.03.001 to G.J.H.

Bibliography

- [1] Agogu  H, Casamayor EO, Joux F, Obernosterer I, Dupuy C, Catala P, Weinbauer MG, Reinthaler T, Herndl GJ, Lebaron P. 2004. Comparison of samplers for the biological characterization of the sea surface microlayer. *Limnology and Oceanography: Methods* 2: 213-25
- [2] Agogu  H, Joux F, Obernosterer I, Lebaron P. 2005. Resistance of marine bacterioneuston to solar radiation. *Applied and Environmental Microbiology* 71: 5282-9
- [3] Aminot A, Kerouel R. 2004. Dissolved organic carbon, nitrogen and phosphorus in the NE Atlantic and the NW Mediterranean with particular reference to non-refractory fractions and degradation. *Deep-Sea Research Part I* 51: 1975-99
- [4] Amon RMW, Fitznar H-P, Benner R. 2001. Linkages among the bioreactivity, chemical composition, and diagenetic state of marine dissolved organic matter. *Limnology and Oceanography* 46: 287-97
- [5] Benner R, Strom M. 1993. A critical evaluation of the analytical blank associated with DOC measurements by high-temperature catalytic oxidation. *Marine Chemistry* 41: 153-60
- [6] Biddanda B, Opsahl SB, R. 1994. Plankton respiration and carbon flux through bacterioplankton on the Louisiana shelf. *Limnology and Oceanography* 39: 1259-75
- [7] Calleja ML, Duarte CM, Navarro N, Agusti S. 2005. Control of air-sea CO₂ disequilibria in the subtropical NE Atlantic by planktonic metabolism under the ocean skin. *Geophysical Research Letters* 32: DOI 10.1029/2004GL022120
- [8] Carlucci AF, Craven DB, Henrichs SM. 1985. Surface-film microheterotrophs: amino acid metabolism and solar radiation effects on their activities. *Marine Biology* 85: 13-22
- [9] Carritt DE, Carpenter JH. 1966. Comparison and evaluation of currently employed modifications of Winkler method for determining dissolved oxygen in seawater - a NASCO Report. *Journal of Marine Research* 24: 287-318
- [10] Del Giorgio PA, Cole JJ. 2000. Bacterial energetics and growth efficiency. In *Microbial Ecology of the Oceans*, ed. DL Kirchman, pp. 289-325. New York: Wiley-Liss
- [11] Falkowska L. 1999. SML; Sea surface microlayer: a field evaluation of teflon plate, glass plate and screen sampling techniques. Part. 1. Thickness of microlayer samples and relation to wind speed. *Oceanologia* 41: 211-22
- [12] Fitznar HP, Lobbes JM, Kattner G. 1999. Determination of enantiomeric amino acids with high-performance liquid chromatography and pre-column derivatisation with *o*-phthaldialdehyde and *N*-isobutrylcysteine in seawater and fossil samples (mollusks). *Journal of Chromatography A* 832: 123-32
- [13] Franklin MP, McDonald IR, Bourne DG, Owens NJP, Upstill-Goddard RC, Murrell JC. 2005. Bacterial diversity in the bacterioneuston (sea surface microlayer): the bacterioneuston through the looking glass. *Environmental Microbiology*

- [14] Fukuda R, Ogawa H, Nagata T, Koike II. 1998. Direct determination of carbon and nitrogen contents of natural bacterial assemblages in marine environments. *Applied and Environmental Microbiology* 64: 3352-8
- [15] Garrett WD. 1967. Organic chemical composition of ocean surface. *Deep-Sea Research Part I* 14: 221-7
- [16] Goldman JC, Caron DA, Dennett MR. 1987. Regulation of gross growth efficiency and ammonium regeneration in bacteria by substrate C:N ratio. *Limnology and Oceanography* 32: 1239-52
- [17] Hardy JT. 1982. The sea surface microlayer: Biology, chemistry and anthropogenic enrichment. *Progress In Oceanography* 11: 307-28
- [18] Harvey GW, Burzell LA. 1972. A simple microlayer method for small samples. *Limnology and Oceanography* 1: 156-7
- [19] Hatcher RF, Parker BC. 1974. Laboratory comparisons of four surface microlayer samplers. *Limnology and Oceanography* 19: 162-5
- [20] Helder W, de Vries R. 1979. An automatic phenolphthorite method for the detection ammonia in sea- and brackish waters. *Netherlands Journal of Sea Research* 13: 154-60
- [21] Jarvis NL. 1967. Adsorption of surface-active material at the sea-air interface. *Limnology and Oceanography* 12: 213-21
- [22] Jørgensen NOG, Tranvik LJ, Berg GM. 1999. Occurrence and bacterial cycling of dissolved nitrogen in the gulf of Riga, the Baltic Sea. *Marine Ecology Progress Series* 191: 1-18
- [23] Kaehler P, Koeve W. 2001. Marine dissolved organic matter: can its C : N ratio explain carbon overconsumption? *Deep-Sea Research Part I* 48: 49-62
- [24] Kaiser K, Benner R. 2005. Hydrolysis-induced racemization of amino acids. *Limnology and Oceanography: Methods* 3: 318-25
- [25] Kirchman D. 1993. Leucine incorporation as a measure of biomass production by heterotrophic bacteria. In *Handbook of methods in aquatic microbial ecology*, ed. PF Kemp, BF Sherr, EB Sherr, JJ Cole, pp. 509-12. Boca Raton: Lewis publishers
- [26] Kirchman DL. 2000. Uptake and regeneration of inorganic nutrients by marine heterotrophic bacteria. In *Microbial ecology of the oceans.*, ed. DL Kirchman, pp. 261-88. New York: Wiley-Liss
- [27] Kroer N. 1993. Bacterial growth efficiency on natural dissolved organic matter. *Limnology and Oceanography* 38: 1282-90
- [28] Kuznetsova M, Lee C, Aller JY. 2004. Enrichment of amino acids in the sea surface microlayer at coastal and open ocean sites in the North Atlantic Ocean. *Limnology and Oceanography* 49: 1605-19

- [29] Lindroth P, Mopper K. 1979. High performance liquid chromatographic separation of subpicomol amounts of amino acids by precolumn fluorescence derivatization with *o*-phthaldialdehyde. *Analytical Chemistry* 51: 1667-74
- [30] Liss PS, Duce RA. 1997. *The sea surface and global change*. New York: Cambridge University Press
- [31] Mimura T, Romano JC, Desouzalima Y. 1988. Microbiomass structure and respiratory activity of microneuston and microplankton in the northwestern Mediterranean Sea influenced by Rhone River water. *Marine Ecology Progress Series* 49: 151-62
- [32] Momzikoff A, Brinis A, Dallot S, Gondry G, Saliot A, Lebaron P. 2004. Field study of the chemical characterization of the top ocean surface using various samplers. *Limnology and Oceanography: Methods* 2: 374-86
- [33] Obernosterer I, Catala P, Reinthaler T, Herndl GJ, Lebaron P. 2005. Enhanced heterotrophic activity in the surface microlayer of the Mediterranean Sea. *Aquatic Microbial Ecology* 39: 1616-564
- [34] Obernosterer I, Reitner B, Herndl GJ. 1999. Contrasting effects of solar radiation on dissolved organic matter and its bioavailability to marine bacterioplankton. *Limnology and Oceanography* 44: 1645-54
- [35] Regan JD, Carrier WL, Gucinski H, Olla BL, Yoshida H, Fujimura RK, Wicklund RI. 1992. DNA as a solar dosimeter in the ocean. *Photochemistry and Photobiology* 56: 35-42
- [36] Reinthaler T, Bakker K, Manuels R, Van Ooijen J, Herndl GJ. submitted. Fully automated spectrophotometric approach to determine oxygen concentrations in seawater via continuous-flow analysis. *submitted to Limnology and Oceanography: Methods*
- [37] Schäfer A, Harms H, Zehnder AJB. 1998. Bacterial accumulation at the air-water interface. *Environmental Science and Technology* 32: 3705-12
- [38] Souza Lima Y. 1985. Dissolved inorganic nutrient enrichment in the sea surface microlayer: Possible effects of abiotic and biotic environmental factors. *Oceanologica acta* 8: 47-58
- [39] Valderrama JC. 1981. The simultaneous analysis of total nitrogen and total phosphorus in natural waters. *Marine Chemistry* 10: 109-22
- [40] Vidal M, Duarte CM, Agusti S. 1999. Dissolved organic nitrogen and phosphorus pools and fluxes in the central Atlantic Ocean. *Limnology and Oceanography* 44: 106-15
- [41] Williams PM, Carlucci AF, Henrichs SM, Van Vleet ES, Horrigan SG, Reid FMH, Robertson KJ. 1986. Chemical and microbiological studies of sea-surface films in the Southern Gulf of California and off the West Coast of Baja California. *Marine Chemistry* 19: 17-98
- [42] Wotton RS, Preston TM. 2005. Surface films: Areas of water bodies that are often overlooked. *Bioscience* 55: 137-45

Chapter 3

Seasonal dynamics of bacterial growth efficiencies in relation to phytoplankton in the southern North Sea¹

Thomas Reinthaler and Gerhard J. Herndl

The main function of heterotrophic bacterioplankton in marine carbon cycling is the conversion of dissolved organic carbon (DOC) into biomass and CO₂. The relative importance of bacterial biomass production (BP) versus respiration (BR) is expressed by the bacterial growth efficiency [BGE = BP/(BP + BR) × 100]. Studies on the dynamics of the BGE of bacterioplankton growing on natural DOC covering entire seasonal cycles are scarce. We measured BP and BR over a seasonal cycle in the southern North Sea at a total of 150 stations to determine seasonal variability in BGE. While BP varied over 1 order of magnitude over the seasonal cycle, BR varied only 2-fold. Cell-specific BP was related to primary production while BR was not. Mean BGE increased from 6 ± 3% in the winter to 25 ± 9% in the spring and summer. Depth-integrated BR was fairly stable over the seasonal cycle, averaging 57% of the particulate primary production. Based on the bacterioplankton respiration and the mean annual BGE of 20%, bacterioplankton organic carbon demand amounts to ~70% of the particulate primary production in the southern North Sea, suggesting that autochthonous organic matter production is sufficient to fuel bacterioplankton carbon demand.

Introduction

Bacterioplankton represent the largest living biomass in the world's ocean [49]. Their main ecological function is to sequester the dissolved organic carbon (DOC) pool by incorporating a fraction of it into biomass and remineralizing the major fraction of DOC to CO₂. Depending on the trophic state of the environment, bacterioplankton contribute between 12% and >50% to total community respiration [36, 38, 44].

Whether high remineralization rates of the prokaryotic community render the vast open-ocean into a net heterotrophic system is currently under debate [10, 11, 17, 51]. While

¹Published in *Aquat. Microbiol. Ecol.* (2005) 39: 7-16

bacterial production (BP) is routinely measured in marine ecosystem studies, bacterial respiration (BR) has only recently received adequate attention. Determining BR rates, however, is as important as BP to estimate the bacterial growth efficiency [$BGE = BP/(BP + BR) \times 100$] and the bacterial carbon demand. Reported BGEs span over a large range from <1% to 80%. The underlying reasons for this large variation are basically unknown [8]. Jahnke and Craven [19] suggested that the variability in the reported BGEs is due to the limited data set on respiration and concomitantly performed production measurements. Del Giorgio et al. [9] argued that BGEs should be in the range from <10 to 25% in most marine surface systems. Attempts to derive respiration rates from BP measurements are problematic because the correlation between BP and BR is usually weak [7]. Rivkin and Legendre [35] found a significant relationship between BGEs and temperature using a data set across a large temperature range; this makes it difficult to apply their model to specific locations with smaller temperature fluctuations [37].

Shelf seas such as the North Sea cover only around 7% of the global ocean surface but contribute ~30% to the oceanic primary production [14]. Most studies on BP and BR are single surveys and surprisingly few marine studies have been performed over a seasonal cycle [23, 40]. In this study, we measured BP, BR and primary production during 6 cruises covering a full seasonal cycle in the non-stratified southern North Sea occupying a total of 150 stations. The ultimate aim of the study was to determine the seasonal relationship between BP and BR and to relate the BGE dynamics to primary production and other physicochemical variables.

Material and Methods

Study site—The study was carried out during 7 cruises aboard the R/V *Pelagia* in the unstratified waters of the southern North Sea (Fig. 3.1), occupying a total of 150 stations between July 2000 and August 2002. The mean depth of the southern North Sea is around 30 m and strong tidal currents and relatively high turbidity are common [26].

Sample preparation for assessing bacterial parameters—For the parameters measured in unfiltered seawater, samples were taken at 5 and 15 m depth as well as 5 m above the bottom with 10 L NOEX bottles mounted on a CTD rosette. Part of the water collected was drawn under gentle vacuum (≤ 200 mbar) and filtered through 0.8- μm polycarbonate filters (Millipore ATTP; 47 mm diameter) to remove most of the non-bacterial particles. To avoid clogging, filters were changed as soon as the flow rate decreased to approximately half the initial rate. Subsequently, the 0.8- μm filtrate was used for bacterial production (BP) and respiration (BR) measurements and for bacterial abundance determination. Bacterial abundance and BP were also determined in unfiltered seawater. All sample handling was performed at in situ temperature ($\pm 2^\circ\text{C}$). Hydrographic properties of the study area are described in detail elsewhere [2]. Additionally, samples were collected for chlorophyll *a* (chl *a*), phytoplankton production and dissolved organic carbon (DOC) as described below.

Bacterial abundance—We fixed 5 mL samples with 37% formaldehyde (4% final conc.), and subsequently determined bacterial abundance by 4',6-diamidino-2-phenylindole (DAPI) staining and epifluorescence microscopy [31] upon return to the lab within 1 wk. Since the abundance of *Archaea* in the coastal North Sea is generally low [28], only DAPI-stained cells with distinct cell boundaries were considered bacteria.

Bacterial production—BP for the unfiltered and 0.8- μm filtered seawater was measured by ^{14}C -leucine incorporation (specific activity: $0.295 \text{ Ci mmol}^{-1}$; final concentration

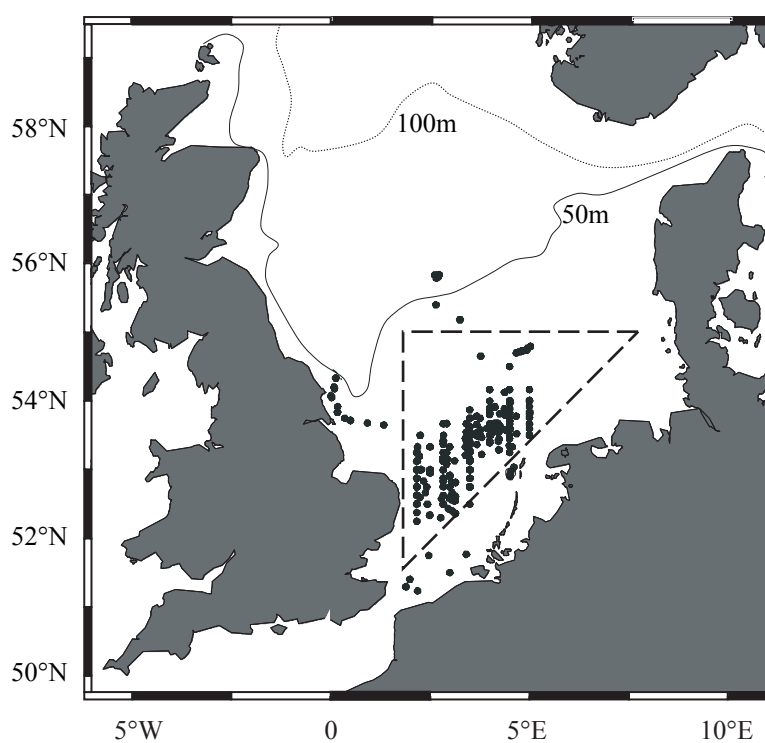


Figure 3.1: Study area. Dots indicate the individual stations occupied during the 7 cruises. Only those stations enclosed by the dashed triangle were considered in the analysis. Continuous and dotted lines mark the 50 m and 100 m isolines, respectively.

10 nmol L⁻¹); 2 samples and 1 blank were incubated in the dark. The blank was fixed with formaldehyde (final concentration 4%, v/v) 10 min prior to adding the tracer. After incubating the samples and the blank at in situ temperature for 60 min, the samples were fixed with formaldehyde (4% final concentration), filtered onto 0.2- μ m nitrocellulose filters (Millipore HA; 25 mm diameter) and rinsed twice with 5 mL ice-cold 5% trichloroacetic acid (Sigma Chemicals) for 5 min. The filters were dissolved in 1 mL ethylacetate and, after 10 min, 8 mL of scintillation cocktail (Insta-Gel Plus, Canberra Packard) was added. The radioactivity incorporated into bacterial cells was counted in a liquid scintillation counter (LKB Wallac, Model 1212). Leucine incorporated into bacterial biomass was converted to carbon production using the empirical conversion factor 0.07×10^{18} cells mol⁻¹ leucine [34] and assuming a bacterial carbon content of 20 fg C cell⁻¹ [22]. The application of this conversion factor resulted in BP estimates similar to the theoretical factor of 1.55 kg C mol⁻¹ leucine, assuming no isotope dilution [41] (data not shown).

Bacterial respiration (BR)—Part of the 0.8- μ m filtrate was carefully transferred to calibrated borosilicate glass BOD bottles with a nominal volume of 120 mL by a sipper system to avoid the formation of air bubbles. For the determination of the initial O₂ concentration (t₀), samples were fixed immediately with Winkler reagents and incubated together with the live samples in a water bath in the dark at in situ temperature ($\pm 1^\circ$ C) for 12 to 24 h before the incubations were terminated (t₁). Triplicate bottles were used for the determination of the initial and final O₂ concentration. All the glassware was washed with 10% HCl and thoroughly rinsed with Milli-Q water prior to use. Sample handling and fixation followed the recommendations of Carrit and Carpenter [6]. Oxygen concentrations of corresponding t₀ and t₁ bottles were measured in one run. The amount of total iodine was determined spectrophotometrically at a wavelength of 456 nm on a Hitachi U-1100 spectrophotometer using a 1 cm flow-through cuvette at 20°C [27, 39]. To increase the sensitivity of the absorbance readings a 4-digit voltmeter (Metex M4650) was connected to the spectrophotometer. Calibration was performed by standard additions of iodate to distilled water, resulting in an empirical coefficient of 0.54455 nmol L⁻¹ cm⁻¹. The samples were withdrawn from the BOD bottles with a Teflon tube and a peristaltic pump (Gilson Minipuls) and directly fed to the flow-through cuvette of the spectrophotometer. The end of the tube was placed near the bottom of the bottles to avoid loss of volatile iodine. The spectrophotometer was zeroed against Milli-Q water. The coefficient of variation of the oxygen determinations was <0.5%. To convert oxygen consumption into carbon we used a respiratory quotient of 1.

Chlorophyll a determination—We gently filtered 1 L water samples collected from 3 depths (5 m, 15 m, 5 m above bottom) through 47 mm Whatman GF/F filters and stored these at -60° C until analysis (within 4 wk). Chl *a* was extracted in 10 mL of 90% acetone at -20° C in the dark for 48 h. Subsequently, the filters were sonicated on ice for 1 min (Branson, model 3200) and centrifuged to remove particles. The chl *a* concentration in the supernatant was determined fluorometrically with a Hitachi F-2000 fluorometer [18].

Primary production (PP) measurement—For particulate PP measurements, the protocol of Gieskes [16] was followed. In brief, before sunrise, seawater was collected from 5 m and transferred into 250 mL polycarbonate bottles, and 10 μ Ci of ¹⁴C-bicarbonate was added to each sample. Subsequently, the samples were placed in 6 tubes of different light transmittance using neutral-density filters. The tubes were held at surface water temperature ($\pm 1^\circ$ C) with a flow-through seawater system. Simulated light intensities ranged from 0.6 to 85% of the surface irradiance. The incubations were run for 24 h; thereafter, the samples were filtered

onto Whatman GF/F glass-fiber filters and fumed over HCl for 3 h. The filters were stored at -20°C and counted in a LKB Wallac liquid scintillation counter after adding 10 mL of Instagel II (Packard Canberra). Dark incorporation of ^{14}C -bicarbonate was subtracted from the incubations in the light. Combining light-attenuation measurements of the water column with the primary production measurements performed under the different light regimens allowed us to calculate integrated PP over the water column.

DOC measurement—Samples for DOC were filtered through rinsed $0.2\text{-}\mu\text{m}$ polycarbonate filters and sealed in pre-combusted (450°C for 4 h) glass ampoules after adding $50\ \mu\text{L}$ of 40% phosphoric acid. Subsequently, the samples were stored frozen at -20°C . DOC concentrations were determined by the high-temperature combustion method using a Shimadzu TOC-5000 analyzer [4]. Standards were prepared with potassium hydrogen phthalate (Nacalai Tesque, Inc. Kyoto, Japan). Ultrapure Milli-Q blanks were run before and after the sample analysis. The blank was on average $16.3 \pm 6.8\ \mu\text{mol L}^{-1}$ and the mean of triplicate injections was calculated for each sample. The average analytical precision of the instrument was $<3\%$.

Calculations and statistical analysis—As no significant differences were detectable between the different stations occupied during the individual cruises, individual parameters from each cruise were pooled. To relate bacterial biomass to phytoplankton biomass a carbon:chl *a* ratio of 30 was used [3]. Depth integration of PP, chl *a*, BP and BR was performed with the trapezoidal method. Areal PP was depth-integrated to the 1% light level while areal BP of unfiltered seawater and BR were integrated over the whole water column. Statistical analyses were done with the software package Statistica from Statsoft on log-transformed data whenever appropriate. For regressions, the ordinary least squares (OLS) and reduced major axis (RMA) regression were calculated. For comparison with other published empirical models OLS is presented, whereas RMA provides a better estimate of the true functional relationship [24 and references therein].

Results

Total versus 0.8- μm filtered bacterial abundance and BP—Bacterial abundance and BP obtained for the $0.8\ \mu\text{m}$ fraction closely correlated with the abundance and production in unfiltered seawater. However, filtration through $0.8\text{-}\mu\text{m}$ filters to exclude non-bacterial particles from the BR measurements reduced BP by $40 \pm 34\%$ compared to the raw seawater, except for July when BP in the $0.8\text{-}\mu\text{m}$ filtered fraction and unfiltered seawater was equal. With increasing abundance and production in the unfiltered seawater, the percentage of bacterial abundance and BP recovered in the $0.8\ \mu\text{m}$ fraction decreased. The loss of cells due to filtration did not change significantly between different months and bacterial abundance recovered in the $0.8\text{-}\mu\text{m}$ fraction was $63 \pm 21\%$ of that in the unfiltered seawater. We used the optical backscatter readings from the CTD to estimate the relative particle load of suspended matter in the water column. From April to August, turbidity was relatively constant and sharply increased in the fall. Total bacterial abundance was not correlated with turbidity, but BP measured in unfiltered seawater showed a weak negative correlation with increasing particle load (Spearman rank correlation: $r = 0.45$; $p < 0.05$; $n = 108$; data not shown). Below, BP is referred to as the production measured in $0.8\text{-}\mu\text{m}$ filtered seawater unless otherwise noted.

Relation of between bacterioplankton abundance, BP and BR—Bacterial abundance of $0.8\text{-}\mu\text{m}$ filtered samples increased from $0.66 \times 10^6\ \text{cells mL}^{-1}$ in April to $1.67 \times 10^6\ \text{cells mL}^{-1}$ in August and declined again toward winter (Fig. 3.2). BP and BR were significantly

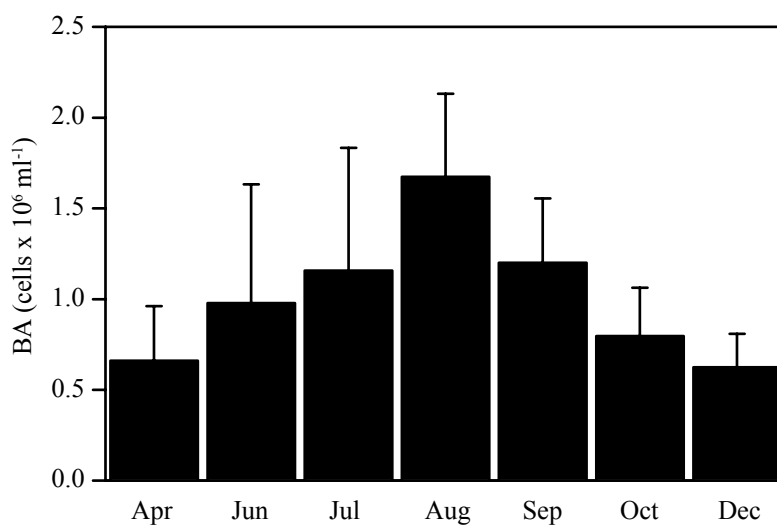


Figure 3.2: Dynamics in bacterioplankton abundance (BA) in the southern North Sea (0.8- μm pre-filtered). Data are averages per cruise; error bars indicate standard deviations of the mean; $n = 11$ to 28 for the different months.

correlated (Fig. 3.3, Table 3.1). BP and temperature explained 61% of the variation in BR by multiple regression analysis, while BP alone explained only 45% of the BR (Table 3.1). In contrast, BP could not be predicted reliably from BR and temperature (Table 3.1).

Cell-specific BP declined steadily from 0.6 $\text{fmol C cell}^{-1} \text{d}^{-1}$ in April to 0.06 $\text{fmol C cell}^{-1} \text{d}^{-1}$ in December. Cell-specific BR was rather constant and varied only between 1 and 2 $\text{fmol C cell}^{-1} \text{d}^{-1}$ (mean: $1.4 \pm 0.71 \text{ fmol C cell}^{-1} \text{d}^{-1}$) with a peak of 2.1 $\text{fmol C cell}^{-1} \text{d}^{-1}$ in August (data not shown).

Chlorophyll a and particulate primary production—Depth-integrated chl *a* concentrations were highest in April with $96.1 \pm 78.8 \text{ mg chl } a \text{ m}^{-2}$, and declined toward December to $21.5 \pm 6.6 \text{ mg chl } a \text{ m}^{-2}$ (Fig. 3.4). Particulate PP followed roughly the pattern of chl *a* (Fig. 3.4). The overall range of depth-integrated PP varied between 1.5 and 244.5 $\text{mmol C m}^{-2} \text{d}^{-1}$ over all the stations, with an annual average of $62.0 \pm 59.8 \text{ mmol C m}^{-2} \text{d}^{-1}$ ($n = 59$). Particulate PP was highest in April and July with 133 and 143 $\text{mmol C m}^{-2} \text{d}^{-1}$, respectively, and lowest in December with an average of 5 $\text{mmol C m}^{-2} \text{d}^{-1}$ (Fig. 3.4).

Relation between phytoplankton and bacterial biomass and activity—Over the seasonal cycle, depth-integrated total bacterial biomass (BB) was similar to depth-integrated phytoplankton biomass (PB), indicated by a BB:PB ratio of ~ 1 (data not shown). However, in April and June, algal biomass dominated over bacterial biomass, whereas bacterial biomass was almost twice as high as phytoplankton biomass in August. During the remaining months, the ratio of total bacterial biomass versus phytoplankton biomass was not different from 1 (Student's *t*-test for single means; $p < 0.001$) (Fig. 3.5). Depth-integrated BP in unfiltered seawater averaged over the different months ranged from 1 to 26 $\text{mmol C m}^{-2} \text{d}^{-1}$. Thus, while particulate PP varied over 2 orders of magnitude, total BP was much less variable (Fig. 3.6a). Total BP as percentage of particulate PP was highest after the bloom period in June and August, amounting to 49% of particulate PP. Over the annual cycle, total BP amounted to $16 \pm 9\%$ of PP. BR did not exhibit any particular trend with depth in the well-mixed study area (data not shown). As for BP, BR was much less variable than phytoplankton production. Depth-integrated

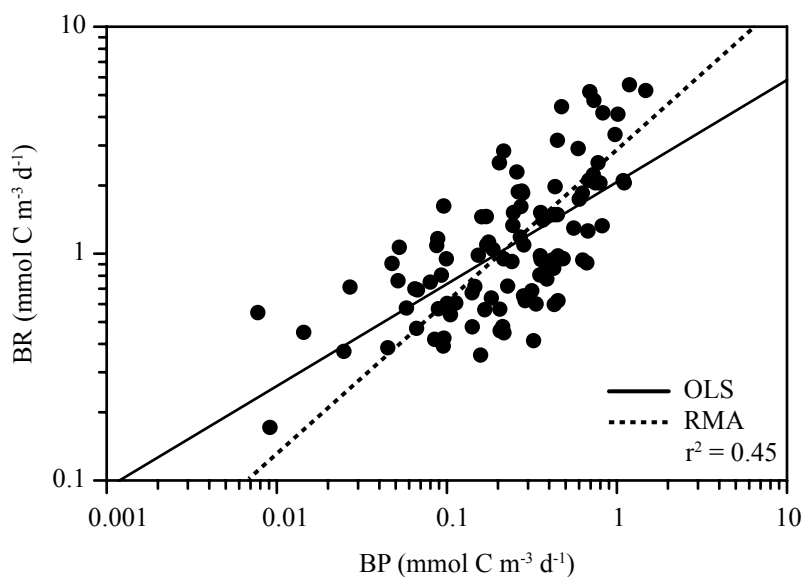


Figure 3.3: (BR) as a function of bacterial production (BP) obtained from 0.8- μm filtered seawater. Ordinary least-squares model (OLS; straight line; $r^2 = 0.45$) and reduced major-axis model (RMA; dotted line; $r^2 = 0.45$) are fitted to the data. Model statistics are presented in Table 3.1.

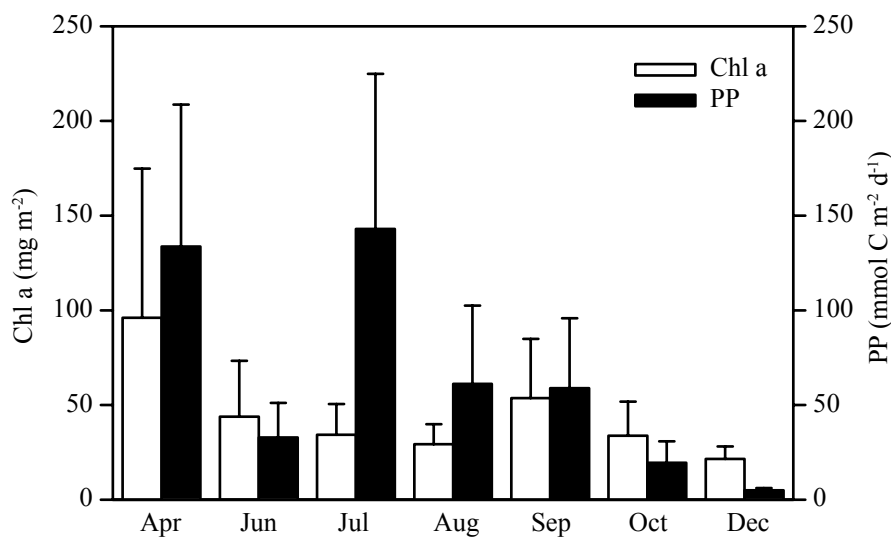


Figure 3.4: Monthly averages (+SD) of depth-integrated chlorophyll *a* (chl *a*) and primary production (PP) measured in the southern North Sea. $n = 4$ to 21 for PP and 11 to 31 for chl *a* for the different month.

Table 3.1: Regression statistics for volumetric and depth-integrated relationships of bacterial production (BP), bacterial respiration (BR), primary production (PP) and temperature (T). All variables were \log_{10} transformed except for temperature. Reduced major axis (RMA) is more appropriate than ordinary least-squares (OLS) when x is measured with error [24]. A conversion factor (CF) must be used when converting from log-transformed to arithmetic scale [45]. Volumetric units of BP and BR in $\text{mmol C m}^{-3} \text{ d}^{-1}$, depth-integrated units in $\text{mmol C m}^{-3} \text{ d}^{-1}$ and T in $^{\circ}\text{C}$; The regressions follow the form: $\log y = \log b_0 + x_1 \log b_1 (+x_2 b_2)$; SEE: standard error of the estimate used to calculate the CF; 95% CI: upper and lower (95%) confidence limit of the estimated parameters; r^2 : coefficient of determination; p : significance level.

Model	y	x_1	x_2	b_0	b_1	b_2	95% CI		r^2	p	SEE	CF		
							b_0	b_1						
Volumetric relationships														
OLS ($n=102$)	BR	BP		0.32 (0.04)	0.45 (0.05)		0.24	0.38	0.35	0.55	0.45	<0.001	0.23	1.15
RMA ($n=102$)	BR	BP		0.46 (0.04)	0.67 (0.05)		0.38	-0.54	0.57	0.77	0.45			
OLS ($n=102$)	BR	BP	T	-0.32 (0.11)	0.32 (0.05)	0.04 (0.01)				0.61		<0.001	0.19	
OLS ($n=102$)	BP	BR	T^*	-0.70 (0.18)	0.98 (0.15)	0.002 (0.01)				0.45		<0.001	0.34	
Depth-integrated relationships														
OLS ($n=55$)	BP	PP		-0.24 (0.16)	0.66 (0.09)		-0.56	0.09	0.48	0.85	0.50	<0.001	0.35	1.38
RMA ($n=55$)	BP	PP		-0.70 (0.16)	0.94 (0.09)		-1.03	-0.38	0.76	1.12	0.50			
OLS ($n=39$)	BR	PP		1.29 (0.12)	0.18 (0.07)		1.04	1.54	0.04	0.33	0.15	<0.01	0.23	1.16
RMA ($n=39$)	BR	PP		0.82 (0.12)	0.48 (0.07)		0.57	1.07	0.33	0.62	0.15			

† numbers in parenthesis are standard errors; n denotes the total number of measurements.

(*) not significant

PP explained only about 15% of the variation in depth-integrated BR (Fig. 3.6b, Table 3.1). About 40% of the depth-integrated BR measurements were higher than areal PP estimates. On a volumetric basis, cell-specific BP of the 0.8- μm filtered fraction significantly correlated with particulate PP (Spearman rank correlation: $r = 0.50$; $p < 0.05$; $n = 54$), while cell-specific BR was not related to particulate PP (Fig. 1.7).

Discussion

Generally, the southern North Sea is a highly dynamic system with strong tidal forces and a permanently well-mixed water column [32]. This probably led to the low spatial variability in phyto- and bacterioplankton biomass and activity we recorded.

It is well known that bottle confinement, such as in BOD bottles, can bias bacterioplankton respiration estimates. An increase in bacterial abundance and community shifts during the

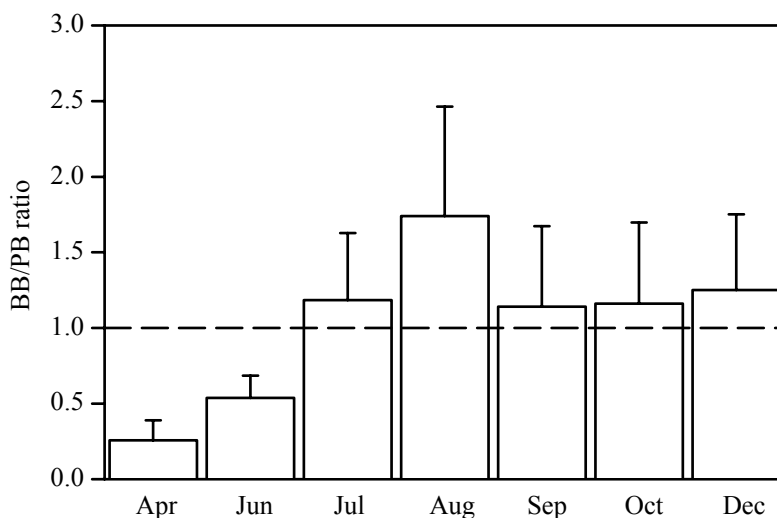


Figure 3.5: Monthly mean (+SD) ratio of depth-integrated total bacterial biomass (BB) and depth-integrated phytoplankton biomass (PB). Dashed line indicates unity.

course of incubations has been reported by several authors [15, 29]. However, Williams [50] found that despite an increase in bacterial abundance during the incubation, the respiration rate is usually linear over incubation times up to 48 h. In our study, the average bacterial turnover rate was $0.2 \pm 0.3 \text{ d}^{-1}$ and most of our incubations for respiration measurements were between 12 and 18 h and never longer than 24 h. Thus, it is unlikely that bacterial abundance increased substantially during our incubations, and consequently shifts in the community composition should also be minimal. Moreover, our regression of BR on BP (Fig. 3.3) was very similar to that obtained by Del Giorgio and Cole [7], further indicating that BR in the southern North Sea is in the range of published respiration rates.

Determining BGE depends on the choice of the conversion factor used in BP estimates and on the respiration quotient (RQ) used. While RQ values are assumed to center around 1 and are considered a minor source of error [7], conversion factors for BP generally vary over a much larger range [12, 21, 34, 41]. We scaled the bacterial production measurements with a conversion factor typical for coastal systems [34]; however, choosing a higher conversion factor of e.g. $3.1 \text{ kg C mol}^{-1}$ leucine [41] would increase our BGEs 1.7 times. We found a clear seasonal pattern in BGE, with a median value of 25% in the spring and summer (mean $25 \pm 9\%$; $n = 60$), decreasing to a median BGE of 14% in the fall (mean $15 \pm 7\%$; $n = 33$) and 5% in the winter (mean $6 \pm 3\%$; $n = 9$) (Fig. 3.8). The annual median BGE in the southern North Sea was 19% (mean $20 \pm 11\%$; $n = 102$), which is similar to the overall BGE of 20% obtained by Del Giorgio and Cole [8] compiling available information from marine surface waters and Carlson et al. [5] from a similar high-latitude system.

The seasonality in BGE is mainly driven by the changes in BP, which varies 6-fold from spring to winter. BR was generally rather uniform over the seasonal cycles although there was a slight increase in cell-specific BR towards the warmer summer months. A peak in respiration coinciding with the annual temperature maximum was reported previously [42 and references therein], but in our study this increase was too small to significantly influence the pattern of BGE. While Sherry et al. [40] found that the seasonal dynamics in BGE were influenced by bacterial respiration rather than production along an E-W transect in the NE Pacific, our finding

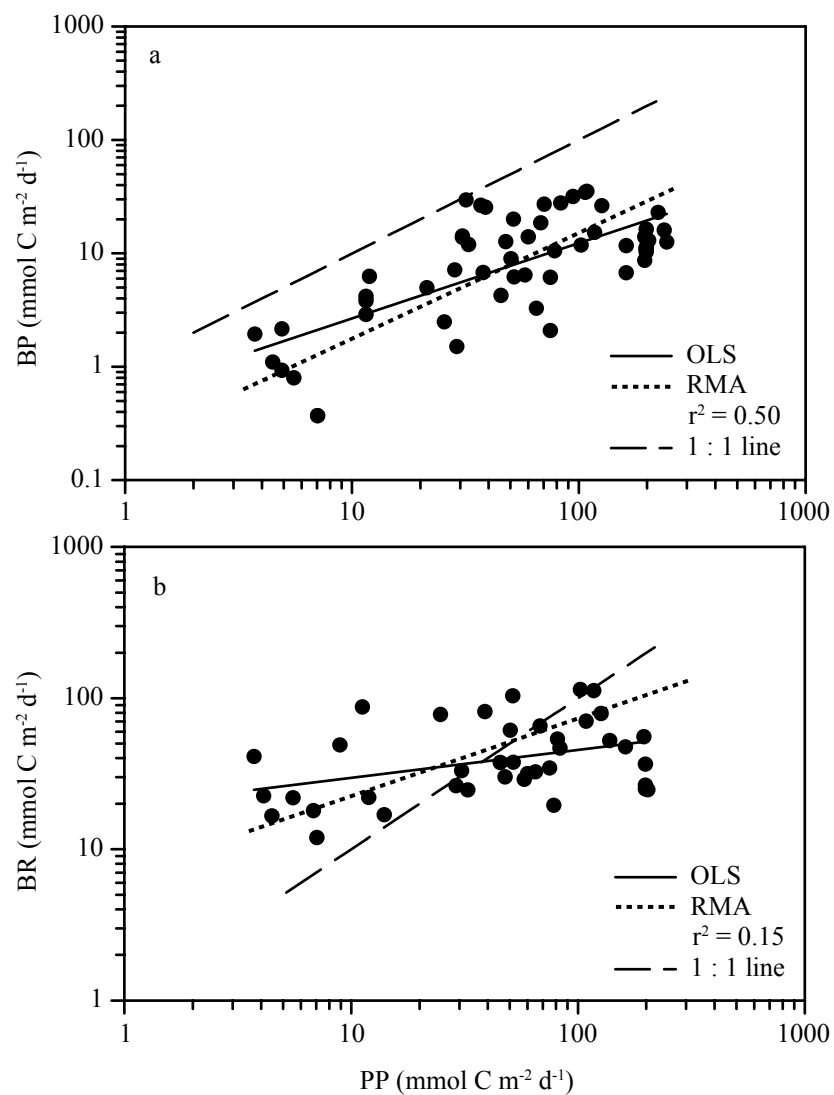


Figure 3.6: (a) Depth-integrated bacterial production (BP) of unfiltered seawaters and (b) depth-integrated bacterial respiration (BR) as a function of primary production (PP). Ordinary least-squares model (OLS) and reduced major-axis model (RMA) are fitted to the data. 1:1 line denotes unity of parameters. Model statistics see Table 3.1.

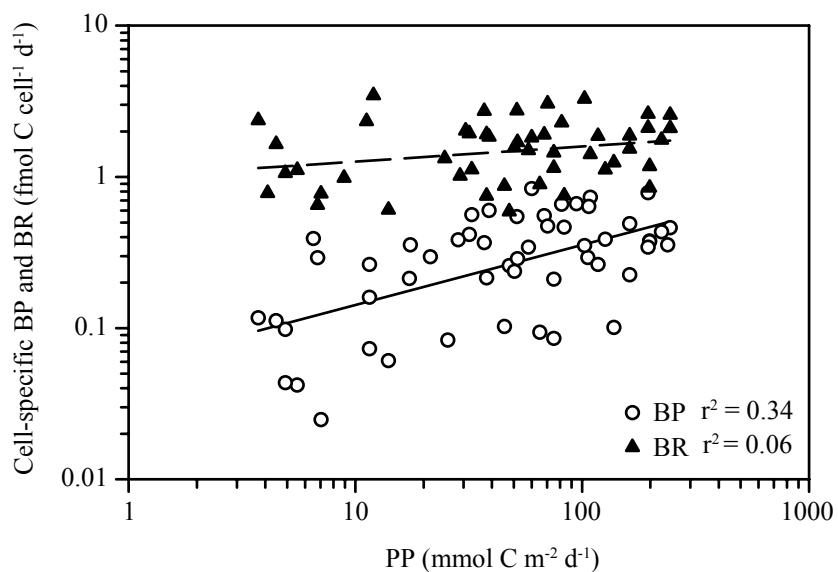


Figure 3.7: Cell-specific bacterial production (BP) and respiration (BR) for $0.8\text{-}\mu\text{m}$ filtered seawater as a function of particulate primary production (PP).

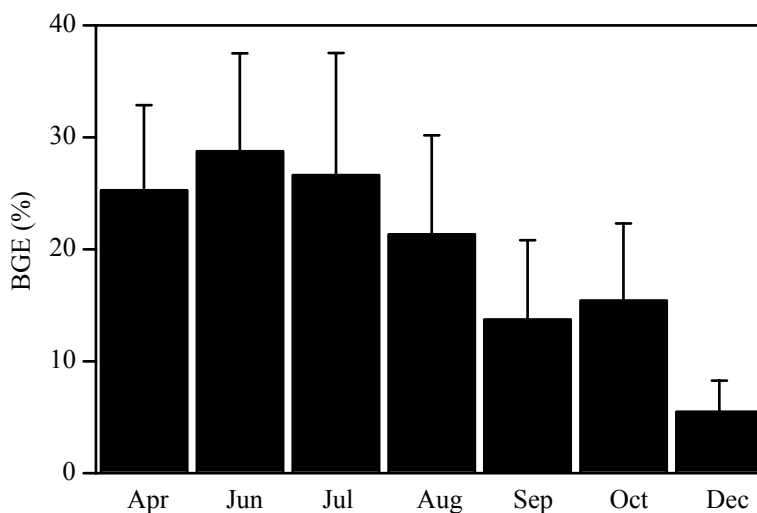


Figure 3.8: Seasonal dynamics of bacterial growth efficiency (BGE) calculated as $\text{BGE} = \text{BP}/(\text{BP} + \text{BR}) \times 100$ from April to December. Means (+SD); $n = 9$ to 21 estimates for the different months.

Table 3.2: Monthly averages of mixed-layer depth (m), salinity (S, PSU), temperature (T , °C) and DOC concentration ($\mu\text{mol L}^{-1}$).

Month	Depth (m)	S	T (°C)	DOC ($\mu\text{mol L}^{-1}$)
Apr	40	30.01	8.8	72.7
($n = 32$)	(20)	(1.19)	(0.8)	(20.5)
Jun	29	34.12	12.2	139.9
($n = 17$)	(7)	(0.29)	(0.3)	(34.7)
Jul	28	34.63	14.9	86.5
($n = 20$)	(6)	(0.28)	(0.2)	(9.6)
Aug	33	34.28	18.4	265.3
($n = 23$)	(7)	(0.30)	(0.5)	(89.0)
Sep	28	34.31	16.6	87.1
($n = 17$)	(6)	(0.21)	(1.2)	(19.9)
Oct	31	34.48	13.1	107.6
($n = 31$)	(8)	(0.23)	(1.2)	(19.2)
Dec	30	34.55	10.3	152.2
($n = 11$)	(8)	(0.48)	(0.9)	(43.5)

† numbers in parenthesis are standard errors;
 n denotes the total number of measurements.

is in agreement with that of Del Giorgio and Cole [8], who concluded that BP was mainly determining BGEs.

Reports on temperature-dependence of bacterioplankton metabolism are contradictory. White et al. [48] used a multiple regression including bacterial abundance and temperature to explain the variability in BP. Pomeroy and Wiebe [30] argued that temperature and substrate availability are both limiting factors for heterotrophic bacteria, while Del Giorgio and Cole [7] concluded that temperature was not an important factor controlling bacterioplankton activity. Over the temperature range of our study (9°C to 18°C; Table 3.2), temperature explained only around 32% of the variability in bacterial production. Thus, in the southern North Sea temperature does not explain the seasonality in BP, and the model from Rivkin and Legendre [35] to derive BGE from BP and temperature cannot be applied here, as they used a much larger temperature range. In a study in the northern North Sea, Robinson et al. [38] calculated BR from the model of Rivkin and Legendre [35], and the resulting estimate grossly underestimated the bacterial contribution to total respiration compared to the model of Del Giorgio and Cole [7] which gave more a reasonable value of ~60% of total respiration.

Other factors causing seasonal fluctuations in BP are changes in the concentrations of readily utilizable dissolved organic matter (DOM) due to variable extracellular release of phytoplankton, grazing activity and/or allochthonous input of organic material via rivers. In our study, phytoplankton biomass (measured as chl a) was not related to bacterial abundance, however, a positive relationship was found between PP and specific BP (Fig. 3.7).

The lowest mean DOC concentrations of around 73 $\mu\text{mol L}^{-1}$ were measured in the spring and DOC peaked in August with an average of 265 $\mu\text{mol L}^{-1}$, but no clear seasonal pattern was apparent (Table 3.2). Søndergaard and Middelboe [43] estimated that in marine environments around 19% of the bulk DOC is labile and used by prokaryotes within 1 and 2 wk. The

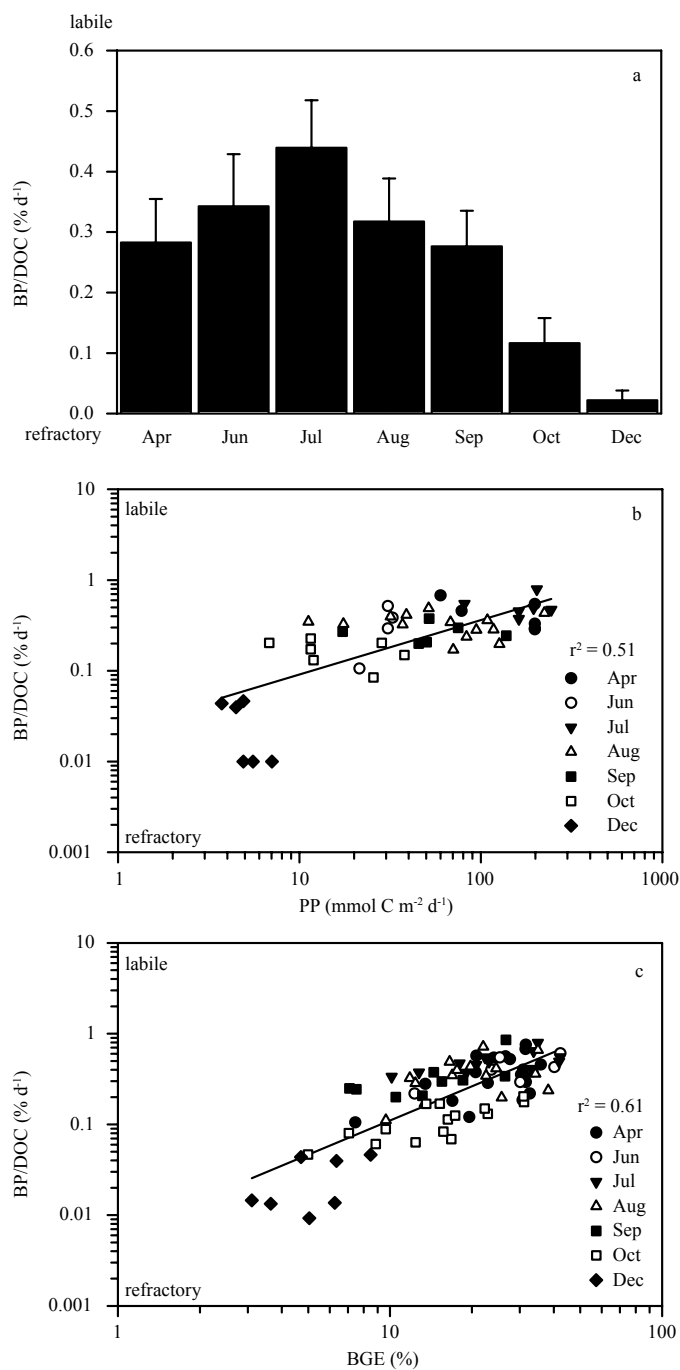


Figure 3.9: Total bacterial production (BP; mmol C m⁻³ d⁻¹) normalized to dissolved organic carbon (DOC; mmol C m⁻³) to indicate relative DOC availability (BP/DOC × 100). (a) Distribution of DOC available over the seasonal cycle, showing ratio of monthly averages; means (+SD). (b) Relation of depth-integrated primary production and available DOC. (c) Dependence of bacterial growth efficiency (BGE) on DOC availability.

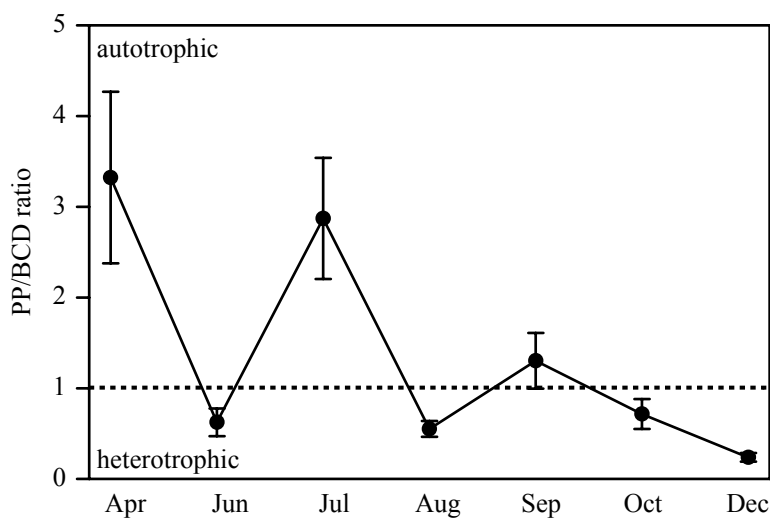


Figure 3.10: Ratio between particulate primary production (PP) and total bacterial carbon demand (BCD) over the seasonal cycle. Means (+SD) of 10 estimates.

more labile components of the DOC pool are directly or indirectly fueled by the release from phytoplankton, and this DOM is remineralized within hours [13, 33]. Natural DOC consists of a continuum of size classes of differing diagenetic state [1], which makes it difficult to directly relate bulk DOC measurements to BP and growth. As a measure of the availability of labile DOC we used the ratio of BP to bulk DOC [25]. In the spring and summer, relatively more labile DOC is available, as indicated by a higher ratio between BP and bulk DOC concentration than in the winter (Fig. 3.9a). The ratio of BP to DOC, as a function of phytoplankton production, indicates that the increase in the relative availability of DOC is related to increased PP (Fig. 3.9b). Therefore, we conclude that the BP in the southern North Sea is mainly coupled to the seasonal dynamics in primary production and that BGE is directly linked to the bioavailability of DOC and indirectly to PP (Fig. 3.9c). While such a conclusion would be expected for open-ocean systems, for a shelf sea such as the North Sea this conclusion is not as obvious, considering the large input of terrigenous material via rivers.

To assess the relative importance of autotrophic versus heterotrophic processes, the ratio of phytoplankton production to bacterial carbon demand (BCD) based on the total BP measurements was calculated. We used the depth-integrated values of PP and BR because, as Williams [51] pointed out, PP should be considered on an areal basis to account for the solar radiation dependency of PP. A considerable part of the phytoplankton production may be lost to the dissolved phase due to extracellular release of DOC [20]. Thus our PP measurements are likely to underestimate actual total phytoplankton production [46]. The PP:BCD ratio was significantly higher than 1 in April and July while in August and December the southern North Sea was heterotrophic (Student's *t*-test for single means; $p < 0.001$) (Fig. 3.10). The remaining months exhibited roughly a metabolic balance, i.e. the ratio was not significantly different from 1 (Fig. 3.10). This pattern generally agrees with a recent study of Thomas et al. [47], who measured fluxes of CO_2 in the North Sea on a seasonal scale. They found that the southern part was slightly heterotrophic throughout the year, except in spring when CO_2 uptake from the atmosphere prevailed.

Recently, evidence has been presented that open ocean systems are slightly heterotrophic

[9, 11, 51]. In marginal seas such as the North Sea, short-term trophic imbalances might be compensated by terrestrial input via rivers and terrestrial runoff. In the southern North Sea, the rivers Humber, Thames and the Rhine provide considerable amounts of DOM [Borges et al. unpublished data]; thus, potentially, even long periods of net system heterotrophy would be possible. Decreasing PP toward the winter was paralleled by decreasing BGE. However, in the spring and early summer the supply of autochthonous DOM supports a relatively high BGE until most of the labile DOM is depleted in August.

In summary, we have shown that seasonality in BP is mainly responsible for the dynamics in BGE which, in turn, is influenced by the bioavailability of the DOC. Remineralization of organic carbon is the main function of prokaryotes in the carbon cycling and, as such, is relatively stable over the annual cycle.

Acknowledgements

We thank Jan Hegeman, Svier Oosterhuis, Anna Nordeloos and Santiago Gonzalez for the primary production, chlorophyll *a* and DOC data. Special thanks go to Goovert van Noort and Christian Winter for help with analysis of the bacterial abundance data and to Martien Baars for his excellent job as chief scientist during the Bloom and Plume project and to the captain and crew of the R/V *Pelagia*. This work was supported by the Dutch Science Foundation (NWO-ALW) project 811.33.002 and the European Commission through the COMET project.

Bibliography

- [1] Amon RMW, Benner R. 1996. Bacterial utilization of different size classes of dissolved organic matter. *Limnology and Oceanography* 41: 41-51
- [2] Baars MA, Oosterhuis S, Kuipers B. 2003. *Plume & Bloom: Water mass patterns and nutrient dynamics in the central part of the southern Bight*, Royal Netherlands Institute for Sea Research, Texel
- [3] Banse K. 1977. Determining the carbon-to-chlorophyll ratio of natural phytoplankton. *Marine Biology* 41: 199-212
- [4] Benner R, Strom M. 1993. A critical evaluation of the analytical blank associated with DOC measurements by high-temperature catalytic oxidation. *Marine Chemistry* 41: 153-60
- [5] Carlson CA, Bates NR, Ducklow HW, Hansell DA. 1999. Estimation of bacterial respiration and growth efficiency in the Ross Sea, Antarctica. *Aquatic Microbial Ecology* 19: 229-44
- [6] Carritt DE, Carpenter JH. 1966. Comparison and evaluation of currently employed modifications of Winkler method for determining dissolved oxygen in seawater - a NASCO Report. *Journal of Marine Research* 24: 287-318
- [7] Del Giorgio PA, Cole JJ. 1998. Bacterial growth efficiency in natural aquatic systems. *Annual Review of Ecology and Systematics* 29: 503-41
- [8] Del Giorgio PA, Cole JJ. 2000. Bacterial energetics and growth efficiency. In *Microbial Ecology of the Oceans*, ed. DL Kirchman, pp. 289-325. New York: Wiley-Liss

- [9] Del Giorgio PA, Cole JJ, Cimperis A. 1997. Respiration rates of bacteria exceed phytoplankton in unproductive aquatic systems. *Nature* 385: 148-51
- [10] Del Giorgio PA, Duarte CM. 2002. Respiration in the open ocean. *Nature* 420: 379-84
- [11] Duarte CM, Agusti S. 1998. The CO₂ balance of unproductive aquatic ecosystems. *Science* 281: 234-6
- [12] Ducklow HW, Kirchman DL, Quinby HL. 1992. Bacterioplankton cell growth and macromolecular synthesis in seawater cultures during the North Atlantic spring phytoplankton bloom, May, 1989. *Microbial Ecology* 24: 125-44
- [13] Fuhrman J. 1987. Close coupling between release and uptake of dissolved free amino acids in seawater studied by an isotope dilution approach. *Marine Ecology Progress Series* 37: 45-52
- [14] Gattuso J-P, Frankignoulle M, Wollast R. 1998. Carbon and carbonate metabolism in coastal aquatic ecosystems. *Annual Review of Ecology and Systematics* 29: 405-34
- [15] Gattuso J-P, Peduzzi S, Pizay M-D, Tonolla M. 2002. Changes in freshwater bacterial community composition during measurements of microbial and community respiration. *Journal of Plankton Research* 24: 1197-206
- [16] Gieskes WWC, Kraay GW, Baars MA. 1979. Current C-14 methods for measuring primary production - gross underestimates in oceanic waters. *Netherlands Journal of Sea Research* 13: 58-78
- [17] Hansell DA, Ducklow HW, Macdonald AM, Baringer MON. 2004. Metabolic poise in the North Atlantic Ocean diagnosed from organic matter transports. *Limnology and Oceanography* 49: 1084-94
- [18] Holm-Hansen O, Lorenzen CL, Holmes RW, Strickland JDH. 1965. Fluorometric determination of chlorophyll. *Journal du Conseil permanent International pour l'Exploration de la Mer* 30: 3-15
- [19] Jahnke RA, Craven DB. 1995. Quantifying the role of heterotrophic bacteria in the carbon cycle - a need for respiration rate measurements. *Limnology and Oceanography* 40: 436-41
- [20] Kaltenböck E, Herndl GJ. 1992. Ecology of amorphous aggregations (marine snow) in the Northern Adriatic Sea: IV. Dissolved nutrients and the autotrophic community associated with marine snow. *Marine Ecology Progress Series* 87: 147-59
- [21] Kirchman DL. 1992. Incorporation of thymidine and leucine in the subarctic Pacific: application to estimating bacterial production. *Marine Ecology Progress Series* 82: 301-9
- [22] Lee S, Fuhrman JA. 1987. Relationships between biovolume and biomass of naturally derived marine bacterioplankton. *Applied and Environmental Microbiology* 53: 1298-303
- [23] Lemée R, Rochelle-Newall E, Van Wambeke F, Pizay M-D, Rinaldi P, Gattuso J-P. 2002. Seasonal variation of bacterial production, respiration and growth efficiency in the open NW Mediterranean Sea. *Aquatic Microbial Ecology* 29: 227-37

- [24] McArdle BH. 2003. Lines, models, and errors: Regression in the field. *Limnology and Oceanography* 48: 1363-6
- [25] Obernosterer I, Reitner B, Herndl GJ. 1999. Contrasting effects of solar radiation on dissolved organic matter and its bioavailability to marine bacterioplankton. *Limnology and Oceanography* 44: 1645-54
- [26] Otto L, Zimmermann JTF. 1990. Physical oceanography of the North Sea. *Netherlands Journal of Sea Research* 26: 163-238
- [27] Pai S-C, Gong G-C, Liu K-K. 1993. Determination of dissolved oxygen in seawater by direct spectrophotometry of total Iodine. *Marine Chemistry* 41: 343-51
- [28] Pernthaler A, Preston CM, Pernthaler J, DeLong EF, Amann R. 2002. Comparison of fluorescently labeled oligonucleotide and polynucleotide probes for the detection of pelagic marine bacteria and archaea. *Applied and Environmental Microbiology* 68: 661-7
- [29] Pomeroy LR, Sheldon JE, Sheldon WM. 1994. Changes in bacterial numbers and leucine assimilation during estimations of microbial respiratory rates in seawater by the precision Winkler method. *Applied and Environmental Microbiology* 60: 328-32
- [30] Pomeroy LR, Wiebe WJ. 2001. Temperature and substrates as interactive limiting factors for marine heterotrophic bacteria. *Aquatic Microbial Ecology* 23: 187-204
- [31] Porter KG, Feig YS. 1980. The use of DAPI for identifying and counting aquatic microflora. *Limnology and Oceanography* 25: 943-8
- [32] Postma H, Zijlstra JJ. 1988. *Continental shelves*. New York: Elsevier. 421 pp.
- [33] Rich J, Gosselin M, Sherr EB, Sherr BF, Kirchman D. 1997. High bacterial production, uptake and concentrations of dissolved organic matter in the central Arctic Ocean. *Deep-Sea Research Part II* 44: 1645-63
- [34] Riemann B, Bell RT, Jørgensen NOG. 1990. Incorporation of thymidine, adenine and leucine into natural bacterial assemblages. *Marine Ecology Progress Series* 65: 87-94
- [35] Rivkin RB, Legendre L. 2001. Biogenic carbon cycling in the upper ocean: Effects of microbial respiration. *Science* 291: 2398-400
- [36] Robinson C, Archer SD, Williams PJIB. 1999. Microbial dynamics in coastal waters of East Antarctica: plankton production and respiration. *Marine Ecology Progress Series* 180: 23-36
- [37] Robinson C, Serret P, Tilstone G, Teira E, Zubkov MV, et al. 2002. Plankton respiration in the Eastern Atlantic Ocean. *Deep-Sea Research Part I* 49: 787-813
- [38] Robinson C, Widdicombe CE, Zubkov MV, Tarran GA, Miller AEJ, Rees AP. 2002. Plankton community respiration during a coccolithophore bloom. *Deep-Sea Research Part II* 49: 2929-50

- [39] Roland F, Caraco NF, Cole JJ, Del Giorgio PA. 1999. Rapid and precise determination of dissolved oxygen by spectrophotometry: evaluation of interference from color and turbidity. *Limnology and Oceanography* 44: 1148-54
- [40] Sherry ND, Boyd PW, Sugimoto K, Harrison PJ. 1999. Seasonal and spatial patterns of heterotrophic bacterial production, respiration, and biomass in the subarctic NE Pacific. *Deep-Sea Research Part II* 46: 2557-78
- [41] Simon M, Azam F. 1989. Protein content and protein synthesis rates of planktonic marine bacteria. *Marine Ecology Progress Series* 51: 201-13
- [42] Smith EM, Kemp WM. 1995. Seasonal and regional variations in plankton community production and respiration for Chesapeake Bay. *Marine Ecology Progress Series* 116: 217-31
- [43] Søndergaard M, Middelboe M. 1995. A cross system analysis of labile dissolved organic carbon. *Marine Ecology Progress Series* 118: 283-94
- [44] Søndergaard M, Williams PJIB, Cauwet G, Riemann B, Robinson C, et al. 2000. Net accumulation and flux of dissolved organic carbon and dissolved organic nitrogen in marine plankton communities. *Limnology and Oceanography* 45: 1097-111
- [45] Sprugel DG. 1983. Correcting for bias in log-transformed allometric equations. *Ecology* 64: 209-10
- [46] Teira E, Pazo MJ, Pablo S, Emilio F. 2001. Dissolved organic carbon production by microbial populations in the Atlantic Ocean. *Limnology and Oceanography* 46: 1370-7
- [47] Thomas H, Bozec Y, Elkalay K, de Baar HJW. 2004. Enhanced open ocean storage of CO₂ from shelf sea pumping. *Science* 304: 1005-8
- [48] White PA, Kalff J, Rasmussen J. B., Gasol JM. 1991. The effect of temperature and algal biomass and bacterial production and specific growth rate in freshwater and marine habitats. *Microbial Ecology* 21: 99-118
- [49] Whitman WB, Coleman DC, Wiebe WJ. 1998. Prokaryotes: the unseen majority. *Proceedings of the National Academy of Sciences of the United States of America* 95: 6578-83
- [50] Williams PJIB. 1981. Microbial contributions to overall marine plankton metabolism: direct measurements of respiration. *Oceanologica Acta* 4: 359-70
- [51] Williams PJIB. 1998. The balance of plankton respiration and photosynthesis in the open oceans. *Nature* 394: 55-7

Chapter 4

Prokaryotic respiration and production in the meso- and bathypelagic realm of the eastern and western North Atlantic basin¹

Thomas Reinthaler, Hendrik van Aken, Cornelis Veth, Philippe Lebaron, Javier Arístegui, Carol Robinson, Peter J. le B. Williams and Gerhard J. Herndl

We measured prokaryotic production and respiration in the major water masses of the North Atlantic down to a depth of ~4000 m by following the progression of the two branches of North Atlantic Deep Water (NADW) in the oceanic conveyor belt. Prokaryotic abundance decreased exponentially with depth from 3 to 0.4×10^5 cells mL⁻¹ in the eastern basin and from 3.6 to 0.3×10^5 cells mL⁻¹ in the western basin. Prokaryotic production measured via ³H-leucine incorporation showed a similar pattern as prokaryotic abundance and decreased with depth from 9.2 to $1.1 \mu\text{mol C m}^{-3} \text{ d}^{-1}$ in the eastern and from 20.6 to $1.2 \mu\text{mol C mm}^{-3} \text{ d}^{-1}$ in the western basin. Prokaryotic respiration, measured via oxygen consumption, ranged from about 300 to $60 \mu\text{mol C m}^{-3} \text{ d}^{-1}$ from ~100 m depth to the NADW. Prokaryotic growth efficiencies of ~2% in the deep waters (depth range ~1200–4000 m) indicate that the prokaryotic carbon demand exceeds dissolved organic matter input and surface primary production by ~2 orders of magnitude. Cell-specific prokaryotic production was rather constant throughout the water column, ranging from 15 to 32×10^{-3} fmol C cell⁻¹ d⁻¹ in the eastern and from 35 to 58×10^{-3} fmol C cell⁻¹ d⁻¹ in the western basin. Along with increasing cell-specific respiration towards the deep water masses and the relatively short turnover time of the prokaryotic community in the dark ocean (34–54 days), prokaryotic activity in the meso- and bathypelagic North Atlantic is higher than previously assumed.

Introduction

Over the past three decades, the role of the ocean in the carbon cycle has been intensively studied, focusing on the food web structure and trophic interactions between the main functional

¹Accepted at *Limnol. and Oceanogr.*

groups of the pelagic food web inhabiting the upper ocean [42] and on the production and remineralization of particulate (POC) and dissolved organic carbon (DOC) [13, 29]. A large dataset on phytoplankton organic carbon production and the export flux of carbon from the euphotic layer to the open ocean seafloor has been acquired mainly via bulk POC and DOC concentrations in the meso- and bathypelagic layers and by sediment trap studies. Based on the decreasing POC and DOC concentrations with depth, the carbon utilization of the meso- and bathypelagic realm has been estimated and modeled [34, 46].

The meso- and bathypelagic realm comprises ~75% of the volume of the global ocean, however, little is known about the microbial activity below 200 m depths due to the scarcity of direct rate measurements. Generally, these deep water layers are considered to support only limited microbial activity. This is deduced mainly from the refractory nature of the bathypelagic dissolved organic matter (DOM) pool with an average age of ~4000–6000 yr [8, 10], and the low temperature at these depths (~2–4°C), retarding metabolic rates. In concert, these two characteristic features of the deep sea led to the commonly accepted view that bathypelagic microbial activity approaches zero.

Prokaryotes are, however, numerous throughout the ocean [58] although prokaryotic abundance typically declines by two orders of magnitude from the surface to the deep oceanic waters [44, 50]. Furthermore, it has been recognized that prokaryotes, notably Bacteria play a key role in the decomposition of non-living organic particles in the surface layers [22] and in mesopelagic waters [17, 37]. The latter two studies presented evidence, that POC concentrations decrease with depth more rapidly than one would deduce from bacterial activity measurements. This suggests that particle-associated bacteria solubilize more POC to DOC than they utilize. This hypothesis has been coined the ‘particle decomposition paradox’ [37]. One cannot rule out, however, that mesopelagic zooplankton are consuming part of this POC pool and thus, account for the difference between mesopelagic bacterial carbon demand and the decrease in POC concentration with depth [7].

Bacterial carbon demand and remineralization rates are often deduced from bacterial production measurements, calculating respiration from an average bacterial growth yield of ~20–30% [23, 45]. Thus, the major fraction of the carbon flow mediated by heterotrophic bacteria, i.e., respiration, is deduced from measurements of a minor fraction, i.e., organic carbon assimilation. Recently, however, oceanic respiration has received considerable attention as it has been recognized as one of the major, albeit poorly constrained, components of the carbon flux in the biosphere [20, 61]. Model estimates suggest, that dark ocean respiration might be higher than hitherto assumed [21]. A higher dark ocean respiration rate than predicted from POC export can only be resolved if fluxes of DOC are much more important, or, if respiration of the dark ocean is grossly overestimated. There is evidence that DOC accumulating in the euphotic layer during the production period is exported into the mesopelagic realm during winter overturning of the water column [14]. The magnitude to which this occurs on a large scale in the open ocean is still unknown and most of the exported DOC is probably respired in the upper mesopelagic zone [3].

For the subtropical North East Atlantic and the Gulf of Mexico, mean mesopelagic respiration amounted to 0.2 ± 0.1 and 0.9 ± 0.6 mmol O₂ m⁻³ d⁻¹, respectively [4, 11]. The few studies on dark ocean respiration rates mainly report potential rates derived from measurements of the activity of the electron transport system (ETS) [2, 47]. Indirectly, dark ocean respiration rates can be obtained from tracer studies [24] and POC fluxes estimated from sediment trap deployments [1].

It has been shown recently, that the global ocean's interior harbors both Bacteria and Archaea [32, 39] with both groups of prokaryotes incorporating leucine. However, Archaea also incorporate inorganic carbon and dominate the total prokaryotic abundance in the meso- and bathypelagic realm of the North Atlantic [32]. Thus, the measured leucine incorporation of deep water prokaryotes is a measure of prokaryotic biomass production rather than restricted to bacterial biomass synthesis only. Therefore, the term 'prokaryotic production' is more appropriate instead of the commonly used term 'bacterial production'. Likewise, the term 'prokaryotic respiration' is used in this paper due to the dominance of Archaea in the deep waters of the North Atlantic although it is unknown at present to what extent Archaea actually contribute to the oxygen consumption of the deep water prokaryotic community.

The aim of this study was to assess prokaryotic respiration and production in the dark ocean, following the eastern and western branch of the North Atlantic Deep Water (NADW) from its origin over 30–50 years of its progression in the oceanic conveyor belt system. We measured prokaryotic production and respiration as prokaryotes are the main drivers of the carbon cycling in the dark ocean along with other basic physicochemical parameters. Specifically, we focused on the major water masses of the North Atlantic down to a depth of ~4000 m. Generally, we found a more active prokaryotic community than expected based on the few published reports on meso- and bathypelagic bacterial activity.

Methods

Study site and sampling—The eastern and western branch of the North Atlantic Deep Water (NADW) were followed with R/V *Pelagia* from near its source of origin in the Greenland Iceland Norwegian Sea (GIN-Sea) over two stretches, each more than 4000 km long and corresponding to 30–50 years of NADW progression in the oceanic conveyor belt system (Fig. 4.1). The TRANSAT-I cruise (September 2002) followed a track from 62.8°N, 13.1°W to 35.3°N, 28.6°W in the eastern basin and TRANSAT-II (May 2003) from 62.5°N, 30.3°W to 37.7°N, 69.7°W in the western basin of the North Atlantic. In total, 42 stations were occupied during TRANSAT-I and 36 stations during the TRANSAT-II cruise. Water was collected with a CTD rosette sampler holding 24 times 12-L NOEX bottles. Samples were taken from the main water masses encountered during the two cruises and from ~100 m depth (thereafter termed subsurface layer, SSL) and the oxygen minimum zone (O₂-min). The main water masses sampled were the Labrador Seawater (LSW), the Iceland Scotland Overflow Water (ISOW), the North Atlantic Deep Water (NADW) and the Denmark Strait Overflow Water (DSOW). These specific water masses were identified based on their temperature and salinity characteristics (Table 4.1) and their oxygen concentrations, using a Seabird SBE43 oxygen sensor mounted on the CTD frame. From these water masses, raw seawater samples were collected for total organic carbon (TOC), prokaryotic abundance and production and ETS measurements. For prokaryotic respiration assays, seawater was filtered over rinsed 0.6- μ m polycarbonate filters (Millipore) to exclude non-prokaryotic particles. Prokaryotic abundance and production were also determined in this 0.6- μ m filtered seawater. Additional samples were taken to determine the relative contribution and activity of Bacteria and Archaea on the prokaryotic community using catalyzed reporter deposition fluorescence in situ hybridization combined with micro-autoradiography (MICRO-CARD-FISH). Results of these measurements are reported elsewhere [see 32, 59].

Prokaryotic abundance—One cm⁻³ samples of unfiltered and 0.6- μ m filtered seawater were fixed with 37% of 0.2- μ m filtered (Acrodisc, Gelman) formaldehyde (2% final conc.), stained

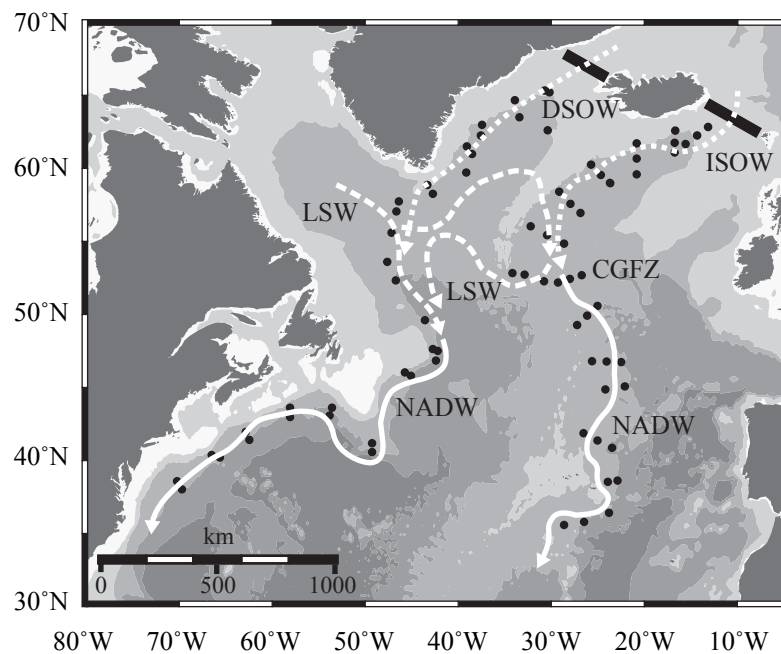


Figure 4.1: Map of the study area in the North Atlantic. Dots indicate the individual stations occupied during TRANSAT-I (eastern basin; Sep 2002) and TRANSAT-II (western basin; May 2003). Lines and arrows indicate the flow of the main water masses (for abbreviations of water masses see Table 1). Filled black bars denote position of the Greenland–Iceland–Scotland Ridge. Charlie-Gibbs Fracture Zone (CGFZ).

with 0.5 μL of SYBR Green I (Molecular Probes) at room temperature in the dark for 15 min and subsequently analyzed on a FACSCalibur flow cytometer (BD Biosciences) [43]. Counts were performed with the argon laser at 488 nm set at an energy output of 15 mW. Prokaryotic cells were enumerated according to their right-angle light scatter and green fluorescence measured at 530 nm. Prokaryotic carbon biomass was calculated assuming a carbon content of 10 fg C per cell which seems more appropriate for deep sea prokaryotes than the generally used 20 fg carbon per cell [23].

Prokaryotic production—Prokaryotic production in the unfiltered and 0.6- μm filtered seawater was measured by ^3H -leucine incorporation (specific activity: $595.7 \times 10^{10} \text{ Bq mmol}^{-1}$ for TRANSAT-I and $558.7 \times 10^{10} \text{ Bq mmol}^{-1}$ for TRANSAT-II; final concentration 10 nmol L^{-1}). Two 10–40 mL samples and 1 blank were incubated in the dark. The blank was fixed immediately with concentrated 0.2- μm filtered formaldehyde (4% final concentration, v/v) 10 min prior to adding the tracer. After incubating the samples and the blank at in situ temperature for 4–12 h, depending on the expected activity, the samples were fixed with formaldehyde (4% final concentration), filtered onto 0.2- μm nitrocellulose filters (Millipore HA; 25mm diameter) and rinsed twice with 5 mL ice-cold 5% trichloroacetic acid (Sigma Chemicals) for 5 min. The filters were dissolved in 1 mL ethylacetate and after 10 min, 8 mL of scintillation cocktail (Insta-Gel Plus, Canberra Packard) was added. The radioactivity incorporated into cells was counted in a liquid scintillation counter (LKB Wallac, Model 1212). Leucine incorporated into prokaryotic biomass was converted to carbon production using the theoretical conversion factor of 3.1 kg C mol^{-1} leu assuming a two-fold isotope dilution [53].

Prokaryotic respiration—The 0.6- μm filtrate was collected in an acid-rinsed (10% HCl and three times with 0.6- μm filtered sample water) glass flask and subsequently transferred to calibrated borosilicate glass BOD-bottles with a nominal volume of 120 cm^3 using silicon tubing fixed to the spigot of the glass flask overflowing the bottles with at least three times the BOD bottle volume. For the determination of the initial O_2 concentration (t_0), samples were fixed immediately with Winkler reagents and incubated together with the live samples in water baths in the dark at in situ temperature ($\pm 1^\circ\text{C}$) for 34 to 96 h when the incubations were terminated (t_1). Triplicate bottles were used for the determination of the initial and final O_2 concentration. All the glassware was washed with 10% HCl and thoroughly rinsed with Milli-Q water prior to use. Oxygen concentrations of the t_0 and t_1 bottles were measured spectrophotometrically in a single run [49] following the standard protocol for the determination of oxygen by Winkler titration [15]. Measurements were done in a temperature-controlled laboratory container (set at 20°C) on a Hitachi U-3010 spectrophotometer with four digits read-out, using a 1 cm flow-through cuvette of 360 μL volume. The samples were withdrawn from the BOD bottles with a peristaltic pump (Gilson Minipuls) pumping the sample through the flow-through cuvette of the spectrophotometer via a Teflon tubing. To avoid loss of volatile iodine, the bottles were covered with parafilm and the lower end of the sampling tube was placed close to the bottom of the BOD bottle. To prevent a photochemical change in color of iodine due to ambient light, the bottles were covered with dark tubes during the analysis. The amount of total iodine was determined at a wavelength of 456 nm calculated from the mean of 6 photometrical readings per sample taken within 3 min.

The spectrophotometer was calibrated using standard additions of potassium iodate (J.T. Baker ACS grade KIO_3) to BOD bottles filled with seawater and adding Winkler chemicals in reverse order. The spectrophotometer was zeroed against a seawater blank. The coefficient of variation between triplicate samples was on average 0.08% at 280 $\text{mmol O}_2 \text{ m}^{-3}$. The final

oxygen consumption rates were converted to carbon units using a respiratory quotient of 1.

Activity of the electron transport system (ETS)—ETS determinations were carried out only during TRANSAT-II following the modifications of the tetrazolium reduction technique as described in Arístegui and Montero [5]. Some minor modifications of the method were made to increase its sensitivity. Briefly, about 10 L of water was filtered through a Whatman GF/F filter (47 mm diameter). Filters were folded into cryovials and immediately stored in liquid nitrogen until analysis in the laboratory. Back in the laboratory, the filters with the collected material were homogenized in 2.5 mL phosphate buffer with a Teflon–glass tissue grinder at 0–4°C for 1.5 min. An 0.9 mL aliquot of the crude homogenate was incubated in duplicate with 0.5 mL of substrate solution and 0.35 mL of 2-(4-iodophenyl)-3-(4-nitrophenyl)-5-phenyltetrazolium chloride (INT) at 18°C for 20 min. The reaction was quenched by adding 0.25 mL of a mixture of formalin and phosphoric acid. The quenched reaction mixture was centrifuged at 5000 rpm at 4°C for 20 min and the absorbance of the particle-free solution measured in a Beckman-DU-650 spectrophotometer at 490 and 750 nm wavelength after the sample was adjusted to room temperature. Readings at 750 nm, to correct for turbidity, were always negligible. In addition to the samples, duplicate controls were run by replacing the crude extract by a clean Whatman GF/F filter homogenized in phosphate buffer. ETS activity was calculated using the equation given in Packard and Williams [48]:

$$\text{ETS}_{\text{ASSAY}}(\text{mmol O}_2 \text{ h}^{-1}) = (H \times S \times \text{OD}_{\text{corr}}) / (1.42 \times V \times f \times t) \times 22.4$$

where H is the volume of the homogenate (in mL), S is the volume of the quenched reaction mixture (in mL), OD_{corr} is the absorbance of the sample measured at 490 nm wavelength and corrected for blank absorbance, V is the volume (in mL) of the seawater filtered through the Whatman GF/F filter, f is the volume of the homogenate used in the assay (in mL), t is the incubation time (in min), the factor 1.42 converts the INT-formazan formed to oxygen units (in μL) and 22.4 converts the μL to mmol. ETS activity was corrected to in situ temperature using the following equation:

$$\text{ETS}_{\text{INSITU}} = \text{ETS}_{\text{ASSAY}} \times e^{E_a/R \times (1/T_{\text{ass}} - 1/T_{\text{is}})}$$

where E_a is the Arrhenius activation energy (in kcal mol^{-1}), R is the gas constant, T_{ass} and T_{is} are the temperatures (in degrees Kelvin) in the assay and in situ, respectively. A calculated activation energy of 16 kcal mol^{-1} was used.

Apparent oxygen utilization (AOU)—AOU is calculated as the difference between the saturation oxygen concentration and the observed oxygen concentration. The saturated oxygen concentration in seawater is dependent on the potential temperature, salinity and pressure of the sampling location. AOU was derived with the software package Ocean Data View of R. Schlitzer (ODV 2005; <http://www.awi-bremerhaven.de/GEO/ODV>) using the CTD measurements of our depth profiles.

Statistical tests—Wherever appropriate, statistical tests were performed with the Tukey-honest significant difference test at a significance level of $p < 0.5$ unless stated otherwise. For significance analysis, data were \log_{10} transformed to obtain heteroscedascity.

Results

General hydrography of the water masses—The average depth, salinity, and temperature of the major water masses of the eastern and western basin of the North Atlantic are given in Table 4.1

Table 4.1: Averaged water mass properties of selected physicochemical parameters in the eastern and western North Atlantic basin. Subsurface layer (SSL), oxygen minimum zone (O₂-min), Labrador Sea Water (LSW), Iceland Scotland Overflow Water (ISOW), North Atlantic Deep Water (NADW), Denmark Strait Overflow Water (DSOW); mean pressure and range $\times 10^1$ kPa), salinity* (Sal), temperature * (T ; °C), apparent oxygen utilization* (AOU; $\mu\text{mol kg}^{-1}$), total organic carbon* (TOC; mmol C m^{-3}).

Basin	Water mass	Pressure ($\times 10^1$ kPa)	Range ($\times 10^1$ kPa)	Sal	T (°C)	AOU ($\mu\text{mol kg}^{-1}$)	TOC (mmol m^{-3})	
Eastern	SSL ($n=35$)	135	90–150	35.48 (0.41)	11.06 (2.89)	19.63 (5.72)	56.0 (7.3)	
	O ₂ -min ($n=38$)	725	350–1030	35.15 (0.19)	7.09 (1.77)	76.08 (14.05)	53.3 (8.2)	
	LSW ($n=39$)	1816	1160–2130	34.91 (0.03)	3.40 (0.21)	37.68 (6.39)	51.3 (6.3)	
	ISOW ($n=23$)	2429	1720–3100	34.97 (0.01)	2.76 (0.29)	41.16 (4.20)	50.1 (6.9)	
	NADW ($n=25$)	2839	2540–3300	34.95 (0.01)	2.98 (0.07)	56.78 (8.97)	49.4 (4.4)	
	Western	SSL ($n=33$)	100	90–110	35.17 (0.58)	8.73 (4.74)	27.73 (19.15)	56.8 (8.7)
		O ₂ -min ($n=15$)	402	180–740	35.08 (0.21)	7.91 (2.39)	103.13 (35.27)	52.9 (12.3)
LSW ($n=32$)		1324	710–2090	34.89 (0.02)	3.44 (0.32)	42.04 (6.03)	52.3 (8.8)	
NADW ($n=25$)		2537	1980–3250	34.92 (0.02)	2.97 (0.19)	54.19 (5.49)	49.6 (8.1)	
DSOW ($n=22$)		3061	1220–3870	34.89 (0.02)	1.95 (0.42)	48.84 (8.98)	54.5 (7.3)	

*top numbers are averages of the water masses; numbers in parenthesis are standard deviations of the mean; n denotes the total number of samples for each water mass.

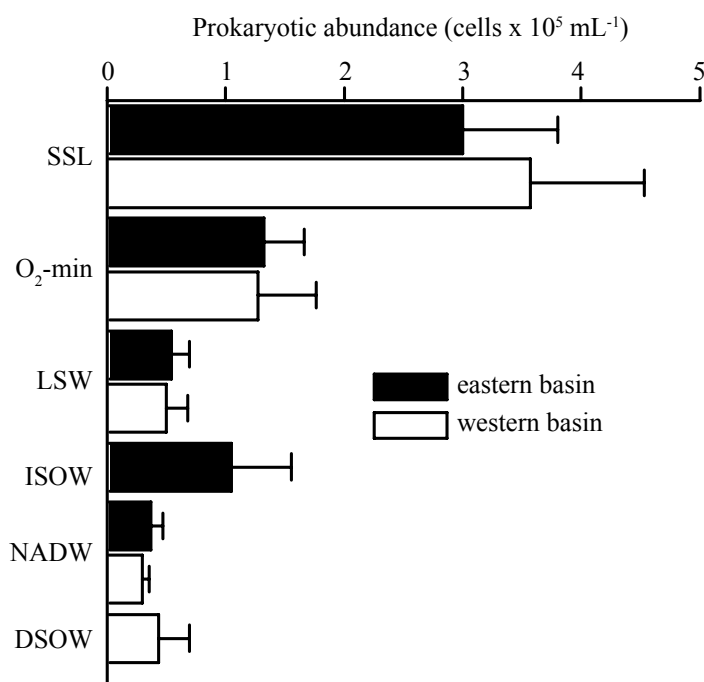


Figure 4.2: Average prokaryotic abundance (cells × 10⁵ mL⁻¹) in the different water masses of the eastern and western North Atlantic basin. Error bars show standard deviations.

along with the mean apparent oxygen utilization (AOU) and TOC concentration. Maximum AOU was found in the oxygen minimum zone (O₂-min). On average, AOU in the O₂-min zone was significantly higher in the western than in the eastern basin ($p < 0.01$, $n = 15$), whereas AOU in the LSW and NADW was similar in both basins (Table 4.1). The TOC concentrations in the water masses of the western basin were slightly more variable than in the eastern basin (Table 4.1). Generally, the TOC concentrations followed the commonly reported decrease with depth. In the western basin, however, the DSOW (depth range: 1200–3900 m) exhibited TOC concentrations not significantly lower than those of the SSL ($p = 0.33$, $n = 22$) indicating that the DSOW is younger than the NADW fueled by DSOW further south (at 60°N) (Table 4.1).

Prokaryotic abundance—In both the eastern and western basin, total prokaryotic abundance decreased exponentially with depth ($r^2 = 0.77$, $p < 0.0001$, $n = 151$ and $r^2 = 0.91$, $p < 0.0001$, $n = 124$, respectively) (Fig. 4.2). Despite this commonly reported pattern, however, prokaryotic abundance was more closely related to the specific water masses than the overall exponential decline in abundance with depth would suggest. The major source waters of the NADW, the ISOW, and the DSOW (see Fig. 4.1), clearly identifiable north of 60°N, supported a higher prokaryotic abundance than the NADW ($p < 0.01$, $n = 20$), reflecting the more recent formation of these two water masses. The ISOW also carried a considerable particle load due to its near-bottom flow over the Iceland-Scotland Ridge (data not shown). Thus, it is likely that the resuspended particles in the ISOW contributed to the higher prokaryotic abundance than subsequently detected in the NADW which is well separated from the seafloor by the Lower Deep Water and the recirculating Antarctic Bottom Water south of 55°N.

Prokaryotic production (PKP) and cell-specific prokaryotic production—Similar to prokaryotic abundance, prokaryotic production (PKP) decreased exponentially with depth ($r^2 = 0.63$, $p < 0.01$, $n = 180$ for the eastern basin and $r^2 = 0.65$, $p < 0.01$, $n = 139$ for the

western basin) and was slightly higher (Student's *t*-test; $p < 0.01$, $n = 103$) in the western than in the eastern basin (Fig. 4.3a). In the eastern basin, PKP decreased from the SSL ($9.2 \pm 3.7 \mu\text{mol C m}^{-3} \text{d}^{-1}$, $n = 31$) to the LSW ($0.9 \pm 0.6 \mu\text{mol C m}^{-3} \text{d}^{-1}$, $n = 33$). PKP in the O₂-min layer between 350–1000 m depth ($2.1 \pm 1.3 \mu\text{mol C m}^{-3} \text{d}^{-1}$, $n = 33$) was similar to that in the ISOW ($2.1 \pm 1.3 \mu\text{mol C m}^{-3} \text{d}^{-1}$, $n = 17$) found at a depth range of 1700–3100 m. Mean PKP in the eastern and the western branch of the NADW was essentially identical ($1.1 \pm 0.8 \mu\text{mol C m}^{-3} \text{d}^{-1}$, $n = 22$ and $1.2 \pm 0.8 \mu\text{mol C m}^{-3} \text{d}^{-1}$, $n = 20$, respectively) and also not significantly different ($p = 0.41$, $n = 20$) from the PKP in the DSOW ($1.3 \pm 0.8 \mu\text{mol C m}^{-3} \text{d}^{-1}$, $n = 16$). PKP in the LSW of the western basin was, on average, twice as high ($p < 0.01$, $n = 26$) as in the eastern basin ($1.9 \pm 1.6 \mu\text{mol C m}^{-3} \text{d}^{-1}$ and $0.9 \pm 0.6 \mu\text{mol C m}^{-3} \text{d}^{-1}$, $n = 34$, respectively) reflecting its formation in the western basin.

While both prokaryotic abundance and production decreased exponentially with depth, cell-specific prokaryotic production showed no systematic change (Fig. 4.3b). In the eastern North Atlantic basin, cell-specific PKP in the NADW ($28.4 \pm 16.0 \times 10^{-3} \text{fmol C cell}^{-1} \text{d}^{-1}$, $n = 22$) was almost as high as in the SSL ($32.3 \pm 11.8 \times 10^{-3} \text{fmol C cell}^{-1} \text{d}^{-1}$, $n = 31$) and about twice as high ($p < 0.01$, $n = 20$) as the cell-specific PKP in the O₂-min layer ($15.2 \pm 7.7 \times 10^{-3} \text{fmol C cell}^{-1} \text{d}^{-1}$, $n = 31$) (Fig. 4.3b). In the western basin, cell-specific PKP ranged from $58.3 \pm 26.6 \times 10^{-3} \text{fmol C cell}^{-1} \text{d}^{-1}$ in the SSL to $30.3 \pm 11.9 \times 10^{-3} \text{fmol C cell}^{-1} \text{d}^{-1}$ in the DSOW (Fig. 4.3b) and was therefore overall 52% higher than the cell-specific PKP in the water masses of the eastern basin (Student's *t*-test; $p < 0.01$, $n = 101$) (Fig. 4.3b). Cell-specific PKP in the LSW of the western basin was 3 times higher than in the LSW of the eastern basin ($p < 0.01$, $n = 25$), again reflecting the more recent formation of the LSW in the western basin and older LSW in the eastern basin. In contrast, cell-specific PKP in the NADW of the western basin was only 34% higher ($p = 0.12$, $n = 20$) than in the eastern basin (Fig. 4.3b).

Bulk prokaryotic respiration (PKR) and cell-specific respiration rates measured via oxygen consumption—Only in the western basin, PKR decreased significantly with depth ($r^2 = 0.20$, $p < 0.01$, $n = 44$) (Fig. 4.4a). In the eastern basin, PKR was not significantly different between the water masses ($p > 0.01$) with the exception of the NADW where PKR was about 21% of that in the SSL ($p < 0.01$) (Fig. 4.4a). Noteworthy, PKR in the ISOW ($224 \pm 97 \mu\text{mol C m}^{-3} \text{d}^{-1}$, $n = 6$) was as high as in the overlying O₂-min layer ($208 \pm 100 \mu\text{mol C m}^{-3} \text{d}^{-1}$, $n = 10$; Fig. 4.4a) reflecting the pattern of the PKP (see Fig. 4.3a). In the western basin, PKR decreased from the SSL to the NADW and DSOW by 41% ($p < 0.01$ for both).

Cell-specific PKR, however, significantly increased from the SSL towards the deeper water masses ($r^2 = 0.30$, $p < 0.0001$ for the eastern and $r^2 = 0.50$, $p < 0.0001$ for the western basin) in both basins (Fig. 4.4b). In contrast to cell-specific PKP, cell-specific PKR was not significantly different (Student's *t*-test, $p = 0.80$, $n = 44$) among the corresponding water masses of the eastern and western basin.

PKR estimated via ETS measurements—In the western basin of the North Atlantic (TRANSAT-II), the respiratory activity of the deep water prokaryotic community was also determined via ETS measurements (Fig. 4.5). While the respiration rates determined via O₂ consumption measurements decreased from the SSL to the NADW by 59% (Fig. 4a), potential respiration estimated via ETS measurements decreased by 85% (Fig. 4.5). Respiration rates estimated via ETS were essentially the same for the different deep water masses (LSW, NADW and DSOW) averaging $20.2 \pm 9.0 \mu\text{mol C m}^{-3} \text{d}^{-1}$ ($n = 45$). Generally, PKR measured via O₂ consumption was ~45% and ~85% higher in the SSL and in the deeper water masses, respectively, than estimated via ETS measurements (compare Fig. 4.4a and Fig. 4.5).

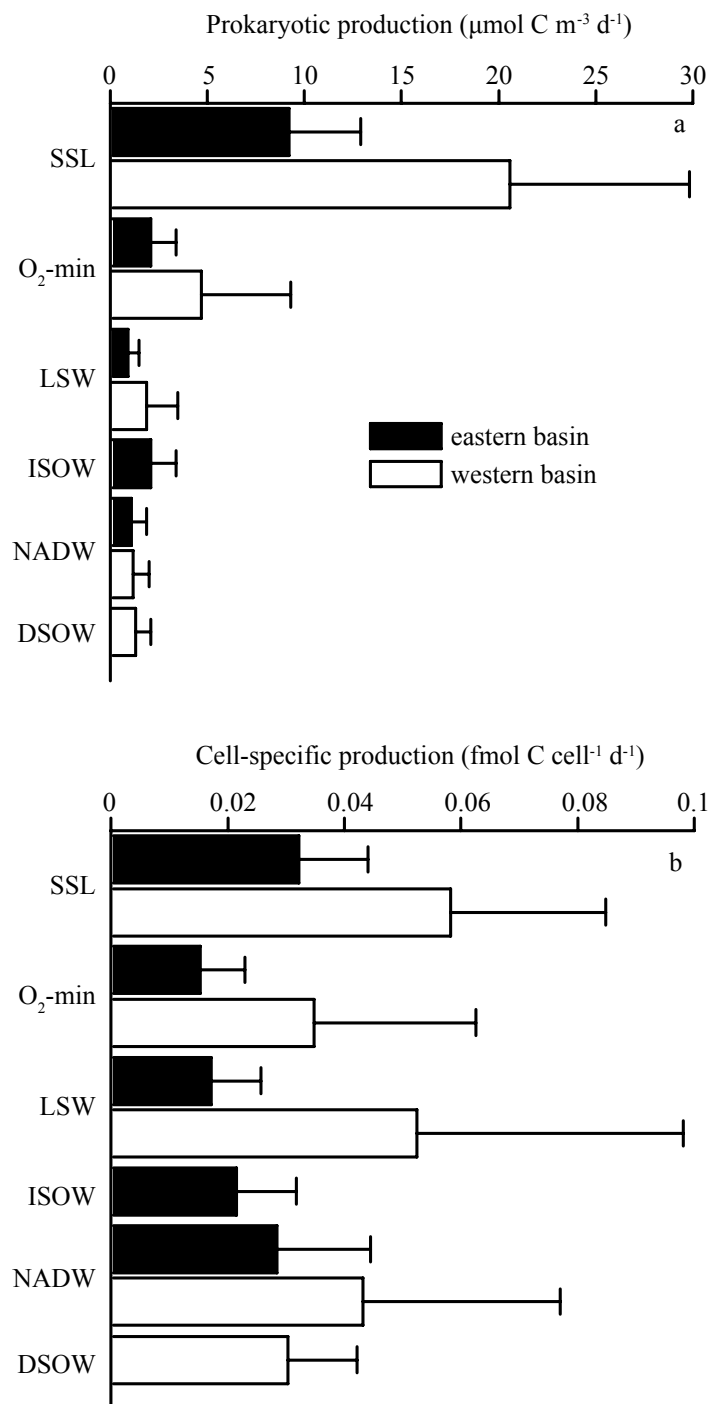


Figure 4.3: (a) Prokaryotic production ($\mu\text{mol C m}^{-3} \text{ d}^{-1}$) and (b) cell-specific prokaryotic production ($\text{fmol C cell}^{-1} \text{ d}^{-1}$) in the different water masses of the eastern and western North Atlantic basin. Error bars show standard deviations; $\text{fmol} = 10^{-15} \text{ mol}$.

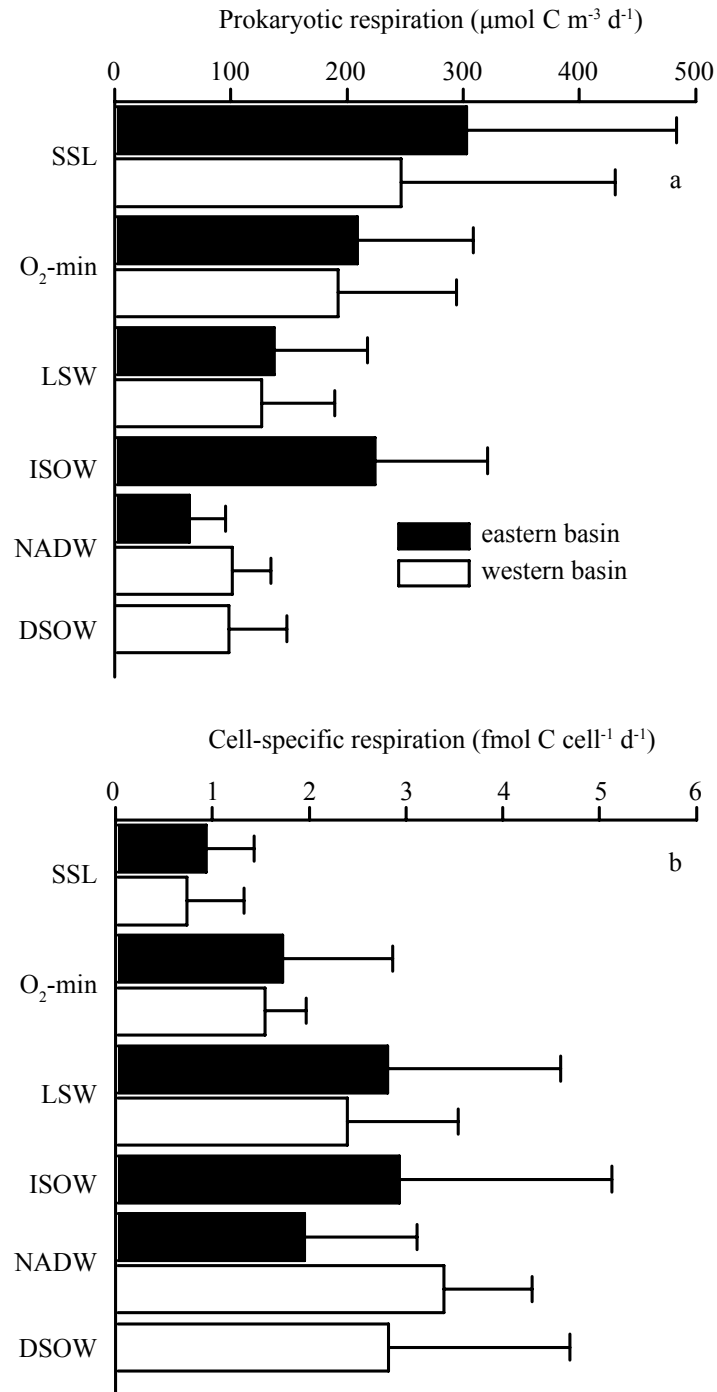


Figure 4.4: (a) Prokaryotic respiration ($\mu\text{mol C m}^{-3} \text{d}^{-1}$) and (b) cell-specific prokaryotic respiration ($\text{fmol C cell}^{-1} \text{d}^{-1}$) in the different water masses of the eastern and western North Atlantic basin. Error bars show standard deviations, $\text{fmol} = 10^{-15} \text{ mol}$.

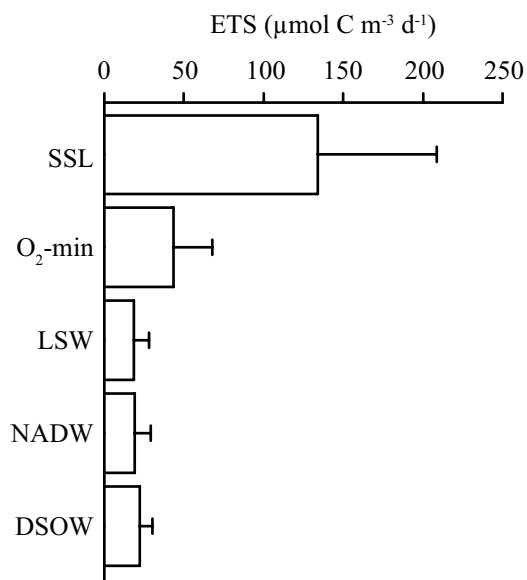


Figure 4.5: Mean potential respiration rates measured via the electron transport system assay (ETS) in the different water masses of the western North Atlantic basin. Error bars show standard deviations.

Prokaryotic growth efficiency (PGE)—For the SSL (depth range 90–150 m), the PGE in the eastern and western basin was, on average, $4 \pm 3\%$ ($n = 13$) and $12 \pm 7\%$ ($n = 11$), respectively (Fig. 4.6). Mean PGE for the water masses below the SSL was $2 \pm 1\%$ ($n = 56$, data from all the water masses below the SSL combined) for both North Atlantic basins. PGE was mainly determined by prokaryotic respiration and only weakly correlated with temperature ($r^2 = 0.13$, $n = 56$; data not shown).

Discussion

Prokaryotic production—Over the incubation period we used, no evidence was found that prokaryotic production in the 0.6- μm filtered seawater was enhanced compared to unfiltered seawater, indicating that the filtration step did not alter the composition or quality of the DOM (Fig. 4.7). Our prokaryotic production estimates of the water masses of the deep North Atlantic are similar to the estimates of Nagata et al. [45] for the deep North Pacific, the deep Arabian Sea (US JGOFS Database) and a site in the southern North Atlantic [50]. For the dark ocean, empirical conversion factors to translate prokaryotic uptake of radiolabeled tracers into cell production are not available. However, while the choice of the conversion factor is crucial for prokaryotic production estimates, its impact on the PGEs is comparatively small due to the high respiration compared to production.

Based on the prokaryotic production and biomass, we calculated the prokaryotic turnover time by dividing prokaryotic abundance by production [41]. In the eastern basin, mean prokaryotic turnover time ranged from 30 to 67 d. In the western basin, prokaryotic turnover times were more uniform throughout the different water masses and ranged from 17 to 39 d (Fig. 4.8). Our prokaryotic biomass estimates are based on flow cytometer counts of prokaryotic cells. Not all of these enumerated cells are alive, however, thus the calculated turnover time is biased by the unknown fraction of inactive or dead cells. In a previous

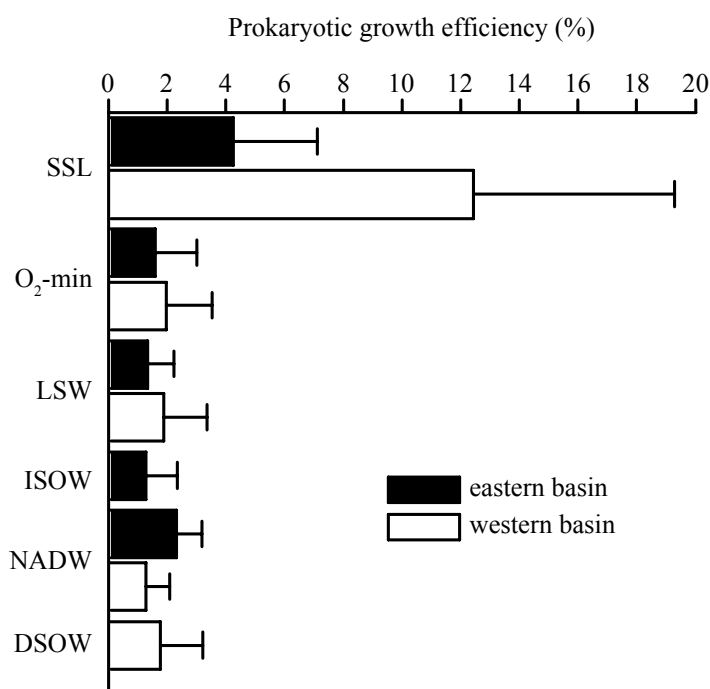


Figure 4.6: Mean prokaryotic growth efficiency (%) based on oxygen consumption measurements in the different water masses of the eastern and western North Atlantic basin. Error bars show standard deviations.

study, CARD-FISH targeting the 16S rRNA was used [58], which might serve as a proxy of active prokaryotes as RNA rapidly degrades when cells decay. About 70% of all the DAPI-stainable cells were detected with fluorescently labeled oligonucleotide probes indicating that they contained sufficient RNA [32]. This 70% might be considered as a conservative estimate of the fraction of living prokaryotic cells. Calculating prokaryotic turnover times using the number of CARD-FISH stainable cells, we arrive at a turnover time of 7 d in the SSL and between 11–20 d in the water masses below, which is a decrease in turnover time of roughly 30–40% in all water masses. Thus, the fraction of deep water prokaryotes potentially metabolically active might be as high as in surface waters.

Prokaryotic respiration (PKR)—Although oxygen consumption measurements have adequate analytical precision, we are aware that they are problematic. Besides the often-cited bottle effect, the long incubation times required to obtain significant differences in the oxygen concentration between the start and the end of the incubation might pose problems. We addressed this potential problem by incubation experiments of 0.6- μm filtered seawater from 400 m and 1000 m depth for up to 192 h. The oxygen concentration decreased linearly, while the increase in prokaryotic abundance in an extra set of bottles incubations was minimal over the maximum incubation period of used for the respiration rates (Fig. 4.9). Furthermore, the decrease in the oxygen concentration between t_0 and t_1 bottles was significant (Student's t -test; $p < 0.0001$, $n = 128$ for the eastern basin and $p < 0.02$; $n = 159$ for the western basin), and well above the precision of the Winkler method (0.1–0.2 mmol O₂ m⁻³). The respiratory quotient (RQ) to convert oxygen utilized to CO₂ produced varies between 0.7 and 1.3 depending on substrate composition [11]. In the absence of reliable data a RQ of 1 is applied. Considering that PGE is mainly influenced by PKR, the error in converting oxygen consumption to CO₂

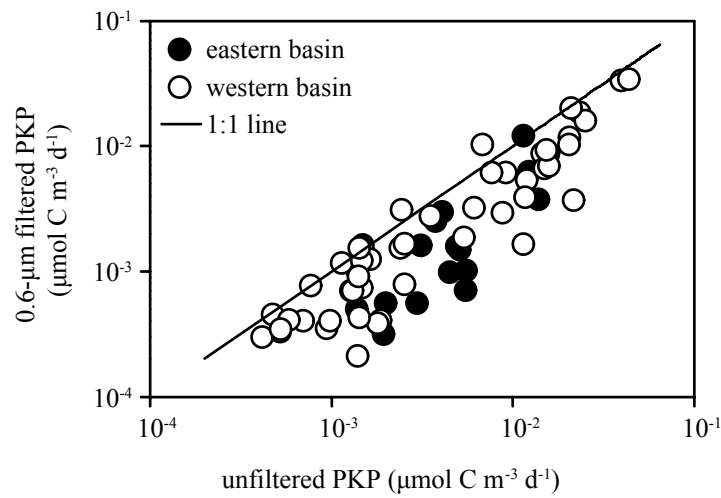


Figure 4.7: Relationship of prokaryotic production (PKP; $\mu\text{mol C m}^{-3} \text{d}^{-1}$) measured in unfiltered and 0.6- μm filtered seawater in the eastern and western basin. The 1:1 line represents unity in rates of both fractions.

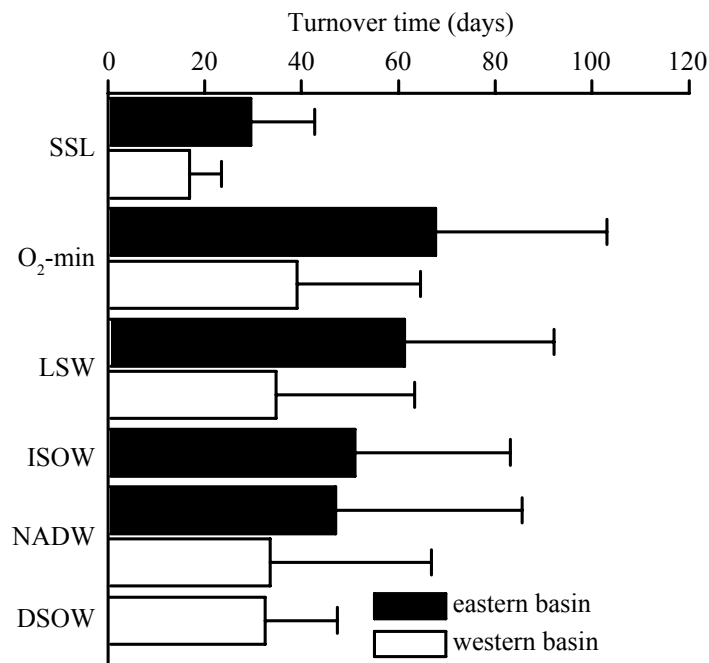


Figure 4.8: Average turnover time (days) of the prokaryotic community in the different water masses of the eastern and western North Atlantic basin. Error bars show standard deviations.

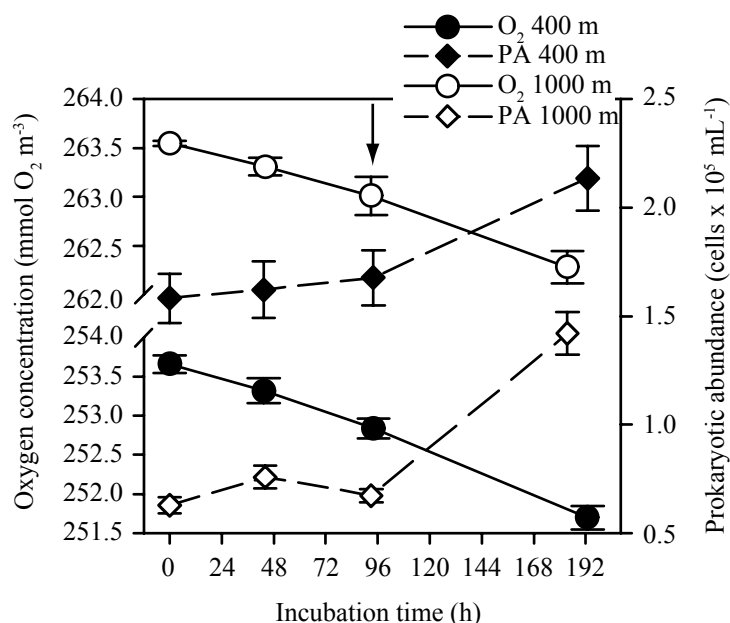


Figure 4.9: Oxygen concentration (O_2 ; mmol m^{-3}) and prokaryotic abundance (PA; $\text{cells} \times 10^5 \text{mL}^{-1}$) in $0.6\text{-}\mu\text{m}$ filtered seawater from 400 m and 1000 m. The arrow denotes the maximum used incubation time for the respiration measurements.

(20–40%), is not as small as usually assumed. The uncertainty in this figure, however, does not change our main conclusions.

For the Gulf of Mexico, Biddanda and Benner [11] reported oxygen consumption rates in the range of $1.7\text{--}0.9 \text{ mmol } O_2 \text{ m}^{-3} \text{ d}^{-1}$ between 100 and 500 m depth. Prokaryotic respiration in the eastern and western basin of the North Atlantic was $\sim 80\%$ lower for similar depths (Fig. 4.4a), however, the temperature in the Gulf of Mexico is high ($22\text{--}9^\circ\text{C}$ in the top 100–500 m). Water mass transport time in combination with the AOU can be used to calculate oxygen utilization rates ($\text{OUR} = \text{AOU}/\text{AGE}_{\text{watermass}}$) [56]. Reported OURs for depths below 250 m are 1 to 2 orders of magnitude lower than our measured PKR [24, 36, 56]. Based on chlorofluorocarbon (CFC) concentrations, the age of the NADW varies between 15 and 25 yr at the equator [25, 54], corresponding to spreading rates of the NADW and LSW of $\sim 1\text{--}2 \text{ cm s}^{-1}$. Using this spreading rate and the AOU, mean OURs in the NADW and LSW amount to $\sim 25\%$ of our measured PKR in the eastern and $\sim 30\%$ in the western Atlantic basin.

Prokaryotic growth efficiency (PGE)—PGEs in the range of 5 to 20% have been reported for surface waters of oligotrophic systems such as the Sargasso Sea, the central North Atlantic and the Mediterranean Sea [19 and references therein]. Our calculated PGEs for the water masses of the North Atlantic's interior are similar to the estimates of Griffith et al. [27] for the outer shelf off Georgia (USA). For various shelf regions, Pomeroy et al. [51] presented bacterial production and respiration data from near-surface waters. Assuming the conversion factors used in our study ($3.1 \text{ kg C mol}^{-1} \text{ leu}$; $\text{RQ} = 1$), the calculated PGEs ranged from 0.6–1.6% and were thus at the lower end of our deep water PGEs. Even lower PGEs of 0.01% were reported from the DYFAMED station in the Mediterranean Sea [43]. Thus, our PGEs obtained for the deep North Atlantic water masses are within the range reported for oligotrophic near-surface waters. For the mesopelagic realm of the Canary region of the North Atlantic, however, higher

PGEs (13–18%) have been reported, likely caused by POC input via lateral advection from the African upwelling [4].

Growth efficiencies based on ETS measurements—ETS measurements should provide the upper limit of possible respiration rates [48]. The relation between the enzymatic INT reduction and oxygen consumption, however, has not been firmly established yet. Commonly, a respiration:ETS ratio (R:ETS) of 0.086 is used, derived from batch culture experiments [18]. The assumed error for this conversion is ~30% [46]. Using our measured ETS rates (Fig. 4.5) and applying the above R:ETS ratio to calculate PGEs, we obtain unrealistically high PGEs ranging between 40–66% for the SSL to the NADW of the western Atlantic basin. Recently, an 8 times higher R:ETS ratio was calculated for the mesopelagic realm based on oxygen consumption and ETS measurements in the subtropical North Atlantic [4]. Using our concurrently measured oxygen consumption (Fig. 4.4a) and ETS measurements (Fig. 4.5), we obtain an average R:ETS ratio of 5.3 over all the water masses (data not shown), which is 2 orders of magnitude higher than the R:ETS ratio obtained for bacteria in batch cultures. Thus, it seems that R:ETS ratios derived from batch cultures with high nutrient availability are of limited value for in situ studies.

Prokaryotic organic carbon demand (PCD) versus POC flux—It is generally assumed that POC exported from the euphotic layer is the main carbon source for the dark ocean and DOC solubilized from POC provides the substrate for deep water prokaryotic plankton [17, 37]. Calculating the PCD from the measured prokaryotic production and respiration ($PCD = PKP + PKR$) integrated over the water column, we arrive at a mean PCD of $436 \text{ mmol C m}^{-3} \text{ d}^{-1}$ averaged over both basins of the North Atlantic. To compare our mean PCD with the carbon flux into the dark ocean, we use the model of Antia et al. [1] which is based on surface primary production and POC flux data ranging from the oligotrophic North Atlantic gyre to subpolar region. The equation of Antia et al. [1] is:

$$\text{POC flux (mmol C m}^{-2} \text{ d}^{-1}) = 0.1 \times PP^{1.77} \times z^{-0.68}$$

where PP is the primary production (in $\text{mmol C m}^{-2} \text{ d}^{-1}$) and z is the depth in m. The surface layer-derived POC arriving at a specific depth can thus be calculated from the above equation and is described by

$$\text{POC available at } z \text{ (mmol C m}^{-3} \text{ d}^{-1}) = 0.068 \times PP^{1.77} \times z^{-1.68}$$

For comparison with our PCD values, we assume a primary production of $100 \text{ mmol C m}^{-2} \text{ d}^{-1}$ reported from the North Atlantic Bloom Experiment (NABE) [23] and a decline in POC supply with depth following the above transformed equation. Clearly, our PCD values are higher than the POC supply at any given depth if a surface primary production of $100 \text{ mmol C m}^{-2} \text{ d}^{-1}$ is assumed (Fig. 4.10). In order to meet the PCD at greater depth, a primary production two orders of magnitude higher than that obtained during the NABE would be required. Particulate primary production measured during NABE are estimates of net primary production [16] and thus might be substantially lower (60–70%) than gross primary production [40, 52]. Thus, even a substantially higher gross primary production would be too low to account for the imbalance between PCD and organic carbon input into the dark ocean. Net heterotrophy in the North Atlantic surface waters, however, might be maintained via import of organic matter and the unique thermohaline circulation pattern, whereas prokaryotic metabolism in deep waters acts as a trap for subducted organic matter [31]. One possible explanation of this apparent paradox is the different time scale over which the two data sets have been obtained. While the POC flux

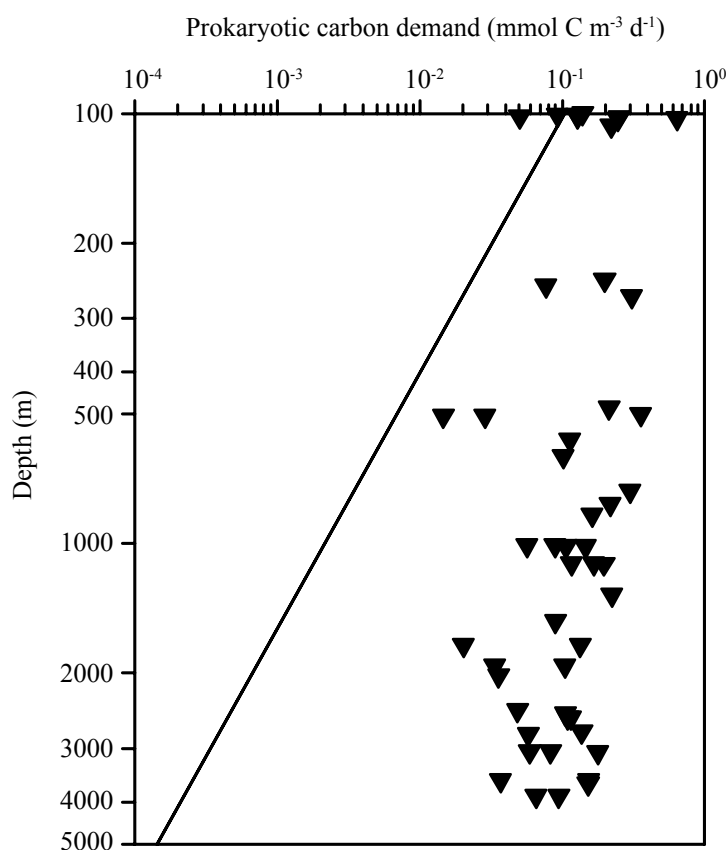


Figure 4.10: Comparison of the prokaryotic carbon demand (PCD) and the availability of sinking POC in the western North Atlantic basin. The line represents the concentration of POC derived from surface primary production based on the POC flux model of Antia et al. [1] assuming a primary production of $100 \text{ mmol C m}^{-2} \text{ d}^{-1}$ (see text). PCD was calculated using the measured prokaryotic production and respiration ($\text{PCD} = \text{PKP} + \text{PKR}$).

data are derived from sediment trap studies, thus, integrating over time spans of up to one year, the PCD values are based on snap-shot measurements of production and respiration.

It is well known that sediment traps preferentially collect fast sinking small particles while slowly-sinking or buoyant large marine snow-type particles are underrepresented in sediment traps [6, 33]. Even in water samples collected with conventional sampling bottles large aggregates are underrepresented since the largely very fragile aggregates are dispersed by the sampling procedure [6]. Nagata et al. [45] found a direct relation between POC flux and bacterial carbon demand in the deep North Pacific. In the Arabian Sea, however, a similar relation was not detectable [30], consequently additional mechanisms of substrate and energy supply were proposed. A re-assessment of the PCD (calculated from a PGE of 15%) in the lagrangian NABE study revealed, that the carbon flux including measured particulate primary production and estimated phytoplankton exudation would cover only ~70% of the PCD in the euphotic zone [23].

Based on $\Delta^{14}\text{C}$ measurements, Bauer et al. [9] calculated that the concentrations of POC and DOC in the deep central gyres of the North West Atlantic are maintained via the relatively larger lateral input from ocean margins rather than from recent surface production. The vertical diffusive flux of DOC in the Middle Atlantic Bight has been estimated to be in the order of $0.2 \text{ mmol C m}^{-3} \text{ d}^{-1}$ and fluxes of $\sim 3 \text{ mmol C m}^{-3} \text{ d}^{-1}$ via downwelling of DOC [14] might also fuel deep water prokaryotic activity. Also, it has been shown that the labile fraction of the DOM pool exported from the euphotic zone is rich in carbon [34]. The relationship between the decrease in DOC concentrations and dark ocean respiration estimated from apparent oxygen utilization suggests, however, that only between 10–20% of the carbon demand in the deeper water layers is fueled by DOC [3].

Cell-specific production and respiration rates—In calculating cell-specific rates we are aware of the uncertainties associated with the presence of non-viable cells. This would of course only give rise to an underestimation of the rates. In the deep water masses, cell-specific production amounted to 50 to 90% of that for surface waters (Fig. 4.3b). Similarly, data on biomass-specific rates of RNA and DNA synthesis by microorganisms in the meso- and bathypelagic suggests that microbial community growth is relatively uniform throughout the water column [38]. The respiration rates, on a per cell basis (Fig. 4.4b), are in the range $1\text{--}5 \text{ fmol C cell}^{-1} \text{ d}^{-1}$, similar to those reported by Blight et al. [12] for surface bacterioplankton. However, with the generally assumed model of decreasing particulate organic matter rain from the euphotic zone, our rates of cell-specific production and respiration cannot be explained. Remarkably, the increase of cell-specific respiration with depth (Fig. 4.4b) was also accompanied by an increasing percentage of cells with a high DNA content, as measured by flowcytometry (data not shown), which has been used to differentiate more active from less active cells [26]. The general decrease of growth yield with depth, is a consequence of the increase in prokaryotic respiration, not a decrease in prokaryotic production. This implies that the more refractory organic matter in the dark ocean might give rise to extra metabolic demands, however, this remains to be shown.

Decompression of the samples retrieved from greater depth prior to measuring production and respiration might have led to a stimulation of prokaryotic activity. Since we obtained prokaryotic growth yields of ~2% for the deep water masses (Fig. 4.6), this would indicate that both production and respiration were stimulated similarly. Grossly over- or underestimating only one of these two parameters would have resulted in unrealistic prokaryotic growth yields. Whether decompression leads to a stimulation or inhibition of prokaryotic activity, however, is

unclear. There is evidence, that deep water prokaryotic activity is overestimated if measured under decompressed conditions [35]. However, other authors report inhibition of prokaryotic activity due to decompression [57].

The finding that the dark ocean PCD exceeds the supply from surface waters has also been reported by others [21, 23, 55] and resolving the discrepancy is a major contemporary challenge. This large discrepancy between the prokaryotic carbon demand and carbon flux might be a result of methodological deficiencies in assessing organic carbon fluxes into the dark ocean and poorly constrained conversion factors needed to convert the rate measurements of leucine uptake into carbon. Prokaryotic production and respiration measurements of deep waters might also be biased due to the depressurization upon retrieval of samples from the dark ocean. The current database on pressurized versus depressurized metabolic activity of deep water prokaryotes is contradictory and needs to be resolved by obtaining prokaryotic activity measurements under realistic pressure conditions on a global scale. Despite these uncertainties, we have shown that an active prokaryotic community exists in the dark ocean, and this adds weight to the emerging view that heterotrophic processes in the meso- and bathypelagic realm might play a major role in the biogeochemical cycles of the oceans.

Acknowledgements

We thank the captain and crew of the *RV Pelagia* for their support at sea. Special thanks go to Denise Cummings for help with the respiration measurements during TRANSAT-II. Santiago Gonzalez performed the TOC measurements and Philippe Catala the flow cytometry analyses. We also thank Jesús Maria Arrieta for invaluable discussions during data analysis. Toshi Nagata is acknowledged for providing his raw data on prokaryotic production of the Pacific. C.R., P.J.leB.W., and J.A. were supported by a UK Natural Environment Research Council grant NER/B/S/2001/00846 awarded to C.R. and P.J.leB.W. C.R. was also supported by the Plymouth Marine Laboratory Core Strategic Research program. The TRANSAT cruises were supported by the Dutch Science Foundation (NWO-ALW), project 811.33.004 to G.J.H.

Bibliography

- [1] Antia A, Koeve W, Fisher G, Lanz T, Schulz-Bull D, et al. 2001. Basin-wide particulate carbon flux in the Atlantic Ocean: Regional export patterns and potential for atmospheric CO₂ sequestration. *Global Biogeochemical Cycles* 15: 845-62
- [2] Arístegui J, Barton ED, Montero MF, García-Muñoz M, Escánez J. 2003. Organic carbon distribution and water column respiration in the NW Africa-Canaries coastal transition zone. *Aquatic Microbial Ecology* 33: 289-301
- [3] Arístegui J, Duarte CM, Agusti S, Doval MD, Alvarez-Salgado XA, Hansell DA. 2002. Dissolved organic carbon support of respiration in the dark ocean. *Science* 298: 1976-
- [4] Arístegui J, Duarte CM, Gasol JM, Alonso-Saez L. 2005. Active mesopelagic prokaryotes support high respiration in the subtropical northeast Atlantic Ocean. *Geophysical Research Letters* 32: doi: 10.1029/2004GL021863

- [5] Arístegui J, Montero MF. 1995. Plankton community respiration in Bransfield Strait (Antarctic Ocean) during austral spring. *Journal of Plankton Research* 17: 1647-59
- [6] Asper VL. 1987. Measuring the flux and sinking speed of marine snow aggregates. *Deep-Sea Research Part I* 34: 1-17
- [7] Banse K. 1990. New views on the degradation and disposition of organic particles as collected by sediment traps in the open sea. *Deep-Sea Research Part I* 37: 1177-95
- [8] Barber RT. 1986. Dissolved organic carbon from deep waters resists microbial oxidation. *Nature* 220: 274-5
- [9] Bauer JE, Druffel ERM, Wolgast DM, Griffin S. 2002. Temporal and regional variability in sources and cycling of DOC and POC in the Northwest Atlantic continental shelf and slope. *Deep-Sea Research Part II* 49: 4387-419
- [10] Bauer JE, Williams PM, Druffel ERM. 1992. C-14 Activity of dissolved organic carbon fractions in the north central Pacific and Sargasso Sea. *Nature* 357: 667-70
- [11] Biddanda B, Benner R. 1997. Major contribution from mesopelagic plankton to heterotrophic metabolism in the upper ocean. *Deep-Sea Research Part I* 44: 2069-85
- [12] Blight SP, Bentley TL, Lefèvre D, Robinson C, Rodrigues R, et al. 1995. Phasing of autotrophic and heterotrophic plankton metabolism in a temperate coastal ecosystem. *Marine Ecology Progress Series* 128: 61-75
- [13] Buesseler KO. 1998. The decoupling of production and particulate export in the surface ocean. *Global Biogeochemical Cycles* 12: 297-310
- [14] Carlson CA, Ducklow HW, Michaels AF. 1994. Annual flux of dissolved organic carbon from the euphotic zone in the northwestern Sargasso Sea. *Nature* 371: 405-8
- [15] Carritt DE, Carpenter JH. 1966. Comparison and evaluation of currently employed modifications of Winkler method for determining dissolved oxygen in seawater - a NASCO Report. *Journal of Marine Research* 24: 287-318
- [16] Chipman DW, Marra J, Takahashi T. 1993. Primary production at 47°N and 20°W in the North Atlantic ocean - a comparison between the C14 incubation method and the mixed layer carbon budget. *Deep-Sea Research Part II* 40: 151-69
- [17] Cho BC, Azam F. 1988. Major role of bacteria in biogeochemical fluxes in the ocean's interior. *Nature* 332: 441-3
- [18] Christensen JP, Owens TG, Devol AH, Packard TT. 1980. Respiration and physiological state in marine bacteria. *Marine Biology* 55: 267-76
- [19] Del Giorgio PA, Cole JJ. 2000. Bacterial energetics and growth efficiency. In *Microbial Ecology of the Oceans*, ed. DL Kirchman, pp. 289-325. New York: Wiley-Liss
- [20] Del Giorgio PA, Cole JJ, Cimperis A. 1997. Respiration rates of bacteria exceed phytoplankton in unproductive aquatic systems. *Nature* 385: 148-51

- [21] Del Giorgio PA, Duarte CM. 2002. Respiration in the open ocean. *Nature* 420: 379-84
- [22] Ducklow HW, Carlson CA. 1992. Oceanic bacterial production. *Advances in Microbial Ecology* 12: 113-81
- [23] Ducklow HW, Kirchman DL, Anderson TR. 2002. The magnitude of spring bacterial production in the North Atlantic Ocean. *Limnology and Oceanography* 47: 1684-93
- [24] Feely RA, Sabine CL, Schlitzer R, Bullister JL, Mecking S, Greeley D. 2004. Oxygen utilization and organic carbon remineralization in the upper water column of the Pacific Ocean. *Journal of Oceanography* 60: 45-52
- [25] Fine RA, Rhein M, Andrié C. 2002. Using a CFC effective age to estimate propagation and storage of climate anomalies in the deep western North Atlantic Ocean. *Geophysical Research Letters* 24: 2227-31
- [26] Gasol JM, Zweifel UL, Peters F, Fuhrman JA, Hagström A. 1999. Significance of size and nucleic acid content heterogeneity as measured by flow cytometry in natural planktonic bacteria. *Applied and Environmental Microbiology* 65: 4475-83
- [27] Griffith PC, Douglas DJ, Wainright SC. 1990. Metabolic activity of size-fractionated microbial plankton in estuarine, nearshore, and continental shelf waters of Georgia. *Marine Ecology Progress Series* 59: 263-70
- [28] Guo L, Santschi PH, Warnken KW. 1995. Dynamics of dissolved organic carbon (DOC) in oceanic environments. *Limnology and Oceanography* 40: 1392-403
- [29] Hansell DA. 2002. DOC in the global ocean carbon cycle. In *Biogeochemistry of marine dissolved organic matter*, ed. DA Hansell, CA Carlson, pp. 685-715. San Diego: Academic Press
- [30] Hansell DA, Ducklow HW. 2003. Bacterioplankton distribution and production in the bathypelagic ocean: Directly coupled to particulate organic carbon export? *Limnology and Oceanography* 48: 150-6
- [31] Hansell DA, Ducklow HW, Macdonald AM, Baringer MON. 2004. Metabolic poise in the North Atlantic Ocean diagnosed from organic matter transports. *Limnology and Oceanography* 49: 1084-94
- [32] Herndl GJ, Reinthaler T, Teira E, van Aken H, Veth C, et al. 2005. Contribution of Archaea to Total Prokaryotic Production in the Deep Atlantic Ocean. *Applied and Environmental Microbiology* 71: 2303-9
- [33] Honjo S, Doherty KW, Agrawal YC, Asper VL. 1984. Direct optical assessment of large amorphous aggregates (marine snow) in the deep ocean. *Deep-Sea Research Part I* 31: 67-76
- [34] Hopkinson CS, Vallino JJ. 2005. Efficient export of carbon to the deep ocean through dissolved organic matter. *Nature* 433: 142-5

- [35] Jannasch HJ, Wirsen CO. 1982. Microbial activities in undecompressed microbial populations from the deep seawater samples. *Applied and Environmental Microbiology* 43: 1116-24
- [36] Jenkins WJ. 1982. Oxygen utilization rates in North Atlantic subtropical gyre and primary production in oligotrophic systems. *Nature* 300: 246-8
- [37] Karl DM, Knauer GA, Martin JH. 1988. Downward flux of particulate organic matter in the ocean - a particle decomposition paradox. *Nature* 332: 438-41
- [38] Karl DM, Winn CD. 1984. Adenine metabolism and nucleic acid synthesis: applications to microbiological oceanography. In *Heterotrophic activity in the sea*, ed. JE Hobbie, PJB Williams, pp. 197-262. New York: Plenum Press
- [39] Karner MB, DeLong EF, Karl DM. 2001. Archaeal dominance in the mesopelagic zone of the Pacific Ocean. *Nature* 409: 507-10.
- [40] Kiddon J, Bender ML, Marra J. 1995. Production and respiration in the 1989 North Atlantic spring bloom - an analysis of irradiance dependent changes. *Deep-Sea Research Part I* 42: 553-76
- [41] Kirchman DL. 2002. Calculation microbial growth rates from data on production and standing stocks. *Marine Ecology Progress Series* 233: 303-6
- [42] Koeve W, Ducklow HW. 2001. JGOFS synthesis and modeling: The North Atlantic Ocean. *Deep-Sea Research Part II* 48: 2141-54
- [43] Lebaron P, Parthuisot N, Catala P. 1998. Comparison of blue nucleic acid dyes for flow cytometric enumeration of bacteria in aquatic systems. *Applied and Environmental Microbiology* 64: 1725-30
- [44] Lemée R, Rochelle-Newall E, Van Wambeke F, Pizay M-D, Rinaldi P, Gattuso J-P. 2002. Seasonal variation of bacterial production, respiration and growth efficiency in the open NW Mediterranean Sea. *Aquatic Microbial Ecology* 29: 227-37
- [45] Nagata T, Fukuda H, Fukuda R, Koike I. 2000. Bacterioplankton distribution and production in deep Pacific waters: Large-scale geographic variations and possible coupling with sinking particle fluxes. *Limnology and Oceanography* 45: 426-35
- [46] Pace ML, Knauer GA, Karl DM, Martin JH. 1987. Primary production, new production and vertical flux in the eastern Pacific Ocean. *Nature* 325: 803-4
- [47] Packard TT, Denis M, Rodier M, Garfield P. 1988. Deep ocean metabolic CO₂ production - calculations from ETS activity. *Deep-Sea Research Part I* 35: 371-82
- [48] Packard TT, Williams PJB. 1981. Rates of respiratory oxygen-consumption and electron-transport in surface seawater from the Northwest Atlantic. *Oceanologica Acta* 4: 351-8
- [49] Pai S-C, Gong G-C, Liu K-K. 1993. Determination of dissolved oxygen in seawater by direct spectrophotometry of total Iodine. *Marine Chemistry* 41: 343-51

- [50] Patching JW, Eardly D. 1997. Bacterial biomass and activity in the deep waters of the eastern Atlantic - evidence of a barophilic community. *Deep-Sea Research Part I* 44: 9-10
- [51] Pomeroy LR, Sheldon JE, Sheldon WM. 1994. Changes in bacterial numbers and leucine assimilation during estimations of microbial respiratory rates in seawater by the precision Winkler method. *Applied and Environmental Microbiology* 60: 328-32
- [52] Robinson C, Serret P, Tilstone G, Teira E, Zubkov MV, et al. 2002. Plankton respiration in the Eastern Atlantic Ocean. *Deep-Sea Research Part I* 49: 787-813
- [53] Simon M, Azam F. 1989. Protein content and protein synthesis rates of planktonic marine bacteria. *Marine Ecology Progress Series* 51: 201-13
- [54] Smethie WM, Fine RA, Putzka A, Jones EP. 2000. Tracing the flow of North Atlantic Deep Water using chlorofluorocarbons. *Journal of Geophysical Research-Oceans* 105: 14297-323
- [55] Smith KL, Jr., Kaufmann RS. 1999. Long-term discrepancy between food supply and demand in the deep eastern North Pacific. *Science* 284: 1174-7
- [56] Suess E. 1980. Particulate organic carbon flux in the oceans-surface productivity and oxygen utilization. *Nature* 288: 260-3
- [57] Tamburini C, Garcin J, Bianchi A. 2003. Role of deep-sea bacteria in organic matter mineralization and adaptation to hydrostatic pressure conditions in the NW Mediterranean Sea. *Aquatic Microbial Ecology* 32: 209-18
- [58] Teira E, Reinthaler T, Pernthaler A, Pernthaler J, Herndl GJ. 2004. Combining catalyzed reporter deposition-fluorescence in situ hybridization and microautoradiography to detect substrate utilization by bacteria and archaea in the deep ocean. *Applied and Environmental Microbiology* 70: 4411-4
- [59] Teira E, Van Aken H, Veth C, Herndl GJ. in press. Archaeal uptake of enantiomeric amino acids in the meso- and bathypelagic waters of the North Atlantic. *Limnology and Oceanography*
- [60] Whitman WB, Coleman DC, Wiebe WJ. 1998. Prokaryotes: the unseen majority. *Proceedings of the National Academy of Sciences of the United States of America* 95: 6578-83
- [61] Williams PJIB. 1998. The balance of plankton respiration and photosynthesis in the open oceans. *Nature* 394: 55-7

Chapter 5

Relationship between bacterioplankton richness, respiration, and production in the southern North Sea¹

Thomas Reinthaler, Christian Winter and Gerhard J. Herndl

We investigated the relationship between bacterioplankton production (BP), respiration (BR), and community composition measured by terminal restriction fragment length polymorphism (T-RFLP) in the southern North Sea over a seasonal cycle. Major changes in bacterioplankton richness were apparent from April to December. While cell-specific BP decreased highly significantly with increasing bacterioplankton richness, cell-specific BR was found to be variable along the richness gradient, suggesting that bacterioplankton respiration is rather independent from shifts in the bacterial community composition. As a consequence, bacterial growth efficiency [BGE = $BP/(BP + BR)$] was negatively related to bacterioplankton richness, explaining ~43% of the variation in BGE. Our results indicate that despite the observed shifts in the community composition, the main function of the bacterioplankton, the remineralization of dissolved organic carbon to CO₂, is rather stable.

Introduction

Marine dissolved organic carbon (DOC) is, besides soil humus the largest organic carbon reservoir in the Earth's biosphere. The fate of this DOC pool is mainly determined by the activity of heterotrophic bacteria, which act as a link or sink of DOC for higher trophic levels of the food web. Thus, the production of biomass and the remineralization of DOC to CO₂ are the two key processes in the transformation of DOC by heterotrophic bacteria [15, 43]. The relationship between these two processes determines the bacterial growth yield. In natural systems, bacterioplankton growth yields range from <5 to >60% [12, 13]. This large variation in bacterial growth yield in natural bacterial communities is mainly caused by variations in substrate availability and is mediated, to a lesser extent, by temperature, although Rivkin and Legendre [43] suggested a direct relationship between temperature and the bacterial growth

¹Published in *Appl. Environ. Microbiol.* (2005) 71: 2260-2266

yield. This relationship only holds for a large temperature range and is not applicable for individual systems such as the North Sea, where seasonal temperature fluctuations are in the range of only 10 to 15°C [41, 44].

The extent to which variations in bacterial growth yield, and particularly in respiration, are related to shifts in the bacterioplankton community composition has not been studied in detail yet. Thus, the link between the phylogenetic composition of the bacterioplankton community and its major function in the carbon cycling, i.e., the remineralization of DOC is unclear, although shifts in bacterioplankton community composition on a seasonal scale have been reported and related to the occurrence of specific phytoplankton blooms [1]. Consequently, microbial communities may respond to changing environmental conditions with physiological adaptation or by shifts in the community composition [2, 11, 37, 54].

Naeem and Li [35] and Morin and McGrady-Steed [34] presented evidence that species loss changes important aspects of ecosystem functioning. In mesocosm experiments, increased biodiversity decreased the variation in the measured CO₂-flux [30]. However, experiments linking biodiversity with ecosystem functioning are usually performed with the aim to maximize experimental control and therefore are likely to miss the spatial and temporal heterogeneity in natural environments [5 and references therein].

In this study we tested the hypothesis that bacterial production and respiration are largely independent of the bacterioplankton community composition. For this purpose, we conducted six cruises in the southern North Sea, covering a full seasonal cycle. We measured bacterial production (BP), and respiration (BR) and the bacterial community composition by terminal restriction fragment length polymorphism (T-RFLP) and compared the patterns of bacterioplankton richness with these bacterial activity measurements.

Material and Methods

Study site—Six cruises were conducted with the *RV Pelagia* between July 2000 and June 2001 in the southern North Sea (Fig. 5.1), occupying at total of 106 stations. For this study, only the core stations between 52°N and 54°N and between 2°E and 5°E were considered (74 stations). Water samples were obtained from 5-m depth with 10 L NOEX bottles mounted on a conductivity-temperature-depth rosette sampler. During most of the cruises, the shallow water column (maximum depth 35 m) was well mixed, and stratification of the water column was only observed during the cruises in the summer months (June to September). Thus, the data presented below are representative for the entire water column during most of the year and of the upper mixed layer during the summer months.

Bacterial abundance—Five-milliliter samples were fixed with 37% formaldehyde (4% final concentration), stained with 4',6-diamidino-2-phenylindole (DAPI) and subsequently filtered immediately onto 0.2- μ m pore-size black polycarbonate filters (Millipore). The filters were mounted on glass slides, covered with coverslips and stored at -20°C in the dark until analysis. Bacterial abundance was determined by epifluorescence microscopy [39] within a week after each cruise.

Bacterial production—Bacterial production on the 0.8- μ m filtered seawater was measured by ¹⁴C-leucine incorporation (specific activity: 0.295 Ci mmol⁻¹; final concentration, 10 nmol L⁻¹). Two samples and 1 blank were incubated in the dark. The blank was fixed immediately with concentrated formaldehyde (final concentration; 4%, v/v) 10 min prior to adding the tracer. After incubating the samples and the blank at the in situ temperature for 60 min, the samples

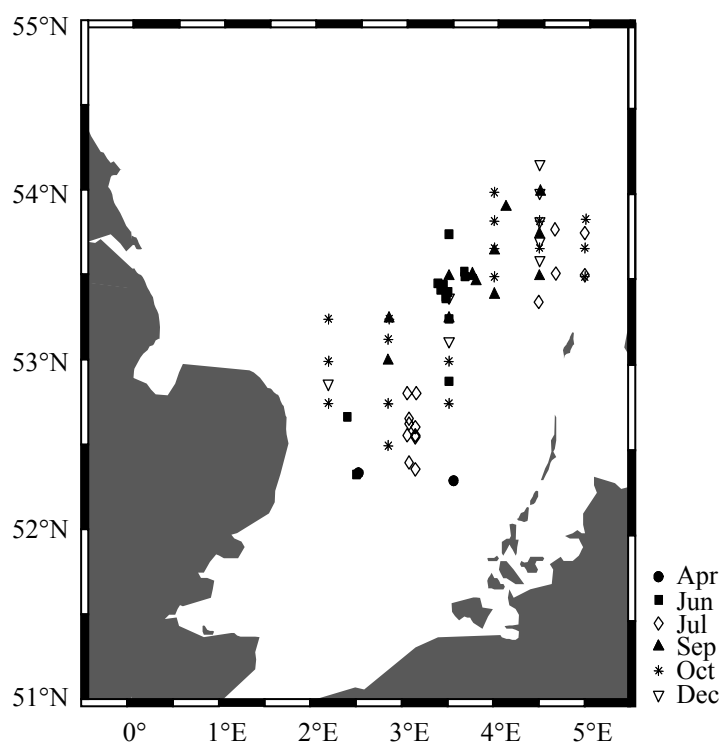


Figure 5.1: Map of the study area. Dots indicate the individual stations occupied during the six cruises. The months of sampling are indicated with different symbols.

were fixed with formaldehyde (4% final concentration), filtered onto 0.45- μm nitrocellulose filters (Millipore HA; 25mm diameter) and rinsed twice with 5 mL ice-cold 5% trichloroacetic acid (Sigma Chemicals) for 5 min. The filters were dissolved in 1 mL ethyl acetate, and after 10 min, 8 mL of scintillation cocktail (Insta-Gel Plus; Canberra Packard) was added. The radioactivity incorporated into bacterial cells was counted in a liquid scintillation counter (LKB Wallac; Model 1212). The amount of leucine incorporated into the bacterial biomass was converted to carbon production using the empirical conversion factor 0.07×10^{18} cells mol^{-1} leu [42] and assuming a carbon content of *Bacteria* of 20 fg C cell^{-1} [25]. Applying this conversion factor resulted in bacterial production estimates similar to the theoretical factor of 1.55 kg C mol^{-1} leu assuming no isotope dilution [48] (data not shown). In the text below, the abbreviation BP is used for bacterioplankton production measured in filtered (0.8- μm) seawater.

Bacterial respiration—The filtrate (filtered through a 0.8- μm filter) was carefully transferred to calibrated borosilicate glass BOD-bottles with a nominal volume of 120 mL by a sipper system to avoid introduction of air bubbles. For determinations of the initial O_2 concentration (t_0), samples were fixed immediately with Winkler reagents and incubated together with the live samples in a water bath in the dark at in situ temperature ($\pm 1^\circ\text{C}$) for 12 to 24 h when the incubations were terminated (t_1). Triplicate bottles were used for the determinations of the initial and final O_2 concentration. All the glassware was washed with 10% HCl and thoroughly rinsed with Milli-Q water prior to use. Oxygen concentrations of the t_0 and t_1 bottles were measured spectrophotometrically in one run [36, 45], essentially according to the standard protocol for the determination of oxygen by Winkler titration [7]. The amount of total iodine was determined at a wavelength of 456 nm. Measurements were

done at 20°C on a Hitachi U-1100 spectrophotometer using a 1 cm flow-through cuvette. To increase the sensitivity of the absorbance readings, we connected a four-digit voltmeter (Metex M4650) to the spectrophotometer. Calibration was performed by standard additions of iodate to distilled water, resulting in an empirical coefficient of 0.54455 nmol L⁻¹ cm⁻¹ (G. Kraay, personal communication). The samples were withdrawn from the BOD bottles with a Teflon tube and a peristaltic pump (Gilson Minipuls) and directly fed to the flow-through cuvette of the spectrophotometer. The end of the tube was placed near the bottom of the bottles to avoid possible loss of volatile iodine. The spectrophotometer was zeroed against Milli-Q water. The coefficient of variation of the oxygen determinations was <0.5%.

T-RFLP sampling and analysis—A total of 19 L of seawater was filtered through 0.8- μ m pore-size filters (Millipore; Isopore ATTP, 142 mm diameter) to exclude most of the non-bacterioplankton particles from the analysis using a stainless steel filter holder and an air-pressure pump. The bacterioplankton fraction (<0.8 μ m) was concentrated to a final volume of 400–550 mL using tangential-flow filtration with an 0.22 μ m pore-size filter cassette (Millipore; Pellicon PTGVPPC05). Subsequently, the bacterial concentrate was filtered onto 0.22- μ m pore-size filters (Millipore; Isopore GVWP, 100 mm diameter) and the filters were frozen in liquid nitrogen and subsequently stored at –80°C until further processing in the lab. The filtration units were thoroughly rinsed with sample water prior to use and soaked in 1 N HCL between sampling.

Extraction of the nucleic acids from the filters was performed as previously described. Briefly, 4 freeze-thaw cycles (–196°C to 37°C) and subsequent treatment with lysozyme (Sigma; cat. # L-7651) and proteinase K (Fluka; cat. # 82456) in 1% sodium dodecyl sulfate was conducted. The liquid phase was extracted with a mixture of phenol, chloroform and isoamylalcohol and the nucleic acids were precipitated with ethanol overnight at –20°C [52]. The resulting pellet was re-dissolved in 100 μ L ultrapure water (Sigma; cat. # W-4502). The nucleic acids in 50 μ L of this solution were further purified using a QIAEX II Gel Extraction Kit (Quiagen) as recommended by the manufacturer for DNA fragments larger than 10 kbp. The nucleic acids were recovered in a final volume of 20 μ L elution buffer (Quiagen) and used for subsequent PCR amplification. The integrity of the DNA was checked by agarose gel electrophoresis.

PCR conditions and chemicals were applied as described by Moeseneder et al. [33]. Briefly, 1–2 μ L of the cleaned nucleic acid extract were used as template in a 50 μ L PCR reaction. The *Bacteria*-specific primer 27F and the universal primer 1492R [24] were used to amplify a ca. 1480bp fragment of the bacterial 16S rRNA gene. The forward primer was fluorescently 5' end-labeled with phosphoramidite fluorochrome 5 carboxy-fluorescein (5'6-FAM) and the reverse primer with 6-carboxy-4',5'-dichloro-2',7'-dimethoxyfluorescein (5',6-JOE; both from Interactiva; Germany). After PCR amplification, excess fluorescently labeled primer was removed by ethanol precipitation and subsequent gel purification in a 1% agarose gel using TAMRA loading dye (Perkin Elmer-Applied Biosystems). The PCR fragments were recovered from the gel using a QIAquick Gel Extraction Kit (Quiagen) in a final volume of 20 μ L elution buffer (Quiagen). The concentration of the PCR fragments was estimated on a 1% agarose gel using a standard (Eurogentec; Smart-Ladder).

Restriction digestion of 50 ng of the purified PCR fragments was performed using 20U of the restriction enzyme *HhaI* together with the recommended buffer (both from Amersham Pharmacia) in a total volume of 100 μ L. Restriction was performed at 37°C for 12 h to ensure complete digestion. The DNA fragments from the restriction digests were recovered

in a final volume of 2 μL ultrapure water (Sigma) by linear polyacrylamide precipitation [32]. T-RFLP analysis was performed on an automated capillary sequencer (Perking Elmer-Applied Biosystems; ABI Prism 310) as previously described [33].

Statistical analyses—The T-RFLP patterns were analyzed by recording the number of peaks (presence versus absence). Due to the variability in the discriminative power of the forward and the reverse primer, subsequent analysis was performed on the combined data set from both primers serving as a relative measure of bacterial community richness [32].

The similarity of the T-RFLP patterns between the different stations was assessed with the Bray-Curtis similarity index which is similar to Sorenson's similarity index when applied to presence/absence data [8]. The resulting similarity matrix was assessed using non-parametric multidimensional scaling (MDS), which is a powerful tool for assessing community profiles obtained by molecular fingerprinting techniques [26, 46, 53]. For the MDS analysis, the recommendations of Clarke and Warwick [8] were followed. With MDS, the complexity of a given similarity matrix is reduced by plotting the data two-dimensionally. The more similar samples are, the closer they appear in the plot. The stress factor is an indication of the goodness of fit of the raw versus the plotted data with values <0.1 representing good ordination of the similarity matrix with little risk of misinterpretation. Higher stress factors were checked with cluster analysis.

Dendrograms of the obtained T-RFLP patterns were constructed by using either the Bray-Curtis similarity matrix or the bootstrapped Jaccard or Simple Match similarity matrixes calculated from the same data set. Clusters were constructed with the unweighted-pair group (UPGMA) method. MDS calculations were done with the software package Primer 5 from Primer-E, other statistical analyses with the software package Statistica from Statsoft.

DOC measurement—Samples for DOC were filtered through rinsed 0.2- μm polycarbonate filters and sealed in combusted (450°C for 4 h) glass ampoules after adding 50 μL of 40% phosphoric acid. Subsequently, the samples were stored frozen at -20°C . DOC concentrations were determined by the high temperature combustion method using a Shimadzu TOC-5000 analyzer [4]. Standards were prepared with potassium hydrogen phthalate (Nacalai Tesque, Inc. Kyoto, Japan). Ultra pure Milli-Q blanks were run before and after the sample analysis. The blank was on average $16.3 \pm 6.8 \mu\text{mol L}^{-1}$ and per sample the mean of triplicate injections was calculated. The average analytical precision of the instrument was $<3\%$.

*Chl *a* measurement*—One-L samples were gently filtered through 47 mm Whatman GF/F filters and stored at -60°C until analysis within 4 weeks. Chlorophyll *a* (Chl *a*) was extracted in 10 mL of 90% acetone at -20°C in the dark for 48 h. Subsequently, the filters were sonicated on ice for 1 min (Branson, model 3200) and centrifuged to remove particles. The Chl *a* concentration in the supernatant was determined fluorometrically with a Hitachi F-2000 fluorometer [21].

Results

Bacterial abundance and production in the 0.8- μm filtered and unfiltered seawater fraction—Total bacterial abundance (BA) and production (BP) were significantly correlated with the respective 0.8- μm filtered fraction (Spearman rank correlation: $r = 0.69$ for BA and $r = 0.84$ for BP, respectively; $p < 0.01$; $n = 74$ for both) (data not shown). Filtration through 0.8- μm filters reduced BA and BP by $\sim 40 \pm 20\%$ compared to the unfiltered seawater samples.

Table 5.1: Monthly means and standard deviations (SD) for selected physico-chemical and biological parameters from the southern North Sea; salinity (S; PSU), Temperature (T ; °C), dissolved organic carbon (DOC; mmol C m^{-3}), Chlorophyll a (Chl a ; mg m^{-3}), bacterioplankton abundance (BA; $\text{cells} \times 10^6 \text{ mL}^{-1}$), bacterioplankton production (BP; $\text{mmol C m}^{-3} \text{ d}^{-1}$), bacterioplankton respiration (BR; $\text{mmol C m}^{-3} \text{ d}^{-1}$) and bacterial growth efficiency (BGE; %).

Month	S	T	DOC	Chl a	BA	BP	BR	BGE
Apr	32.2	9.7	98.4	6.6	1.0	1.75	2.4	42
($n = 6$)	(1.1)	(0.3)	(22.9)	(1.8)	(0.4)	(0.71)	(0.9)	(5)
Jun	34.0	12.2	173.8	1.7	1.0	0.53	1.6	25
($n = 13$)	(0.1)	(0.3)	(76.2)	(0.8)	(0.7)	(0.17)	(1.1)	(12)
Jul	34.7	14.9	96.0	1.3	1.2	0.44	1.7	24
($n = 15$)	(0.3)	(0.2)	(22.7)	(0.8)	(0.7)	(0.15)	(0.9)	(13)
Sep	23.4	17.0	129.1	2.2	1.2	0.22	1.6	15
($n = 13$)	(0.2)	(0.3)	(73.7)	(1.2)	(0.4)	(0.18)	(1.0)	(13)
Oct	34.5	13.6	137.7	1.3	0.8	0.13	0.7	18
($n = 19$)	(0.3)	(0.9)	(40.9)	(0.4)	(0.3)	(0.08)	(0.5)	(10)
Dec	34.7	10.6	186.8	0.8	0.6	0.03	0.8	5
($n = 8$)	(0.4)	(0.7)	(116.0)	(0.2)	(0.1)	(0.02)	(0.7)	(2)
All*	34.2	13.6	137.3	1.7	1.0	0.40	1.4	21
($n = 74$)	(0.8)	(2.3)	(69.2)	(1.5)	(0.5)	(0.49)	(1.0)	(14)

*All groups is the grand average over the seasonal cycle calculated from raw data;
 n =number of stations;

Seasonal dynamics in physicochemical parameters—Low salinity values were recorded in April but varied only within a rather narrow range during the rest of the year. Temperature changed significantly between the months (least significant difference test; $p < 0.05$) with lowest temperatures in spring and winter and an average maximum temperature in September. Monthly averages in DOC concentration showed no clear pattern and varied around an annual average of $137 \pm 69 \text{ mmol C m}^{-3}$. Chl a concentrations peaked in April and in September and were low during the other months (Table 5.1)

Seasonal dynamics in microbiological parameters—The mean BA was $\sim 1.0 \pm 0.5 \times 10^6 \text{ mL}^{-1}$. BP decreased significantly from the late spring towards the winter (least significant difference test; $p < 0.0001$). Highest BP was measured in April with $1.7 \text{ mmol C m}^{-3} \text{ d}^{-1}$, while in December, BP was only $0.03 \text{ mmol C m}^{-3} \text{ d}^{-1}$. BR was variable over the seasonal cycle, with an average, $1.4 \pm 1.0 \text{ mmol C m}^{-3} \text{ d}^{-1}$. Bacterial growth efficiencies (BGEs) ranged from 42% in April to 5% in December with an overall average of $\sim 21 \pm 14\%$ (Table 5.1). Monthly averages in BGEs were variable but overall decreased significantly from spring to winter (analysis of variance [ANOVA]; $p < 0.05$).

Spatial versus seasonal heterogeneity in the richness of the bacterial community—As indicated by the dendrogram based on the Bray-Curtis similarity index (Fig. 5.2), bacterial communities were more closely related within individual months than between different months. An MDS plot highlights the seasonal heterogeneity of the bacterial community, but spatial dissimilarities are also visible (Fig. 5.3). Major changes in the bacterioplankton community composition from April to June were apparent, while between July and December

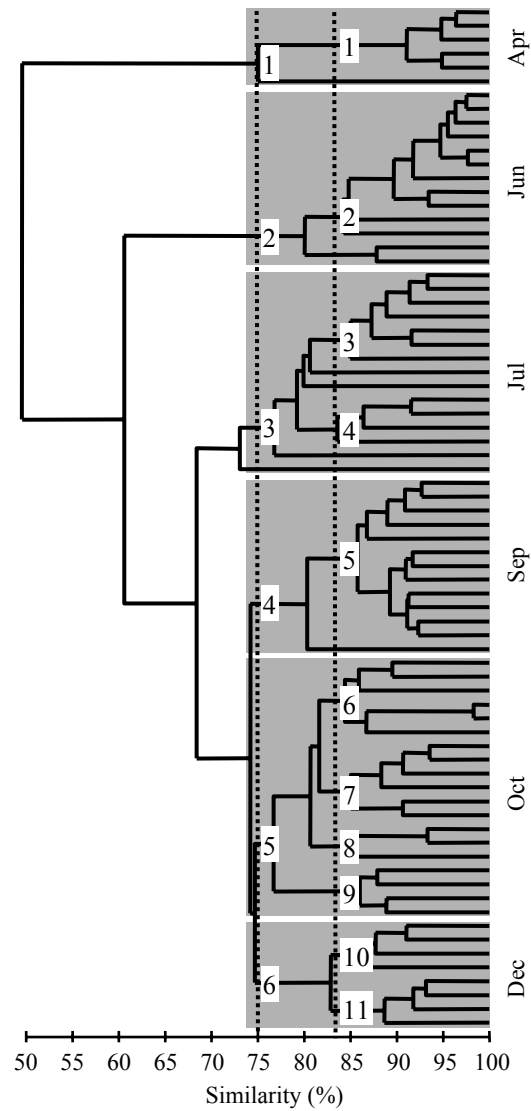


Figure 5.2: Cluster analysis of the T-RFLP patterns from an annual cycle in the southern North Sea by the unweighted-pair group (UPGMA) method using average linkages. The distance matrix was calculated by using the Bray-Curtis similarity index. The main groups are shaded and correspond to the month of sampling, and the branches represent stations. Subgroups are indicated with a dotted lines for relative similarities of 75 and 83%. Numbers next to the lines denote the groups used in the analysis in Fig. 5.7.

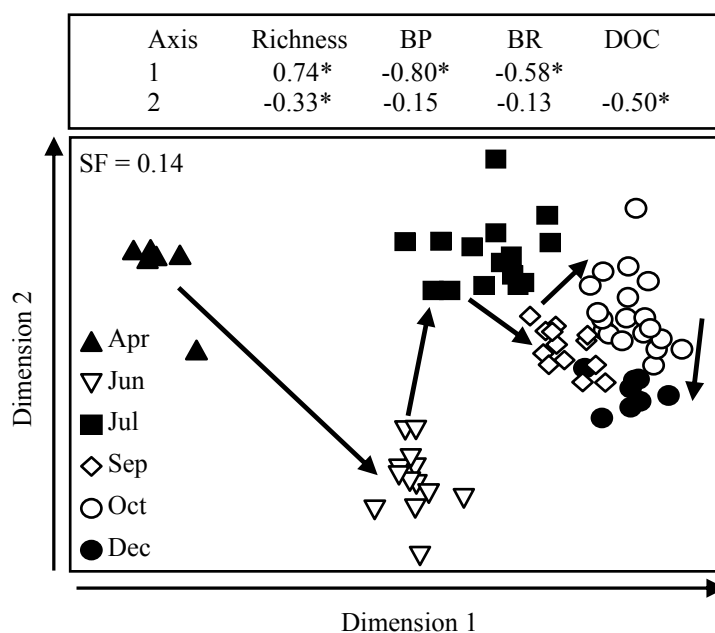


Figure 5.3: Two-dimensional MDS plot of the T-RFLP patterns of the bacterioplankton community of the southern North Sea. The configuration found by MDS was based on a Bray-Curtis similarity matrix from the bacterial richness between the stations. The months are indicated by different symbols. The arrows inside the panel indicate the seasonal sequence from spring to the winter. The arrows on axis 1 and dimension 2 indicate the direction in which scores increase. Spearman rank correlations were calculated between the scores of the dimension found for the different stations and richness, bacterial production (BP), bacterial respiration (BR), chlorophyll *a* (Chl *a*), dissolved organic carbon (DOC) and temperature (T); SF = Stress factor; (*) denotes $p < 0.01$.

these changes were much smaller (Fig. 5.3).

Relationship between environmental variables and bacterial richness, BP and BR—A nonparametric analysis of potentially important environmental variables indicated only a few significant correlations (Table 5.2). Salinity was correlated with BP or BR only when the data for April were included in the data set. DOC and temperature showed no substantial relationship with either bacterial richness, BP or BR. Increasing bacterial richness explained the decreasing BP ($r^2 = 0.50$; $p < 0.0001$; $n = 71$) better than it explained the changes in BR ($r^2 = 0.21$; $p < 0.0001$; $n = 72$) (data not shown). Cell-specific BP decreased exponentially with increasing bacterioplankton richness (Fig. 5.4a). At about the average richness calculated for the total data set (~52 operational taxonomic units), cell-specific BP leveled off (Fig. 5.4a). The decline in cell-specific BR was less pronounced and more variable (Fig. 5.4b).

Relationship of bacterial richness and BGE—In summer, estimated community richness was lower than in the fall and winter. The monthly averaged bacterioplankton richness increased significantly from spring to winter from 15 to ~80 operational taxonomic units (one-way ANOVA; $r^2 = 0.68$; $p < 0.0001$), while BGE significantly decreased from April to December from ~42% in spring to 5% in winter (one-way ANOVA; $r^2 = 0.45$; $p < 0.0001$) (Fig. 5.5a). As a consequence, BGE was negatively related to bacterioplankton richness explaining ~43% of the variation in BGE (Fig. 5.5b).

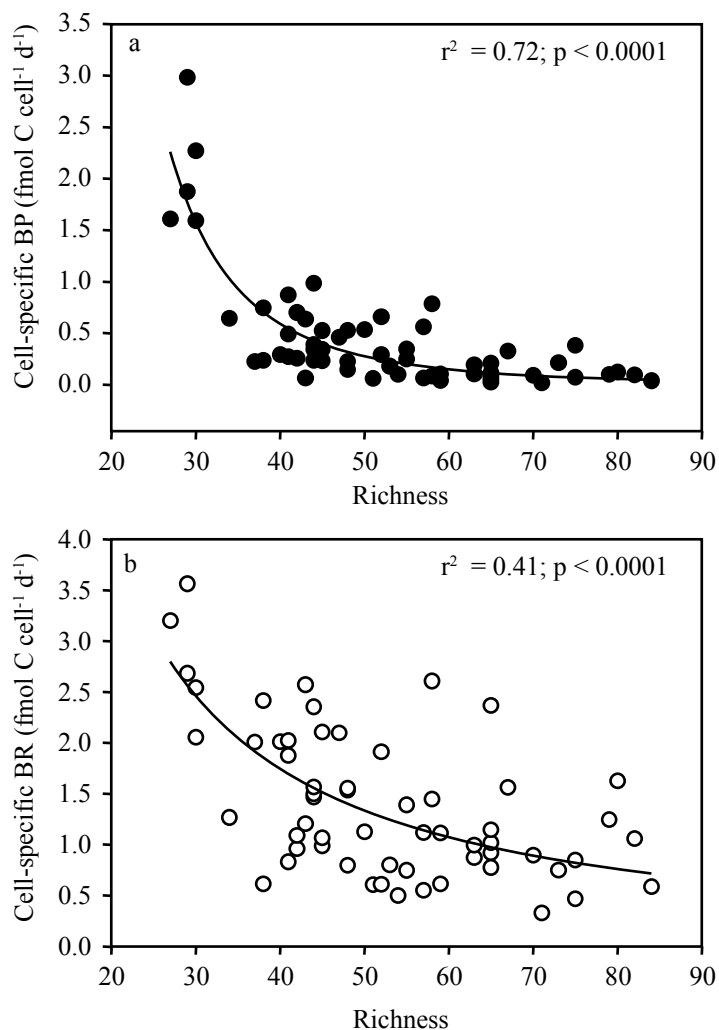


Figure 5.4: Relation between bacterioplankton richness and cell-specific bacterial production (BP; $\text{fmol C cell}^{-1} \text{d}^{-1}$) (a) or cell-specific respiration (BR; $\text{fmol C cell}^{-1} \text{d}^{-1}$) (b). The exponential decreases are illustrated by a power regression model fit to the raw data.

Table 5.2: Spearman rank correlations of biological and selected physico-chemical parameters. OTUs of $0.8\text{-}\mu\text{m}$ filtered bacterioplankton (Richness), bacterioplankton respiration (BR) bacterioplankton production (BP), salinity (Sal), temperature (T) and chlorophyll a (Chl a); ^aAll parameters were log-transformed before analysis except T ; Total $n = 74$.

Parameter	Spearman rank correlation value ^a		
	Richness	BP	BR
Salinity	0.32	0.40*	-0.32*
T	0.19	-0.07	0.08
DOC	0.14	-0.30	-0.21
Chl a	-0.21	0.36*	0.37*

(*) denotes $p < 0.01$ significance level.

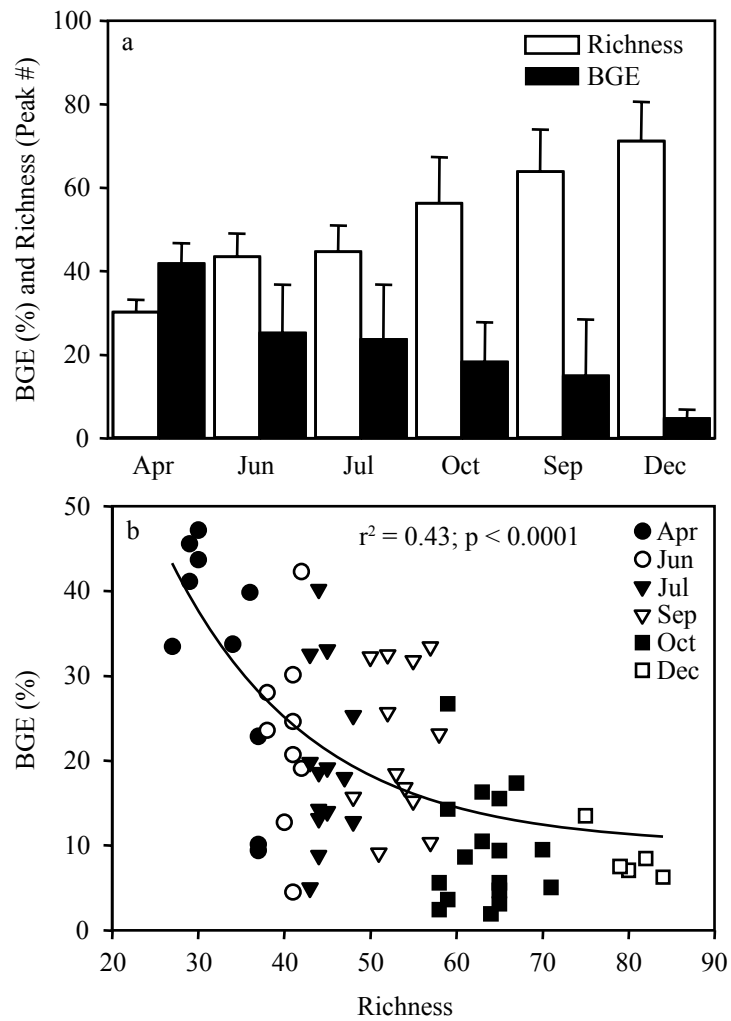


Figure 5.5: Dynamics of bacterial growth efficiency (BGE) and richness over the seasonal cycle in the southern North Sea. (a) Monthly averages of BGE and bacterioplankton richness measured by T-RFLP. Error bars indicate standard deviations of the mean ($n = 8$ to 19). (b) Relationship between BGE and bacterioplankton richness, with months indicated by different symbols.

Discussion

The selective amplification of T-RFLP templates due to a potential PCR bias could lead to differences between the measured and the actual in situ community composition [49, 51]. Furthermore, it is known that even specific primers for the profiling of bacterioplankton amplify 16S rRNA genes of chloroplasts [40]. Thus, we primarily examined the 0.8- μm filtered fraction of the bacterioplankton community. A variable fraction of the total bacterial community was lost in the filtration step. Because the southern North Sea is shallow (mean depth, 30 m), it seems likely that resuspension of sediment particles with associated bacteria contributed to the variability of the total versus free-living bacterioplankton. However, the correlation between BP measured in unfiltered and that measured in 0.8- μm filtered seawater was high, and therefore we consider our data to be representative for the free-living bacterioplankton community.

Evidence that biodiversity can influence rates of ecosystem processes has come from experimental studies [20, 27, 30, 35]. Usually, the opposing view that ecosystem function affects species diversity is reported. However, relationships between diversity and productivity are, in fact, two-dimensional projections of a three-dimensional relationship among factors, e.g., site productivity, metabolic rates and species diversity [18, 47]. Thus, conclusions from effects of changes in bacterial richness on ecosystem properties seem appropriate.

There is much debate about the relationship between species diversity as a function of productivity [27, 47]. Chl *a* is commonly used as a simple indicator for phytoplankton productivity, and some studies have interpreted changes in bacterial community composition as a consequence of gradients in Chl *a* concentrations [23, 38]. However, analyzing the pattern of α -, and β - proteobacteria and *Bacteroidetes* richness individually, Horner-Devine et al. [22] found that the richness within the individual groups changed differently along a Chl *a* gradient but the overall bacterial richness showed no trend. Also in our study, only a weak correlation was found between Chl *a* and bacterioplankton richness (Table 5.2). Due to the effects of statistical averaging, diverse communities may appear more stable than they actually are, as pointed out by Doak et al. [14] and Tilman [50]. This effect might mask productivity versus richness patterns in whole community analysis.

In seawater cultures, Covert and Moran [10] and Carlson et al. [6] found that shifts in the bacterial community were related to the quality of the DOC. In the southern North Sea, DOC concentrations showed no clear seasonality (Table 5.1) and, consequently, no substantial correlation with bacterial richness (Table 5.2). However, a negative correlation in the MDS plot was apparent (Fig. 5.3). Bulk DOC measurements are usually not a good indicator for the direct availability of substrate to bacteria since the DOC pool consists to more than 80% of semi-labile to refractory compounds [3]. Nevertheless, the weak gradient detected suggests that changes in DOC concentration and/or composition play a role in structuring the composition of bacterial communities in the southern North Sea. This was also evident from a previous study performed at a coastal site of the North Sea for which the wax and wane of a phytoplankton bloom were monitored [1].

Generally, low BP is measured in the winter. In early summer, BP and BR are high [41] but community richness is low in the southern North Sea (Fig. 5.5a). From published reports, Mittelbach et al. [31] deduced that both hump-shaped and positive relationships of species diversity as a function of productivity are common in nature. In many studies, however, primary production is compared to the diversity of animals, i.e., complex feedback interactions between productivity and diversity are to be expected. Thus, direct productivity estimates of the studied

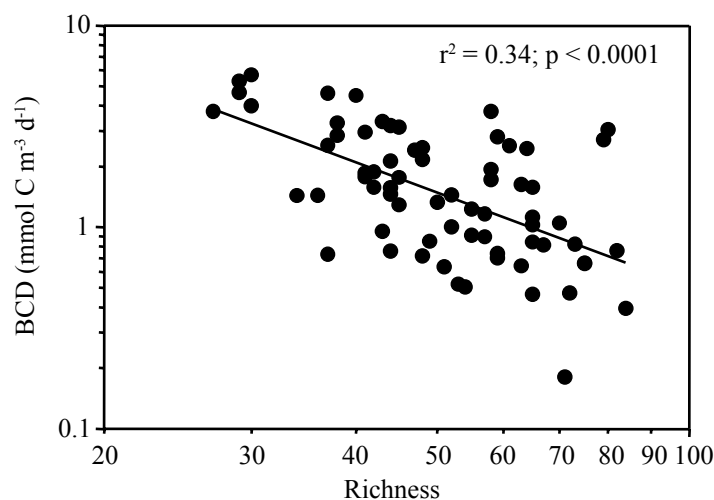


Figure 5.6: Relationship between bacterioplankton richness and bacterial carbon demand (BCD; $\text{mmol C m}^{-3} \text{d}^{-1}$).

organisms should be used [19]. The bacterial carbon demand (BCD), calculated as the sum of BP and BR reveals the carbon flux mediated by the bacterial community. We found a broad negative relationship between bacterial richness and the BCD (Fig. 5.6). This would argue for a highly active bacterial assemblage in spring with few community members and reduced productivity with increasing bacterial richness.

The question arises, whether the combined physicochemical effects constrain BP or whether changes in bacterial richness control BP. Reinthaler and Herndl [41] found a link between primary production and BP and a direct relationship between bacterial growth efficiency and the availability of labile DOC. However, in chemostats kept under constant environmental conditions, Fernández et al. [17] found that functional performance was constant over 2 years albeit considerable changes in the bacterial community composition, driven by the interactions among the different members of the community. Although we have no direct evidence that bacterioplankton richness influences BP, the negative relation between cell-specific BP and bacterial richness is apparent (Fig. 5.4a).

Generally, the stability-diversity hypotheses argue that with increasing diversity or species richness, community responses tend to become more stable [16, 29]. We assessed the stability-diversity relationship for North Sea bacterioplankton, using the bacterioplankton richness and activity, by constructing a dendrogram based on the similarity matrix and then intersecting the resulting tree at relative similarities of 75 and 83% (Fig. 5.2) in a way to allow calculation of averages and standard deviations. The tendency of variance to increase with the mean is a major source of bias in variability estimates [9]. McArdle et al. [28] argued that the standard deviation of log-transformed raw data [standard deviation (SD) of $\log(x_i)$] is less sensitive to highly skewed distributions, as is often the case for aggregate community properties, than the coefficient of variation.

When the standard deviation of log-transformed cell-specific BP obtained from the individual months was plotted against the respective average of bacterioplankton richness, a significant increase in variability with increasing richness became apparent ($r^2 = 0.70; p < 0.002$) (Fig. 5.7a). This suggests that increasing richness leads to an increased instability of

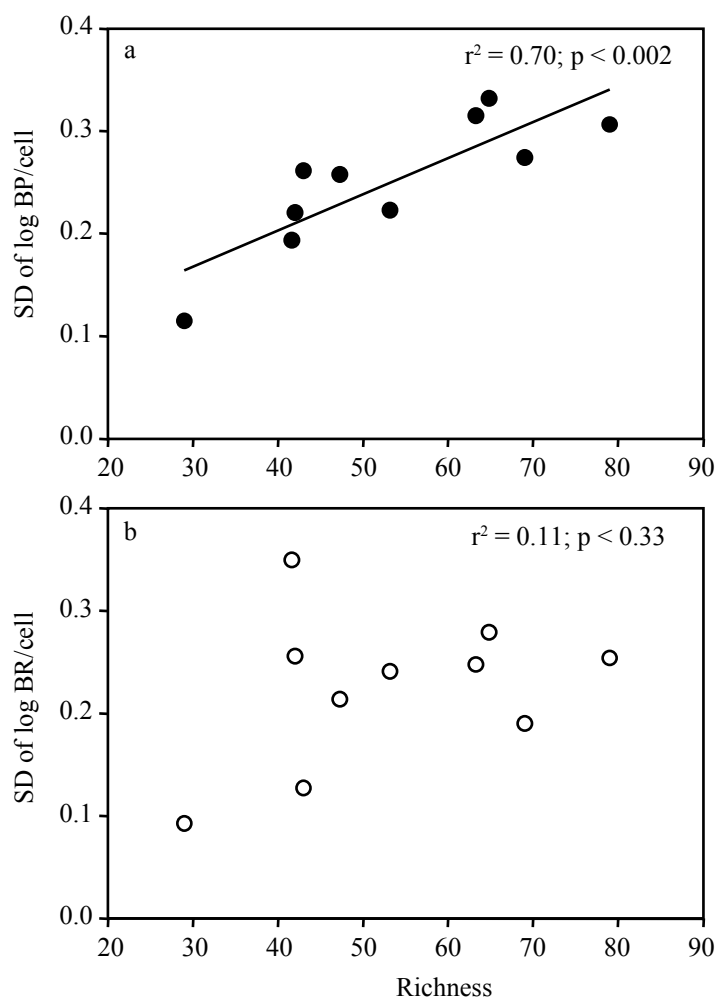


Figure 5.7: Relationship between the standard deviations (SD) of log-transformed raw data [SD of $\log(x_i)$] and averages of bacterioplankton richness calculated for the subgroups >83% relative similarity, as indicated in the dendrogram in Fig. 5.2. The graph shows the relationship between richness and SD of log BP/cell (a) or SD of log BR/cell (b).

cell-specific BP. However, the variability of cell-specific BR barely increased along the richness gradient (Fig. 5.7b). This is in contrast to McGrady-Steed et al. [30] who measured the CO₂ flux in mesocosms supplied with increasing species richness of a manipulated aquatic microbial assemblage. They found that with increasing biodiversity ecosystem respiration becomes more predictable, i.e., the standard deviation of replicates with similar species richness decreased with increasing richness. Our data on natural bacterioplankton assemblages, however, suggest that bacterioplankton respiration is rather independent of shifts in bacterioplankton community richness. Thus, the main function of heterotrophic bacterioplankton, i.e., the remineralization of DOC to CO₂ is rather stable over the seasonal cycle.

Acknowledgements

We thank the captain and crew of the R/V *Pelagia* for their support at sea. Martien Baars and Corina Brussaard are gratefully acknowledged as chief scientists during the cruises. We also thank Govert van Noort, Anna Noordeloos and Santiago Gonzalez for help with data analysis. This work was supported by the Dutch Science Foundation (NWO-ALW) project 811.33.002) and the European Commission through the COMET and AIRWIN project.

Bibliography

- [1] Arrieta JM, Herndl GJ. 2002. Changes in bacterial β -glucosidase diversity during a coastal phytoplankton bloom. *Limnology and Oceanography* 47: 594-9
- [2] Arrieta JM, Weinbauer MG, Lute C, Herndl GJ. 2004. Response of bacterioplankton to iron fertilization in the Southern Ocean. *Limnology and Oceanography* 49: 799-808
- [3] Benner R, Pakulski JD, Mccarthy M, Hedges JI, Hatcher PG. 1992. Bulk chemical characteristics of dissolved organic matter in the ocean. *Science* 255: 1561-4
- [4] Benner R, Strom M. 1993. A critical evaluation of the analytical blank associated with DOC measurements by high-temperature catalytic oxidation. *Marine Chemistry* 41: 153-60
- [5] Cardinale BJ, Ives AR, Inchausti P. 2004. Effects of species diversity on the primary productivity of ecosystems: extending our spatial and temporal scales of inference. *Oikos* 103: 437-50
- [6] Carlson CA, Giovannoni SJ, Hansell DA, Goldberg SJ, Parsons R, Vergin K. 2004. Interactions among dissolved organic carbon, microbial processes, and community structure in the mesopelagic zone of the northwestern Sargasso Sea. *Limnology and Oceanography* 49: 1073-83
- [7] Carritt DE, Carpenter JH. 1966. Comparison and evaluation of currently employed modifications of Winkler method for determining dissolved oxygen in seawater - a NASCO Report. *Journal of Marine Research* 24: 287-318
- [8] Clarke KR, Warwick RM. 2001. *Change in marine communities: an approach to statistical analysis and interpretation*. Plymouth, UK: PRIMER-E. 172 pp.

- [9] Cottingham KL, Brown BL, Lennon JT. 2001. Biodiversity may regulate the temporal variability of ecological systems. *Ecology Letters* 4: 72-85
- [10] Covert JS, Moran MA. 2001. Molecular characterization of estuarine bacterial communities that use high- and low-molecular weight fractions of dissolved organic carbon. *Aquatic Microbial Ecology* 25: 127-39
- [11] Crump BC, Kling GW, Bahr M, Hobbie JE. 2003. Bacterioplankton community shifts in an Arctic lake correlate with seasonal changes in organic matter source. *Applied and Environmental Microbiology* 69: 2253-68
- [12] Del Giorgio PA, Cole JJ. 2000. Bacterial energetics and growth efficiency. In *Microbial Ecology of the Oceans*, ed. DL Kirchman, pp. 289-325. New York: Wiley-Liss
- [13] Del Giorgio PA, Cole JJ, Cimperis A. 1997. Respiration rates of bacteria exceed phytoplankton in unproductive aquatic systems. *Nature* 385: 148-51
- [14] Doak DF, Bigger D, Harding EK, Marvier MA, O'Malley RE, Thomson D. 1998. The statistical inevitability of stability-diversity relationships in community ecology. *American Naturalist* 151: 264-76
- [15] Ducklow HW, Carlson CA. 1992. Oceanic bacterial production. *Advances in Microbial Ecology* 12: 113-81
- [16] Elton CS. 1958. *Ecology of invasions by animals and plants*. New York: John Wiley & Sons. 181 pp.
- [17] Fernández AS, Huang S, Seston S, Xing J, Hickey R, et al. 1999. How stable is stable? Function versus community composition. *Applied and Environmental Microbiology* 65: 3697-704
- [18] Gessner MO, Inchausti P, Persson L, Raffaelli DG, Giller PS. 2004. Biodiversity effects on ecosystem functioning insights from aquatic systems. *Oikos* 104: 419-22
- [19] Groner E, Novoplansky A. 2003. Reconsidering diversity-productivity relationships: directness of productivity estimates matters. *Ecology Letters* 6: 695-9
- [20] Hector A, Schmid B, Beierkuhnlein C, Caldeira MC. 1999. Plant diversity and productivity experiments in European grasslands. *Science* 286: 1123-7
- [21] Holm-Hansen O, Lorenzen CL, Holmes RW, Strickland JDH. 1965. Fluorometric determination of chlorophyll. *Journal du Conseil permanent International pour l'Exploration de la Mer* 30: 3-15
- [22] Horner-Devine MC, Leibold MA, Smith VH, Bohannon BJM. 2003. Bacterial diversity patterns along a gradient of primary productivity. *Ecology Letters* 6: 613-22
- [23] Kerkhof LJ, Voytek MA, Sherrell RM, Millie D, Schofield O. 1999. Variability in bacterial community structure during upwelling in the coastal ocean. *Hydrobiologia* 401: 139-48

- [24] Lane DJ. 1991. 16S/23S rRNA sequencing. In *Nucleic acid techniques in bacterial systematics*, ed. E Stackebrandt, M Goodfellow, pp. 115-76. New York: John Wiley & Sons
- [25] Lee S, Fuhrman JA. 1987. Relationships between biovolume and biomass of naturally derived marine bacterioplankton. *Applied and Environmental Microbiology* 53: 1298-303
- [26] Lindström ES. 2001. Investigating influential factors on bacterioplankton community composition: results from a field study of five mesotrophic lakes. *Microbial Ecology* 42: 598-605
- [27] Loreau M, Naeem S, Inchausti P, Bengtsson J, Grime JP, et al. 2001. Biodiversity and ecosystem functioning: current knowledge and future challenges. *Science* 294: 804-8
- [28] McArdle BH, Gaston KJ, Lawton JH. 1990. Variation in the size of animal populations: patterns, problems and artefacts. *Journal of Animal Ecology* 59: 439-54
- [29] McCann KS. 2000. The diversity-stability debate. *Nature* 405: 228-33
- [30] McGrady-Steed J, Harris PM, Morin PJ. 1997. Biodiversity regulates ecosystem predictability. *Nature* 390: 162-5
- [31] Mittelbach GG, Steiner CF, Scheiner SM, Gross KL, Reynolds HL, et al. 2001. What is the observed relationship between species richness and productivity? *Ecology* 82: 2381-96
- [32] Moeseneder MM, Winter C, Arrieta JM, Herndl GJ. 2001. Terminal-restriction fragment length polymorphism (T-RFLP) screening of a marine archaeal clone library to determine the different phylotypes. *Journal of Microbiological Methods* 44: 159-72
- [33] Moeseneder MM, Winter C, Herndl GJ. 2001. Horizontal and vertical complexity of attached and free-living bacteria of the eastern Mediterranean Sea, determined by 16S rDNA and 16S rRNA fingerprints. *Limnology and Oceanography* 46(1): 95-107
- [34] Morin PJ, McGrady-Steed J. 2004. Biodiversity and ecosystem functioning in aquatic microbial systems: a new analysis of temporal variation and species richness-predictability relations. *Oikos* 104: 458-66
- [35] Naeem S, Li SB. 1997. Biodiversity enhances ecosystem reliability. *Nature* 390: 507-9
- [36] Pai S-C, Gong G-C, Liu K-K. 1993. Determination of dissolved oxygen in seawater by direct spectrophotometry of total Iodine. *Marine Chemistry* 41: 343-51
- [37] Pinhassi J, A. Hagström. 2000. Seasonal succession in marine bacterioplankton. *Aquatic Microbial Ecology* 21: 245-56
- [38] Pinhassi J, Sala MM, Havskum H, Peters F, Guadayol O, et al. 2004. Changes in bacterioplankton composition under different phytoplankton regimens. *Applied and Environmental Microbiology* 70: 6753-66
- [39] Porter KG, Feig YS. 1980. The use of DAPI for identifying and counting aquatic microflora. *Limnology and Oceanography* 25: 943-8

- [40] Rappe MS, Suzuki MT, Vergin KL, Giovannoni SJ. 1998. Phylogenetic diversity of ultraplankton plastid small-subunit rRNA genes recovered in environmental nucleic acid samples from the Pacific and Atlantic coasts of the United States. *Applied and Environmental Microbiology* 64: 294-303
- [41] Reinthaler T, Herndl GJ. 2005. Seasonal dynamics of bacterial growth efficiencies in relation to phytoplankton in the southern North Sea. *Aquatic Microbial Ecology* 39: 7-16
- [42] Riemann B, Bell RT, Jørgensen NOG. 1990. Incorporation of thymidine, adenine and leucine into natural bacterial assemblages. *Marine Ecology Progress Series* 65: 87-94
- [43] Rivkin RB, Legendre L. 2001. Biogenic carbon cycling in the upper ocean: Effects of microbial respiration. *Science* 291: 2398-400
- [44] Robinson C, Widdicombe CE, Zubkov MV, Tarran GA, Miller AEJ, Rees AP. 2002. Plankton community respiration during a coccolithophore bloom. *Deep-Sea Research Part II* 49: 2929-50
- [45] Roland F, Caraco NF, Cole JJ, Del Giorgio PA. 1999. Rapid and precise determination of dissolved oxygen by spectrophotometry: evaluation of interference from color and turbidity. *Limnology and Oceanography* 44: 1148-54
- [46] Schäfer H, Bernard L, Courties C, Lebaron P, Servais P, et al. 2001. Microbial community dynamics in Mediterranean nutrient-enriched seawater mesocosms: changes in the genetic diversity of bacterial populations. *FEMS Microbiology Ecology* 34: 243-53
- [47] Schmid B. 2002. The species richness-productivity controversy. *Trends in Ecology & Evolution* 17: 113-4
- [48] Simon M, Azam F. 1989. Protein content and protein synthesis rates of planktonic marine bacteria. *Marine Ecology Progress Series* 51: 201-13
- [49] Suzuki MT, Giovannoni SJ. 1996. Bias caused by template annealing in the amplification of mixtures of 16S rRNA genes by PCR. *Applied and Environmental Microbiology* 62: 625-30
- [50] Tilman D. 1999. The ecological consequences of changes in biodiversity: A search for general principles. *Ecology* 80: 1455-74
- [51] v. Wintzingerode F, Gobel UB, Stackebrandt E. 1997. Determination of microbial diversity in environmental samples: pitfalls of PCR-based rRNA analysis. *FEMS Microbiology Reviews* 21: 213-29
- [52] Winter C, Moeseneder MM, Herndl GJ. 2001. Impact of UV radiation on bacterioplankton community composition. *Applied and Environmental Microbiology* 67: 665-72.
- [53] Yannarell AC, Triplett EW. 2004. Within and between lake variability in the composition of bacterioplankton communities: investigations using multiple spatial scales. *Applied and Environmental Microbiology* 70: 214-23

- [54] Yu Z, Mohn WW. 2001. Bacterial Diversity and Community Structure in an Aerated Lagoon Revealed by Ribosomal Intergenic Spacer Analyses and 16S Ribosomal DNA Sequencing. *Applied and Environmental Microbiology* 67: 1565-74

Summary

Following a gradient in system's productivity from the Mauritanian upwelling into the oligotrophic subtropical Atlantic, bacterial respiration (BR) in the euphotic layer was in the range of 36 to 76% of total community respiration. This suggests that depending on the trophic status, BR in the surface ocean does not always constitute the main fraction of system's respiration and more organic matter might be remineralized by larger sized planktonic organisms than by bacteria.

The sea-surface microlayer (SML) is the boundary layer between the ocean and the atmosphere and its chemical composition and biological activity might substantially influence the gas exchange between the ocean and the atmosphere. BR in the surface microlayer and the underlying waters (30 cm depth) contributed on average 58% to total community respiration. In the underlying water, bacterial growth efficiency (BGE) exhibited the typical range for open ocean surface waters ranging from 9 to 14%, however, calculated BGE in the SML was only between 0.2 and 2%, thus extremely low. Concentrations of dissolved organic nitrogen (DON) and phosphorus (DOP) and particularly free amino acids were significantly enriched in the SML as compared to the underlying waters. Despite the high concentrations of free amino acids in the SML, usually taken up efficiently by bacteria, bacterial production (BP) was consistently low whereas BR was elevated by a factor of ~ 15 over the background value of $\sim 0.8 \pm 0.8 \mu\text{mol O}_2 \text{ L}^{-1} \text{ d}^{-1}$ in the underlying water. This suggests that the dissolved organic matter (DOM) accumulating in the SML is not readily available to bacteria. A combination of factors might be responsible for this characteristic feature of the SML. One reason could be UV-radiation retarding bacterial activity, however, low BGEs were also obtained in the early morning when bacteria should have recovered already from the UV stress of the previous day. Another explanation might be nutrient limitation due to the disproportionate conversion of dissolved organic carbon (DOC), DON or DOP to more labile constituents upon UV irradiation in the initially refractory DOM.

Shelf seas such as the North Sea are sites of high primary production and heterotrophic microbial activity. Changing bacterial carbon demand in concert with the seasonality in primary production determines whether systems are net auto- or heterotrophic. On an annual scale, BGE was $\sim 20 \pm 11\%$, however, seasonally, BGE ranged from $25 \pm 9\%$ in spring and summer to $6 \pm 3\%$ in the winter. BGE was mainly determined by the dynamics in BP. Cell-specific BP varied over one order of magnitude from spring to winter (0.6 to $0.06 \text{ fmol C cell}^{-1} \text{ d}^{-1}$). During that time, cell-specific BR was rather stable and varied only between 1 and $2 \text{ fmol C cell}^{-1} \text{ d}^{-1}$. Estimated bioavailability of DOC to support BP was linked to the dynamics in particulate primary production. Thus, despite the high input of terrigenous organic matter via rivers into the North Sea, autochthonously produced organic matter determines BP and BGE.

It is generally assumed that particulate organic carbon, exported from the euphotic zone, is the main carbon source for meso- and bathypelagic waters. However, evidence accumulates

suggesting that the local carbon export from the surface water does not match the respiration rates estimated for the dark ocean. The average BGE was 2% in the dark ocean of the North Atlantic and prokaryotic respiration was more stable than prokaryotic production mirroring the findings obtained in the North Sea. Generally, higher prokaryotic activity was observed than previously reported for the dark ocean, however, the high prokaryotic carbon demand measured cannot be explained by conventional models of carbon fluxes. This discrepancy between the prokaryotic carbon demand and the carbon supply rate might be due to stimulation of prokaryotic activity due to decompression of the samples prior to the rate measurements. Thus, the high microbial activity we measured highlights the need to perform these rate measurements under realistic pressure conditions but also indicates that deep water prokaryotes have the potential to exhibit higher metabolic activity than hitherto assumed.

There is a lively debate on the relation between biodiversity and ecosystem function and stability. We investigated the richness of the bacterial community by T-RFLP fingerprinting of 16S rRNA gene fragments in the North Sea. A highly active bacterial assemblage with few dominating phylotypes was found in spring and reduced productivity with increasing bacterial richness in winter. The monthly variability of cell-specific BP as a function of seasonal bacterioplankton richness suggested, that increasing richness is related to enhanced variability of cell-specific bacterial growth. However, cell-specific BR remained remarkably constant over the range of observed bacterioplankton richness. This suggests that despite the observed shifts in the community composition, the main function of heterotrophic bacterioplankton, i.e., the remineralization of DOC to CO₂ is rather stable over the seasonal cycle.

Synoptic analysis of the collected data

Generally, bacterial growth efficiency increases with increasing bacterial production [3]. Recent reports suggest that, on a seasonal scale, BP is mainly responsible for the dynamics of BGE [6, 9, 11], but do similar relations exist on a broader scale between different open ocean regions and different trophic sites? To synthesize a more global view, the data collected between May and September in the southern North Sea (NS), subtropical Atlantic (SATL) and the western Mediterranean Sea (WMED) were grouped according to the trophic status of the systems, i.e., into more eutrophic or oligotrophic sites, according to the relative inorganic nutrient load. This division is somewhat arbitrary, however, the definition of ‘trophic state’ of a system itself is blurred [2]. Temperature has been suggested to significantly affect BGE [10], however, no clear direct relationship was found in the present dataset although temperature ranged from ~14 to 26°C (Fig. 1a). Average bulk DOC concentrations, as indicator for potential substrate sources to bacteria were in the range of 58 to 127 mmol C m⁻³ (Fig. 1b). Nevertheless, only a weak relationship with either BP or BR was found. Seasonal deviations from optimum temperature or substrate concentration limit bacterial growth in varying degrees [7, 12]. Furthermore, natural DOC consists of a continuum of size classes of differing diagenetic state [1], which makes it difficult to directly relate bulk DOC measurements to BP and growth. Consequently we assume that the combined effects defining the general trophic state is dominating over direct relationships of BP or BR with temperature and DOC.

Converting BP measurements into units of carbon is a source of uncertainty in BGE estimates [4, 8]. For this survey, a conversion factor of 1.5 kg carbon mol⁻¹ leucine was assumed for all the data [5]. Within the different trophic categories, BP varied only over one order of magnitude from 0.29 ± 0.19 mmol C m⁻³ d⁻¹ in the eutrophic surface waters to 0.03

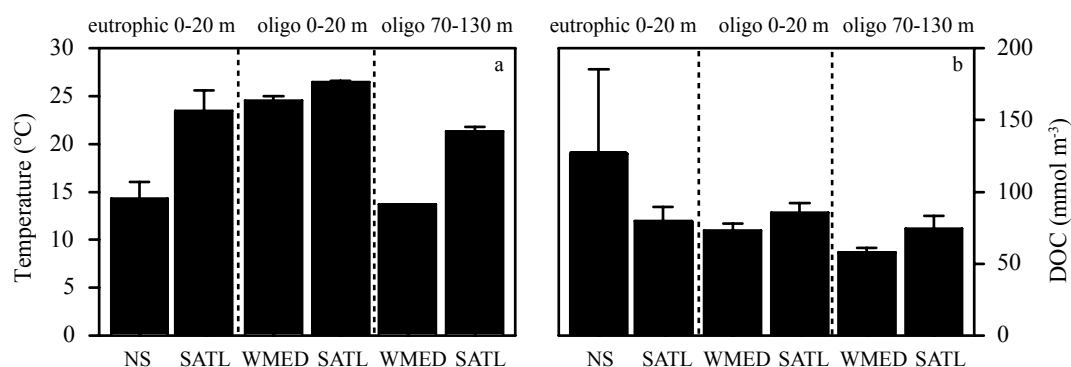


Figure 1: Average Temperature (°C) (a) and dissolved organic carbon (DOC; mmol m⁻³) (b) in the North Sea (NS), subtropical Atlantic (SATL) and the western Mediterranean (WMED).

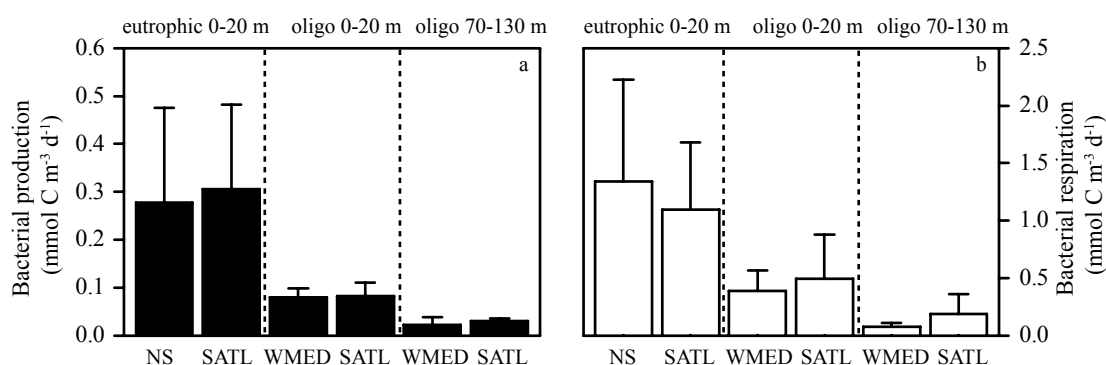


Figure 2: Bacterial production (mmol C m⁻³ d⁻¹) (a) and bacterial respiration (mmol C m⁻³ d⁻¹) (b) at the different trophic sites.

± 0.01 mmol C m⁻³ d⁻¹ in the more oligotrophic deeper water layers. From the more eutrophic sites towards the more oligotrophic sites, however, BP decreased by ~91% (Fig. 2a). Similar to BP, the variation in respiration within the individual groups was lower than between the different sites. Averaged BR (converted to carbon units by a respiratory quotient of 1) ranged from 1.27 ± 0.82 mmol C m⁻³ d⁻¹ in the eutrophic regions to low respiration rates of 0.15 ± 0.15 mmol C m⁻³ d⁻¹ in the deeper oligotrophic water layers (Fig. 2b) which is an overall decrease in respiration rates by 88%.

We estimated the relative availability of DOC by normalizing the BP measurements to bulk DOC (Fig. 3). Although this index is quite crude, it shows the relative importance the DOC might play at the different sites, with the most refractory DOM in the WMED and the most labile DOM in the productive region of the subtropical Atlantic.

Despite the range in BP and BR between the regions and trophic sites, the calculated mean BGE ($19.3 \pm 8.6\%$; $n = 144$) showed rather low variability (Fig. 4). However, the magnitude in BGE was affected differently by BP and BR at the different trophic sites (Fig. 5). BGE in eutrophic surface regions is more influenced by BP as suggested previously [3, 9, 11]. In oligotrophic surface regions, however, most of the variability in BGE is explained by BR whereas in the deeper layers of oligotrophic sites, the combination of very low BP and BR determines the BGE.

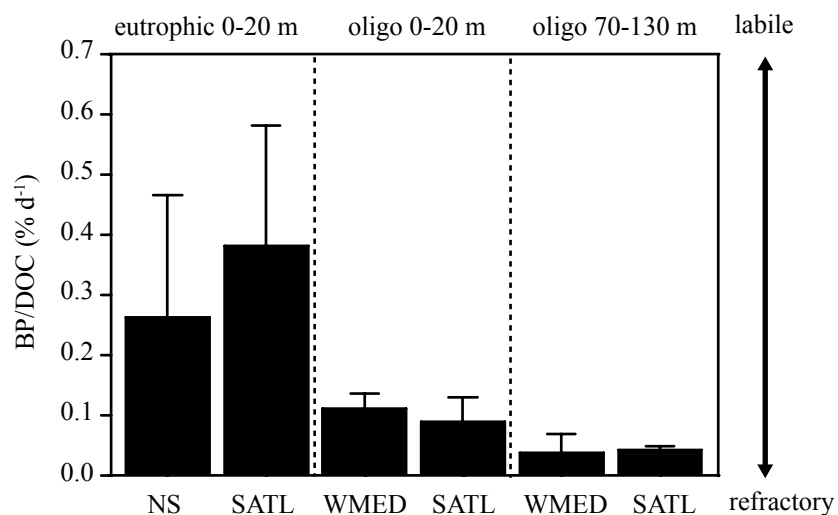


Figure 3: Bacterial production normalized to DOC (% d⁻¹). Higher percentages are indicative for relatively more labile organic matter, low values show more refractory DOC.

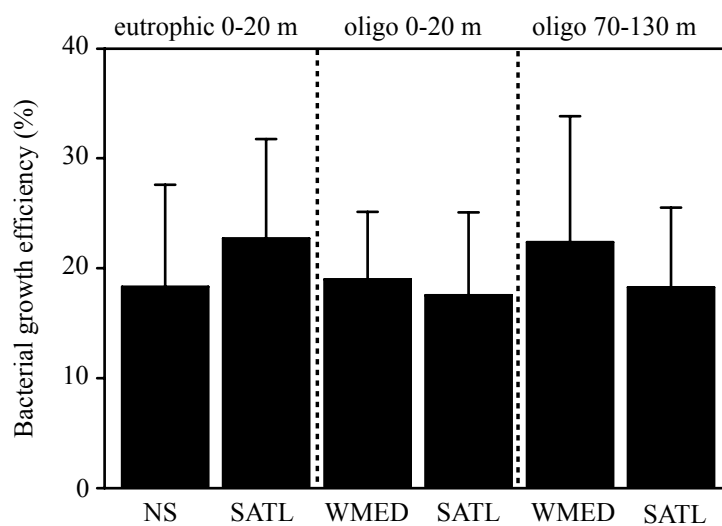


Figure 4: Bacterial growth efficiency (%) at the different trophic sites of the ocean.

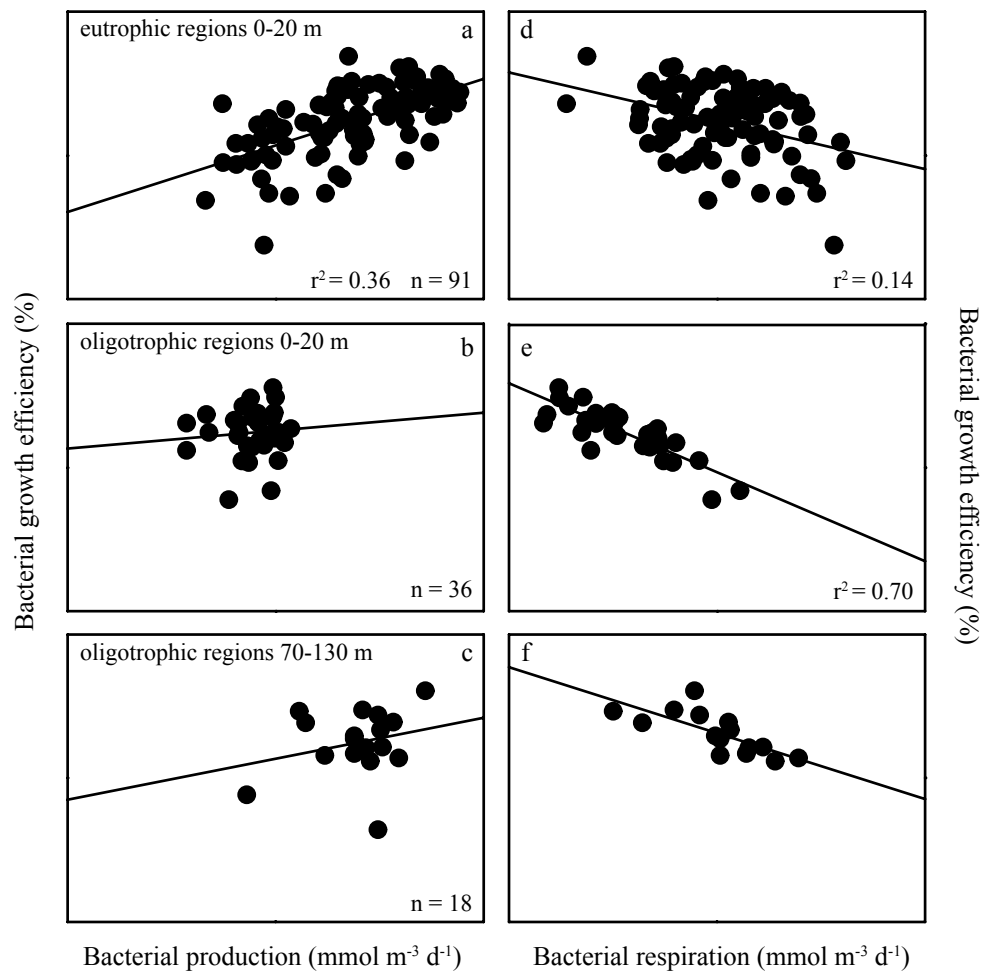


Figure 5: Relationship of bacterial growth efficiency and bacterial production (a-c) or bacterial respiration (d-f) at the different trophic sites.

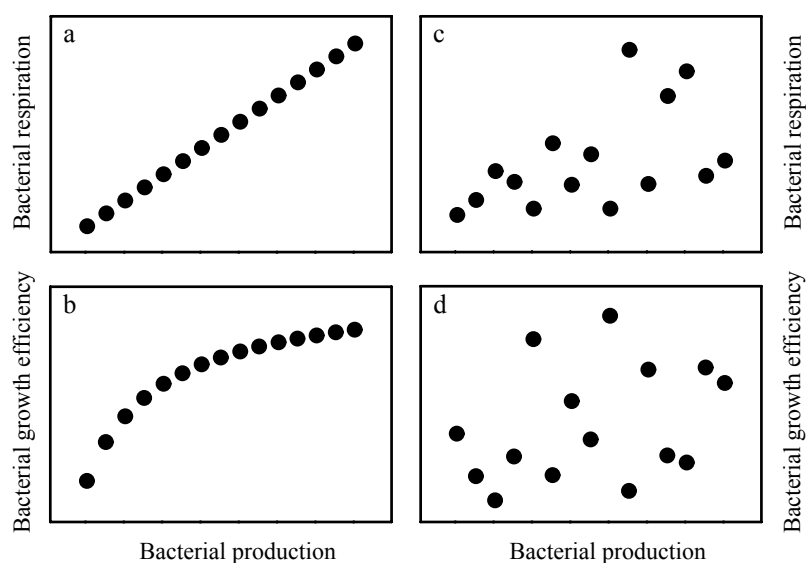


Figure 6: Model relationships of bacterial production, bacterial respiration and bacterial growth efficiency. Bacterial respiration was calculated assuming a fixed relationship to bacterial production (a, b). Bacterial respiration derived from random numbers in the range typical for open ocean waters (c, d).

The relation between BGE and BP or BR is partly determined by the equation $[BGE = BP/(BP + BR)]$. If BR would be a fixed function of BP (Fig. 6a) then BGE would asymptotically rise to reach a maximum value (Fig. 6b). If, however, BR is only weakly related to BP (Fig. 6c), BGE might vary randomly along a gradient of BP (Fig. 6d). Thus, apparently at oligotrophic sites, BP tends to be uncoupled from BGE and probably a variable fraction of the available energy is used for cell maintenance. A similar conclusion was reached by Del Giorgio and Cole [3] who assumed, however, that the patterns found between BP and BGE could have been driven to some extent by the variability in the data they compiled from different studies using various methods.

Ultimately, bacterial production and respiration should be linked to the available organic matter, however, it becomes clear in the different chapters of this thesis that the relationship between bulk DOC and bacterial production or respiration is either weak or not existent at all. Thus besides the many assumption involved in measuring bacterial production and respiration accurately, perhaps the biggest problem in determining the degree of variability in BGE is the unknown composition of the natural DOM pool and its bioavailability to bacteria.

Bibliography

- [1] Amon RMW, Benner R. 1996. Bacterial utilization of different size classes of dissolved organic matter. *Limnology and Oceanography* 41: 41-51
- [2] Carlson RE, Simpson J. 1996. A coordinator's guide to volunteer lake monitoring methods. *North American Lake Management Society*: 96

- [3] Del Giorgio PA, Cole JJ. 2000. Bacterial energetics and growth efficiency. In *Microbial Ecology of the Oceans*, ed. DL Kirchman, pp. 289-325. New York: Wiley-Liss
- [4] Ducklow HW, Kirchman DL, Anderson TR. 2002. The magnitude of spring bacterial production in the North Atlantic Ocean. *Limnology and Oceanography* 47: 1684-93
- [5] Kirchman D. 1993. Leucine incorporation as a measure of biomass production by heterotrophic bacteria. In *Handbook of methods in aquatic microbial ecology*, ed. PF Kemp, BF Sherr, EB Sherr, JJ Cole, pp. 509-12. Boca Raton: Lewis publishers
- [6] Lemée R, Rochelle-Newall E, Van Wambeke F, Pizay M-D, Rinaldi P, Gattuso J-P. 2002. Seasonal variation of bacterial production, respiration and growth efficiency in the open NW Mediterranean Sea. *Aquatic Microbial Ecology* 29: 227-37
- [7] Pomeroy LR, Wiebe WJ. 2001. Temperature and substrates as interactive limiting factors for marine heterotrophic bacteria. *Aquatic Microbial Ecology* 23: 187-204
- [8] Reinthaler T, Aristegui J, Robinson C, Williams PJIB, Lebaron P, et al. Prokaryotic respiration and production in the meso- and bathypelagic realm of the eastern and western North Atlantic basin. *submitted to Limnology and Oceanography*
- [9] Reinthaler T, Herndl GJ. 2005. Seasonal dynamics of bacterial growth efficiencies in relation to phytoplankton in the southern North Sea. *Aquatic Microbial Ecology* 39: 7-16
- [10] Rivkin RB, Legendre L. 2001. Biogenic carbon cycling in the upper ocean: Effects of microbial respiration. *Science* 291: 2398-400
- [11] Sherry ND, Boyd PW, Sugimoto K, Harrison PJ. 1999. Seasonal and spatial patterns of heterotrophic bacterial production, respiration, and biomass in the subarctic NE Pacific. *Deep-Sea Research Part II* 46: 2557-78
- [12] Wiebe WJ, Pomeroy LR. 1999. *The temperature-substrate controversy resolved?* Presented at 8th international symposium on microbial ecology, Canada, Halifax

Samenvatting

Bacteriële respiratie in de eufotische zone van ecosystemen met een hoge productiviteit (zoals het opwellingsgebied bij Mauretanië) tot de laag productieve oligotrofe subtropische Atlantische Oceaan varieert van 36 tot 76% van de totale respiratie. Dit suggereert, dat organisch materiaal in de bovenste laag van de oceaan voor een groot deel door organismen groter dan bacteriën geremineeraliseerd kan worden.

De zogeheten microlaag direct aan het zee-oppervlak (SML, surface microlayer) vormt de grens tussen de oceaan en de atmosfeer. De chemische samenstelling ervan zou de uitwisseling van gassen tussen zee en lucht substantieel kunnen beïnvloeden. Bacteriële respiratie (BR) in de SML en de direct eronder liggende waterlaag (30 cm diepte) bedroeg gemiddeld 58% van de totale respiratie. De bacteriële groei-efficiëntie (BGE, bacterial growth efficiency) in de onderliggende wateren lag in het bereik voor open oceanen (9–14%). De BGE in de SML was extreem laag en bedroeg maar 0.2–2%.

De concentraties van opgeloste organisch stikstof (DON, dissolved organic nitrogen), fosfaat (DOP, dissolved organic phosphate) en vrije aminozuren waren in de SML significant hoger dan in het onderliggende water. Ondanks die hogere concentratie van vrije aminozuren in de SML en de over het algemeen gemakkelijke opname van deze organische verbindingen door bacteriën, was de bacteriële productie laag en de BR juist hoog (15 maal hoger dan in de in de onderliggende wateren). Dit suggereert dat het opgeloste organische materiaal (DOM, dissolved organic matter) dat zich ophoopt in de SML niet gemakkelijk beschikbaar is voor de bacteriën. Verschillende factoren zouden hiervoor verantwoordelijk kunnen zijn. UV straling, waarvan bekend is dat dit een negatief effect heeft op bacteriële activiteit zou een verklaring kunnen zijn. Echter, lage BGE was ook waargenomen in de vroege ochtend wanneer de bacteriën hersteld zouden moeten zijn van eventuele UV-stress van de vorige dag. Een gebrek aan beschikbare voedingstoffen zou een andere verklaring kunnen zijn. Als gevolg van de blootstelling aan UV straling zou een onevenredig groot gedeelte van de, aanvankelijk gemakkelijk afbreekbare, opgeloste organische koolstof (DOC, dissolved organic carbon) DON of DOP, kunnen worden omgezet in minder gemakkelijk afbreekbare verbindingen.

Kustzeeën zoals de Noordzee zijn gebieden met hoge primaire productie en heterotrofe microbiële activiteit. Veranderingen in de bacteriële vraag naar koolstof die gelijk opgaan met de seizoensafhankelijke variatie in primaire productie bepalen of een ecosysteem netto auto- of heterotroof is. Op jaarbasis was de BGE $20 \pm 9\%$, maar in de winter slechts $6 \pm 3\%$. De BGE werd voornamelijk bepaald door de dynamiek in de bacteriële productie (BP). Cel-specifieke BP was een factor tien groter in het voorjaar dan in de winter (0.6 resp. 0.06 fmol C per cel per dag). Variabiliteit in de particuliere primaire productie had zijn weerslag op de geschatte biobeschikbaarheid van DOC die nodig is voor de BP. Dus ondanks de hoge toevoer van terrogeen organische stof vanuit rivieren bepaalt de autogeen geproduceerde organische stof de bacteriële productie en BGE in de Noordzee.

Het wordt algemeen aangenomen dat de particuliere organische koolstof vanuit de eufotische zone de belangrijkste bron van koolstof is voor de meso- en bathypelagische wateren. Er is echter toenemend bewijs dat het lokale transport van koolstof vanuit de oppervlaktewateren naar de waterlagen daaronder niet overeenkomt met de respiratiesnelheden in de diepe oceaan. De gemiddelde BGE in de diepzee van de Noord Atlantische Oceaan was 2%, en was stabiel dan de prokaryote productie. Dit komt overeen met de bevindingen in de Noordzee. Over het algemeen observeerden we een hogere prokaryote activiteit dan tot nu toe werd vermeld voor de diepe oceaan. De hoge gemeten vraag naar koolstof van prokaryoten kan niet worden verklaard door conventionele koolstoffluxmodellen. Het verschil tussen de prokaryote koolstofvraag en -aanbod zou veroorzaakt kunnen zijn door verhoogde activiteit van de prokaryoten als gevolg van het drukverschil tussen diepzee en oppervlak. Hoewel onze metingen suggereren dat prokaryoten uit de diepe oceaan potentieel een hogere metabolische activiteit kunnen hebben dan tot nu toe aangenomen, maken de resultaten ook duidelijk dat er behoefte is om de metingen te herhalen onder realistische hoge druk omstandigheden.

Er is een levendig debat gaande over de relatie tussen biodiversiteit en de functie en stabiliteit van het ecosysteem. Wij hebben de rijkdom van de bacteriële gemeenschap in de Noordzee bestudeerd met behulp van T-RFLP van 16S rRNA genfragmenten (genetische 'vingerafdrukken'). Een actieve bacteriële gemeenschap met slechts enkele dominerende fylotypen werd gevonden in het voorjaar. Dit in tegenstelling tot de wintersituatie met een gereduceerde productiviteit die een toegenomen bacteriële rijkdom liet zien. De maandelijkse variabiliteit in cel-specifieke BP als functie van de seizoensafhankelijke bacteriële rijkdom suggereert dat toenemende rijkdom in bacteriële fylotypen is gerelateerd aan een toenemende variatie in cel-specifieke bacteriële groei. De cel-specifieke BR bleef echter opmerkelijk constant. Dit impliceert dat ondanks de waargenomen seizoensveranderingen in de samenstelling van de bacteriële gemeenschap de belangrijkste functie van deze heterotrofe bacteriën, zijnde de remineralizatie van DOC naar CO₂ stabiel is.

Acknowledgements

With all the difficulties inherent in being a foreigner in any foreign country, especially on Texel, there are some good reasons to do a PHD at the NIOZ. The excellent working conditions are one of them, but most of all it is the people here that run the show.

First I want to thank Gerhard Herndl who gave me the chance to work under his guidance and also for being a friend. His schedule is filled in every possible hour of the day (minus 4 hours of sleep) still, his office door was always open to ask for advice and if not during the week, then we would meet at the weekend to sort out things. He sent me on quite some missions, both scientific and administrative, which at times had only little to do with my core project. However, I learned a great deal through these side tasks for me personally and also for my future in science. Above all he is a great socializer and most of the time was there when his ‘staff’ had parties, never being the first to leave. Thus, the relationship between promoter and promovendus probably can’t get any better.

Through the years on the island, many people have helped to keep me up and running. During the day it was my colleagues at the BIO and other departments whom I want to thank for the big and small advice on my work. I am especially grateful to Karel Bakker, Rinus Manuels, Jan van Ooijen, Santiago González, Herman Boekel, Harry Witte and Arjan Smit for their help in providing analytical assistance and technical know how. I am indebted to the crew of the RV Pelagia with whom I shared in total eight month at sea, for solving whatever technical problem there was on board.

Texel is a migration zone for friends that come and go, however, they will all leave their marks in my memory. For almost four years I shared the office with Txetxu Arrieta. The discussions and exchange of thoughts about our work and private matters were always of great help for me. I shared numerous ‘counseling’ nights with Jörg Dutz, Marja Koski, Christian Winter, Conny Maier, Maite Pérez, Markus Weinbauer, Heidi Pirker, Eva Teira and Ines Wilhartitz; Thank you for the good, the bad and the ugly! My thanks also go to Willem Warmerdam and Corina Brussaard who always have an open house for me and for the nice dinners. Together with Geraldine Kramer, Eva Sintes, Stefan Groenewold, Ben Abbas, Joana Cardoso, Anne-Claire Baudoux, Yann Bozec, Marian Keuning, Micha Rijkenberg, Cornelia Wuchter, Verónica Parada, Tereza Amaro, Furu Mienis, Jasper de Goeij, Marta Varela, Craig Robertson I thank you for making Texel a home for me.

Mein besonderer Dank gilt meinen Eltern. Sie waren es die mir meine Laufbahn ermöglicht haben, ohne wenn und aber. Ich danke auch allen Freunden in Österreich die mich nicht vergessen haben, trotz grosser Distanz und nur sehr gelegentlichen Besuchen meinerseits in Vorarlberg, Wien und Innsbruck. Bei Elmar und Katharina Skarlounik war ich immer willkommen und ihre exzellente Küche und Gastfreundschaft ist nachstrebenswert. Bei Ulrike Hartmann und Markus Kornfehl durfte ich lernen wie man in Österreich Arbeit, Familie und Hausbau unter einen Hut bringt. Durch meinen Bruder Stephan und seine Frau Sonja fühle

Acknowledgements

ich mich der Musik immer noch verbunden wie damals. Zu guter Letzt, die moralische Unterstützung und Treue die ich von meiner Frau Barbara erfahren habe kann mit nichts dieser Welt aufgewogen werden. Mir bleibt nur soviel zu sagen, ohne sie wäre ich nur halb soviel.

Curriculum Vitae

Education

- 1992–1994 University of Innsbruck, Austria; General Biology
- 1994–1997 University of Vienna, Austria; Zoology with special emphasize on anatomy, aquatic microbiology and marine ecology.
- 1997–1999 Department of Marine Biology, Vienna–M.Sc. Thesis: ‘Coexistence and nutrition by the Mediterranean holothuroids *Holothuria tubulosa* and *Holothuria polii* (Echinodermata) at the island of Elba, Italy’ supervision Prof. Dr. Joerg Ott
- 1999–2000 Educational journey to South Pacific islands, Australia and South East Asia
- 2000–2005 Royal Netherlands Institute for Sea Research, Netherlands–Ph.D. Thesis: ‘Response of bacterioplankton activity to changing physical parameters’ supervision Prof. Dr. Gerhard J. Herndl
- 2000–present Scientific and technical assistance in COMET, AIRWIN, TRANSAT and ARCHIMEDES project, granted by the European Union or NWO to G. J. Herndl

Publication List

- Agogu , H, EO Casamayor, F Joux, I Obernosterer, C Dupuy, P Catala, MG Weinbauer, T Reinthaler, GJ Herndl, and P Lebaron. 2004. *Comparison of samplers for the biological characterization of the sea surface microlayer*. Limnology and Oceanography: Methods 2:213-225.
- Herndl, GJ, T Reinthaler, E Teira, H van Aken, C Veth, A Pernthaler, and J Pernthaler. 2005. *Contribution of archaea to total prokaryotic production in the deep atlantic ocean*. Applied and Environmental Microbiology 71:2303-2309.
- Joux, F, H Agogue, I Obernosterer, C Dupuy, T Reinthaler, GJ Herndl, and P Lebaron. *Microbial community structure in the sea surface microlayer at two contrasting coastal sites in the northwestern mediterranean sea*. in press at Aquatic Microbial Ecology.
- Obernosterer, I, P Catala, T Reinthaler, GJ Herndl, and P Lebaron. 2005. *Enhanced heterotrophic activity in the surface microlayer of the mediterranean sea*. Aquatic Microbial Ecology 39:1616-1564.
- Reinthaler, T, K Bakker, R Manuels, J Van Ooijen, and GJ Herndl. submitted. *Fully automated spectrophotometric approach to determine oxygen concentrations in seawater via continuous-flow analysis*. submitted to Limnology and Oceanography: Methods.
- Reinthaler, T, and GJ Herndl. *Bacterial production and respiration in the sea surface microlayer of the open ocean*. submitted to Limnology and Oceanography.
- Reinthaler, T, and GJ Herndl. 2005. *Seasonal dynamics of bacterial growth efficiencies in relation to phytoplankton in the southern North Sea*. Aquatic Microbial Ecology 39:7-16.

- Reinthaler, T, HM van Aken, C Veth, P Lebaron, J Aristegui, C Robinson, PJIB. Williams, and GJ Herndl. *Prokaryotic respiration and production in the meso- and bathypelagic realm of the eastern and western North Atlantic basin*. accepted at Limnology and Oceanography.
- Reinthaler, T, C Winter, and GJ Herndl. 2005. *Relationship between bacterioplankton richness, respiration, and production in the southern North Sea*. Applied and Environmental Microbiology 71:2260-2266.
- Teira, E, T Reinthaler, A Pernthaler, J Pernthaler, and GJ Herndl. 2004. *Combining catalyzed reporter deposition-fluorescence in situ hybridization and microautoradiography to detect substrate utilization by bacteria and archaea in the deep ocean*. Applied and Environmental Microbiology 70:4411-4414.
- Waengberg, S-A, KI Andreasson, K Garde, K Gustavson, P Hendriksen, and T Reinthaler. *Impact of UVB radiation on primary production in an arctic bay- model calculations*. submitted to Aquatic Sciences.

Meetings and Workshops

- 1998 May 5th European conference on Echinoderms, Milan, Italy; Poster
T. Reinthaler and S. Scheiblaue: 'Ecological monitoring of *Holothuria tubulosa* and *H. polii* (Echinodermata: Holothuroidea) in nearshore waters of Elba, Italy'
- 2002 Oct 8th Symposium on Aquatic Microbial Ecology (SAME), Taormina, Italy; Talk
T. Reinthaler and G. J. Herndl: 'Seasonal dynamics of organic carbon remineralization by heterotrophic bacteria in the Southern North Sea'
H. Agogué, F. Joux, E. Casamayor, P. Lebaron, G. J. Herndl, M. Weinbauer and T. Reinthaler: 'Structure of microbial food webs at the air-water interface'
- 2003 Jan Verwey meeting, Texel, Netherlands; . Reinthaler and G. J. Herndl; Talk
'Seasonal dynamics of organic carbon remineralization by heterotrophic bacteria in the Southern North Sea'
- 2004 Feb Ocean Sciences meeting, Honolulu, USA; Talk
T. Reinthaler, J. Aristegui, P. J. Le B. Williams and G. J. Herndl: 'Prokaryotic production and growth yield in the North Atlantic Deep Waters'
- 2004 Jun CIESM congress, Barcelona, Spain; Talk
J. M. Arrieta, E. Sintes, T. Reinthaler and G. J. Herndl: 'Ectoenzymatic hydrolytic activities in the sea surface microlayer'
- 2004 Jul Workshop on aquatic ecosystem respiration, Barcelona, Spain; Talk
T. Reinthaler, J. Aristegui, P. J. Le B. Williams and G. J. Herndl: 'Prokaryotic production and growth yield in the North Atlantic Deep Waters'
- 2005 Apr EGU general assembly meeting, Vienna, Austria; Talk
T. Reinthaler and G. J. Herndl: 'Bacterial and dark community respiration in the euphotic layer along a transect from the Mauritanian upwelling into the subtropical Atlantic gyre'
- 2005 Jun Workshop on respiration and planktonic food webs, Vigo, Spain; Talk
G. J. Herndl and T. Reinthaler: 'Prokaryotic respiration of the meso- and bathypelagic realm'
- 2005 Jun ASLO summer meeting, Santiago di Compostela, Spain; Talk
T. Reinthaler and G. J. Herndl: 'Bacterial respiration and growth efficiency: a system comparison of oceanic sites'
A. Waengberg, K. Andreasson, K. Garde, K. Gustavson, P. Henriksen and T. Reinthaler: 'How sensitive are estimates of inhibition of photosynthesis by UV-B radiation in arctic phytoplankton for different biological and environmental factors?'

Professional Experience

Methods

Oxygen measurement by spectrophotometry
Bacterial production measurements by ³H-Thymidine and ¹⁴C-Leucine incorporation
Epifluorescence microscopy
Fluorescent and spectrophotometric measurements of dissolved organic matter
Bacterial enumeration by different staining techniques (Acridine Orange, DAPI, Propidium Iodide)
Micro-CARD-FISH (Autoradiography combined with catalyzed reporter deposition fluorescent in situ hybridization)
Size fractionation of dissolved organic matter by ultrafiltration
Experience with of solar irradiation measurements (PUV, Macam)
In depth knowledge of software relevant for oceanographic research: e.g. Ocean Data View (ODV),
Global mapping tools (GMT), Surfer, Statistical software (Statistica, Primer5)

Other Methods

Fluorometric determination of bacterial extracellular enzymatic activity
Bacterial community structure by T-RFLP
Bacterial counting by flowcytometry
Electron transport system (ETS) measuring potential community respiration
DOC measurement by HTC method
Amino acid analysis by HPLC method
Image analysis with Laser Scanning Microscopy (LSM–Zeiss)
Scuba Diving
Underwater marine ecological methodology
Knowledge on webdesign (Dreamweaver, Flash, Photoshop, Illustrator)

Courses

Radioactivity course Level 5
STCW 95' basic course – Seaman's book

Teaching

2001 Oct	Assistant teacher for university Utrecht during microbial oceanography course held at the NIOZ
2002 Jun	Assistant teacher for University Groningen during biological oceanography course held at the NIOZ
2003 May	Co-mentor for trainee with topic: 'Bacterial dissolved organic matter utilization in a coastal marine system'
2004 Jun	Lecture at University of Groningen: Pelagic Food Webs, 6 hours
2005 Mai	Lecture at University of Groningen: Pelagic Food Webs, 3 hours

Affiliations

American Society of Limnology and Oceanography
American Society for Microbiology
European Geological Union

Reviewer for

Limnology and Oceanography
Limnology and Oceanography: Methods
Journal of Sea Research

Scientific Expeditions

2000 Sep	Plume & Bloom 3 – RV Pelagia, Southern North Sea
2000 Dec	Plume & Bloom 4 – RV Pelagia, Southern North Sea
2001 May	COMET 1 – RV Navicula, Westerschelde, Netherlands
2001 Jun	COMET 2 – RV Pelagia, Mediterranean Sea and North Sea
2001 Jul	COMET 3 – field campaign Spitzbergen, Norway
2001 Sep	CANOBA – RV Pelagia, North Sea
2002 Mar	AIRWIN 2 – field campaign Barcelona and Banyuls sur Mer
2002 Jun	AIRWIN 3 – field campaign Barcelona and Banyuls sur Mer
2002 Sep	TRANSAT 1 – RV Pelagia, North East Atlantic
2003 May	TRANSAT 2 – RV Pelagia, North West Atlantic
2003 Jul	AIRWIN 3 – field campaign Banyuls sur Mer
2003 Sep	BADE 1 – RV Pelagia, Mediterranean Sea
2004 Sep	BADE 2 – RV Pelagia, subtropical North East Atlantic
2005 Nov	ARCHIMEDES 1 – RV Pelagia, subtropical North Atlantic